An Enhanced Oil Recovery Micromodel Study with Associative and Conventional Polymers

Diploma Thesis

Markus Buchgraber

Submitted to the

Department of Petroleum Engineering

University of Leoben, Austria

September 2008

I declare in lieu of oath, that I wrote this thesis and performed the associated research myself, using only literature cited in this volume.

_____

Markus BUCHGRABER
Leoben, October 2008

Acknowledgements

I would like to thank my advisors, Prof. Anthony Kovscek and Dr. Louis Castanier, for their assistance and guidance in research and for their remarkable support in case of experimental difficulties. I also gratefully acknowledge the support of all the members and Industrial Affiliates of the Stanford Petroleum Research Institute (SUPRI-A).

Furthermore, I would like to thank Dr. Clemens Torsten for all the preparation work and organization and his indispensable phone calls, which gave me new inspiration and motivation for this work.

I also would like to thank Prof. Leonhard Ganzer for his advice and support during my master thesis in Stanford and Leoben.

I am very grateful to OMV for giving me this great and unique opportunity and financial support to pursue my master thesis at Stanford University.
Also special thanks to SNF Floerger for providing the polymers and information.

Finally, I want to thank my family for their incredible support during my semesters abroad. Your help, patience and love made it a lot easier to do my research and finish my studies. Mom, Dad, Christian and my dear Verena, thanks for being with me in good as well as in hard times!

Table of Contents

List of Figures

List of Tables

Abstract

Half of the recovery of the worldwide oil production is due to waterflooding projects. Mainly lighter oils with lower in situ viscosities are recovered by water flooding. Buckley-Leverett and Darcy´s Law can describe the displacement process of these stable displacements very well. Higher viscous oils suffer from unfavourable mobility ratios and, therefore, show unstable displacement.

Viscous fingers cause an early breakthrough leaving a lot of bypassed oil behind them and having high watercuts early in their flooding life. This behaviour can hardly be described by the Buckley Leverett equation and does not predict reservoir performance very accurately.

By adding polymer into the injection water and, therefore, increasing the viscosity, the displacement process will have a more favourable mobility ratio and hence a more stable displacement. In addition, the effect of the plugging of high permeability paths so that bypassed areas get in contact with the displacement fluid, is desired.

Polymer flooding has been done for almost 40 years with hydrolysed polyacrylamide or xanthan, which are referred to as conventional polymers. A new type of polymer, a so-called associative polymer, has been developed recently. It has a greater resistance against salinity and at the same concentration a higher viscosity than conventional polymers, which would reduce the costs of a polymer flooding project significantly.

The purpose of this study is to improve the understanding of the immiscible displacement of conventional and associative polymer solutions with dead oil (450 cP). Forced imbibitions experiments were conducted to observe front stability, breakthrough-time and recovery and ultimate recovery for different polymer concentrations and polymers.

Experiments were conducted in a micromodel which had geometrically and topologically the same homogenous pore space as Berea sandstone. It acts as an artificial reservoir and is an etched silicon wafer bonded with glass to build the flow channels. The main advantage compared to conventional core experiments is that the displacement process can be observed at meso and micro scale with a microscope without any CT-scanning tools. Records in form of high resolution photographs and videos describe the displacement process at micro and meso scale.

Initial water saturation, water saturation at breakthrough, swept area at breakthrough and ultimate recovery are determined and calculated with digital analyses. Additional data recorded before and

during experiments are oil and polymer viscosity, mobility ratios, shear rates for polymer solution in the micromodel, absolute and relative permeabilities, injection rate and pump pressure.

Analyses stated that with increasing polymer concentration recovery, sweep efficiency and front stability also improved. Associative polymer solutions did not convince significantly in terms of recovery but showed better front stabilities than conventional polymer solutions. For this set of experiments best results were obtained with polymer concentrations of 1250 ppm to 1500 ppm. It was also shown that there exists a upper limit for polymer concentration. Exceeding this led to a pore plugging effect and poor recovery.

Kurzfassung

Die Hälfte des weltweit geförderten Erdöls wird mit Hilfe von Wasserfluten gewonnen. Hauptsächlich werden dabei Erdölfelder mit leichtem Öl und niedriger Viskosität gefördert. Um diese Prozesse mathematisch zu beschreiben, können die Gleichungen von Buckley und Leverett und das Gesetz von Darcy verwendet werden.

Höher viskoses, schweres Öl hat mit Hilfe von Wasserfluten sehr schlechte Erfolgsergebnisse. Grund dafür sind unvorteilhafte Mobilitätsverhältnisse, die zu einem nicht stabilem Verdrängungsprozess führen. Viskose Finger bilden sich und führen zu einem Durchbruch der Wasserfront. Hohe verfrühte Wasserproduktionen und nicht kontaktierte Reservoirgebiete mit hohen Ölsättigungen sind die Folge.

Das Beimischen von kleinen Mengen von Polymeren kann die Viskosität des Injektionswassers signifikant erhöhen und zu besseren Mobilitätsverhältnissen, die stabilere Verdrängungsverhältnisse haben, führen. Zusätzlich werden Kanäle erhöhter Permeabilität verstopft und das Flutwasser so zu nicht kontaktierten Bereichen geleitet.

Der Prozess des Polymerfluten wird seit mehr als 40 Jahren kommerziell eingesetzt. Die am häufigsten verwendeten Polymere sind hydrolisierte Polyacrylamide und Xanthan. Sie werden als konventionelle Polymere bezeichnet.

Seit kurzem wurde ein sogenanntes assoziatives Polymer getestet. Durch funktionelle Gruppen besitzt es eine höhere Resistenz gegen Salinität und kann bei gleicher Konzentration höhere Viskositäten als konventionelle Polymere haben.

Das Ziel dieser Studie war es das Verständnis von unmischbaren Verdrängungsvorgängen von konventionellen und assoziativen Polymer-Lösungen mit mittelschweren Ölen (250cp) zu verbessern. Forced Imbibtion Experimente mit verschiedenen Polymer Konzentrationen wurden durchgeführt um Frontstabilität, Durchbruchszeit -und Entölung und Endentölung zu bestimmen und zu beobachten. Als poröses Medium dienten Micromodels, welche die gleichen geometrischen und topologischen homogenen Porenstrukturen von Berea Sandstein aufweisen. Eine geätzte Silkonscheibe, die durch eine Glasplatte abgedeckt und verklebt wird, bildet den künstlichen Kern mit den nachgeahmten Porenkanälen. Vorteil dieser Technik ist, dass der Verdrängungsvorgang visuell im Micro- als auch im Mesobereich mit Hilfe eines Mikroskops beobachtet werden kann und kein Röntgengerät verwendet werden muss.

Hochaufgelöste Photographien im Micro- und Mesobereich beschreiben anfängliche Wassersättigung, Wassersättigungen zur Front Durchbruchszeit, Endentölung und geflutete Bereiche. Zusätzliche Daten, die vor und während der Experimente aufgenommen wurden wie absolute und relative Permeabilität, Viskositäten des Öls und der Polymer Lösungen, Mobilitätsverhältnisse, Scheer Raten und Injektionsraten sowie dazugehörige Pumpendrücke sollen für ein besseres Verständnis der Flutversuche sorgen.

Auswertungen ergaben dass mit erhöhten Polymer Konzentrationen, Entölungsgrad, geflutete Bereiche und Frontstabilitäten auch entscheidend gesteigert werden konnten. Assoziative Polymerlösungen ergaben keine besseren Entölungen als konventionelle Polymerlösungen, führten aber zu stabileren Fronten. Beste Ergebnisse für diese Experimentreihe ergaben Polymerkonzentrationen mit 1250ppm bis 1500ppm. Zusätzlich konnte gezeigt werden, dass es eine kritische Polymerkonzentration gibt. Experimente mit höheren Konzentrationen führten zu Porenverstopfungen und schlechten Entölungen.

Introduction

Primary oil production relies on the natural energy present in a hydrocarbon bearing zone. The main energy sources are water and gas, which displace the oil to the production wells. Most often this process contributes to only a minor part of the production of the original oil in place. Thus, different supplemental recovery techniques have been developed and invented through the last decades to increase the recovery for reservoirs.

Volumetric sweep efficiency and microscopic displacement efficiency determine the viability of a displacement process in an oil reservoir. Enhanced oil recovery (EOR) usually utilizes the injection of different fluids into the reservoir. The injected fluids supplement the displacement process with natural energy in the reservoir. Chemical flooding (alkaline flooding or micellar polymer flooding), miscible displacement (carbon dioxide or hydrocarbon injection), and thermal recovery (steamflood or in-situ combustion) are the three major types of enhanced oil recovery. The selection of one of those specific techniques depend on reservoir temperature, pressure, depth, net pay, permeability, residual oil and water saturation, porosity and fluid properties, such as oil API gravity and viscosity.[1]

Mobility control and chemical processes are the main processes involved in enhanced oil recovery techniques. Polymer flooding utilizes the mobility control process. A polymer flood application is designed to develop a favourable mobility ratio between the injected polymer solution and the oil bank being displaced ahead of the polymer solution slug. The main target is to produce a uniform displacement in vertical and horizontal direction to avoid viscous water fingers, which take the shortest path to the production well. Figure 1 represents a desired displacement process during a polymer flood and an undesired case, where viscous fingers cause an early breakthrough in a water flood project. During the last decades, the molecular weight and quality of polymers have improved their flood efficiency and success rate significantly. Therefore, the interest in users, manufactures and research facilities has significantly increased. Rheological properties and the behaviour by displacing heavy and intermediate viscous oils are the target of current investigations. As a rule of thumb, polymer flood applications were applied for oils with viscosities less than 100 centipoises (cp). Nowadays oil viscosities up to 2000 cp have been tested with

polymer solutions. A reason for that is the increased oil price, which broads the sometimes risky application of enhanced oil recovery techniques. In addition, the advent of new technology, combining two technologies like horizontal wells and polymer flooding, can make the initiation of a polymer flood quite economically and technically successful.

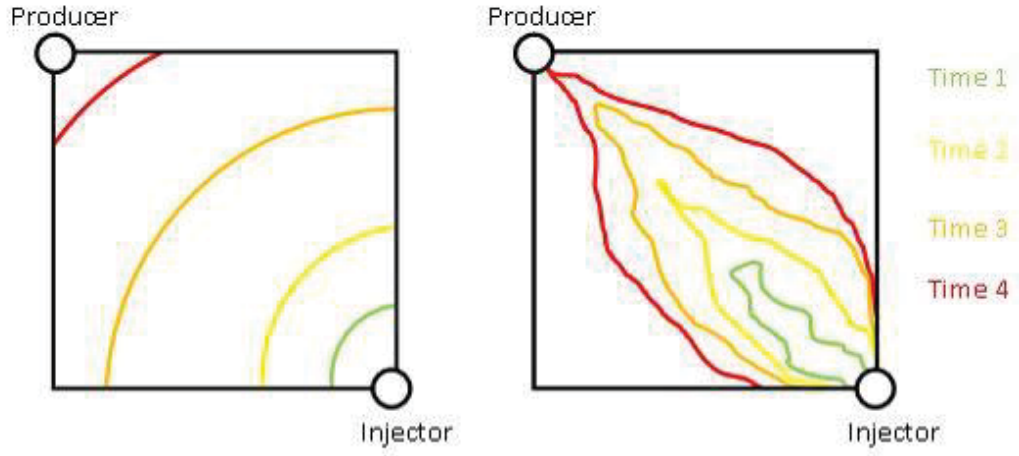

Figure 1: Five spot displacement pattern: stable and unstable displacement

A polymer flood project requires more technical equipment and knowledge compared to conventional water floods. A number of polymer projects have been implemented since the 1960's. However, the mobility control process alone does not employ the microscopic displacement efficiency and suffers from a low recovery efficiency, thus the incremental oil recovery is limited, usually under 10% of the original oil in place (OOIP). Analyzed statistical data from the DOE of the field wide projects showed that the median recovery of oil was 2.91% OOIP[2].

This study investigates the behaviour of so-called associative polymers, which have special functional groups which provide a better viscosity than conventional polymers of the same concentration. Additionally, they are suitable for mixing with very high saline reservoir brines. Different concentrations of conventional and associative polymers solutions were tested to understand the relationship of polymer concentration with sweep efficiency and recovery. Polymer solution can also be used with surfactants and alkali agents. For the purpose of this work, only polymer solution mixed with brine is used to observe and understand the flow mechanism. Instead of a real core, micromodels act as an artificial core. An etched silicon wafer bonded with a

pyrex glass represents the pore structure of a Berea sandstone and provides artificial flow channels. High resolution photographs on micro and meso scale are used to describe flow behaviour and pattern and to determine recovery and sweep efficiency. As a baseline, a water flood experiments was conducted. Additionally, the influence of a late start of a polymer injection after breakthrough has been tested and evaluated. Also, the possible recovery of residual oil with a polymer solution has been tested. Rheological experiments with oil and augmented polymers give a better understanding of shear rate and viscosity behaviour during the experiments.

The first chapters will give an overview about polymer flooding including the advantages, screening criteria and field development and evaluation processes for a polymer flood. Next chapters will deal with the chemical and rheological properties of polymer solutions. Followed by this, the experimental apparatus and the experimental procedure including are described in more detail. The final part presents the results and a follow up.

Viscous Fingering

Buckley and Leverett´s displacing theory assumes that water displaces oil as a smooth and substantially straight interface. Viscous fingers which developed in displacement experiments disproved Buckley and Leverett´s theory. In general viscous fingers refer to the onset and evolution of instabilities that evolve in the displacement of fluids in a porous system. Most often instabilities are intimately linked to viscosity variations between phases. Viscous structures typically consist of fingers invading into the displaced fluid and propagating through the porous medium and leaving clusters of the displaced fluid behind. Once the path of displacing fluid has broken through and flows into the production well, the production well will henceforth preferentially produce the displacing fluid, which flows more easily because of the lower viscosity and better fractional flow characteristic. Viscous fingers depend on viscosity ratios, relative permeability curves, initial water saturation and flow rates of injected fluid.

One of the first experiments, which showed the viscous displacement process of water by oil was made by van Meurs[3] [4] . Fine powdered glass served as a porous medium. He came up with the conclusion that a water drive at favourable viscosity ratios is efficient, but the presence of stratified layers with different permeabilities can reduce its success significantly. Furthermore, he stated that unfavourable viscosity ratios lead to poor sweep efficiency and the influence of stratification was minor. A displacement of viscosity ratio of a unity led to a stable displacement. He was able to visualize the viscous fingers depending on injected fluid, W_i, as can be seen in Fig. 2.

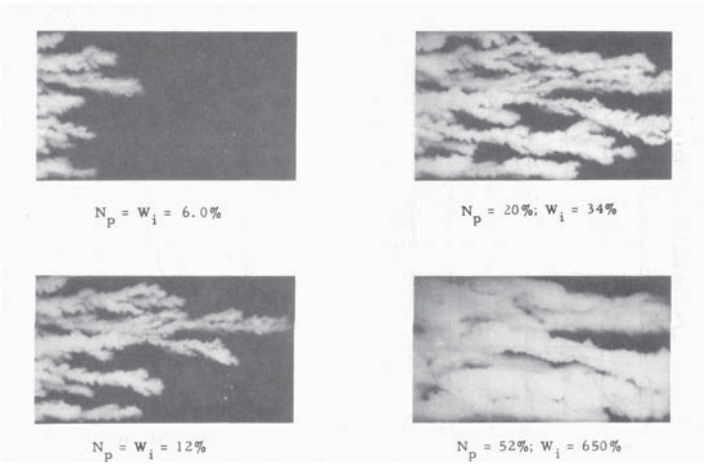

Figure 2: Development of viscous fingers according to van Meurs.

In 1963, Benham and Olsen studied the behaviour of viscous fingers in an open and packed Hele-Shaw model (1 ft x 4 ft). Flow velocities of 0.06 to 0.2 ft/hour and mobility ratios from 1 to 9.3 were used for the displacement experiments. Results indicated that the length of viscous fingers increased linearly with increasing mobility ratio and increasing flow rate. They were not able to determine the initiation point of a viscous finger but they observed that fingers decreased towards the end of the model due to microscopic dispersion or diffusion effects[5].

Saffman and Taylor[6] used a Hele-Shaw model to demonstrate the instability problems. A less viscous fluid was injected into a more viscous one constrained between two parallel thin glass plates. Wave-like projections, known today as viscous fingers, exhibited the resulting interface between the fluids. They investigated that on the one hand surface tension served to stabilize the system by trying to minimize the surface, and on the other hand the viscosity difference destabilized the system promoting the growth of the fingers. Results show that single fingers were produced, and that unless the flow is very slow λ = (width of finger)/(width of channel) is close to ½ , so that behind the tips of the advancing fingers the widths of the two columns of fluid were equal.

Other experiments with lower viscous fluids for displacing like air and water stated that λ is only a function of viscosity, speed of advance and interfacial tension.

Van Meurs and van der Peol [7] conducted linear displacement experiments with oil and water at unfavourable mobility ratios in a transparent porous medium. Experimental observations described mathematically and led to accurate expressions of oil production and pressure drops across the porous media as a function of cumulative water injection with the oil-water viscosity ratio as a parameter. The theoretical results were applied to sand filled tubes and to field scale applications. Both led to satisfying predictions in oil and water production and breakthrough time.

Polymer Flooding Mechanism

By adding small amounts of soluble polymers into water a very viscous aqueous solution can be obtained. This viscous fluid can reduces mobility ratios in flooding operations significantly. It was regarded as one of the most successful EOR methods in the 80s, although by definition polymer flooding projects did not increase the volumetric sweep efficiency of the reservoir rock. The remaining oil saturation after a polymer flood is the same as after a water flood. Nevertheless it was observed that polymer solutions can interact with the rock surface and change wettability to more water wet characteristics leading to residual oil recovery. Compared to other EOR methods like chemical floods, which reduce the interfacial tension and therefore reduce the residual oil saturation, polymer floods cannot produce significant amounts of residual oil. Polymer flooding does not reduce the residual oil saturation noticeable, but is rather a way of reaching the residual oil saturation more quickly and allows it to be reached more economically. Hence, almost the same physical laws used for water floods can be applied for the injection of the polymer solution.
To make the oil recovery process with polymer solution more efficient there are three potential ways:

- through the effects of polymers on fractional flow
- by decreasing the water/oil mobility ratio, and
- by diverting injected water from zones that have been swept

Relative permeability relationships and viscosities of oil and water are the main parameters influencing the way and success of a reservoir approaching its ultimate residual oil saturation. Those two factors are combined and used in the formulation of the fractional flow. Assuming that the oil and the water are flowing simultaneously through a segment of a porous medium, the fractional flow of crude oil, f_o, and water, f_w, can be expressed as in Eq. 1. [3]

$$f_o = \frac{1}{1 + \frac{\mu_o k_{rw}}{\mu_w k_{ro}}}$$

$$f_w = \frac{1}{1 + \frac{\mu_w k_{ro}}{\mu_o k_{rw}}}$$

Any change of the term $\frac{\mu_o k_{rw}}{\mu_w k_{ro}}$,which increases the fractional flow of the oil, will lead to an improvement of recovery. Polymers, when added to water, have the ability of increasing the viscosity of water, μ_w. Another effect is that once they have flooded a zone, they can reduce the permeability to water, k_{rw}. This effect occurs at parts of the reservoir having high mobile oil saturation, anywhere where the relative permeability to oil is above zero. But having already very low mobile oil saturation and therefore a low k_{ro}, changes in μ_w and k_{rw} will not result in any significant changes in the fractional flow of oil. Hence the fractional flow effect is more significant to projects where polymer flooding has been applied early in a field life when mobile oil saturation is still high. Oil viscosities also contribute to the fractional flow. Areas of higher oil viscosity will show greater tendency of water flowing than oil.

As a result the water breakthrough and therefore the water production will be early in the field life and a lot of mobile bypassed oil will be left in the reservoir. Thus fractional flow effects show more likely in viscous oil reservoirs. Below characteristic flow curves are plotted for oil having a viscosity of 15 cp and the displacing fluids water with 1 cp and a polymer solution having 15 cp. The saturation at the front for the polymer flood S_{pf} and the water flood S_{wf} and also the saturation at the breakthrough S_{btp} and S_{btw} are given in Fig. 3. Both saturations at the front and at breakthrough are distinctly higher for the polymer flood than for the waterflood. This shows the better performance of a polymer flood to a water flood. In Fig 4. the corresponding mobility ratios to Fig.3 can be seen. It is shown that mobility ratios in water floods at low water saturations can be below 1, whereas for polymer floods at high saturations, the mobility ratio can exceed 1 as well.

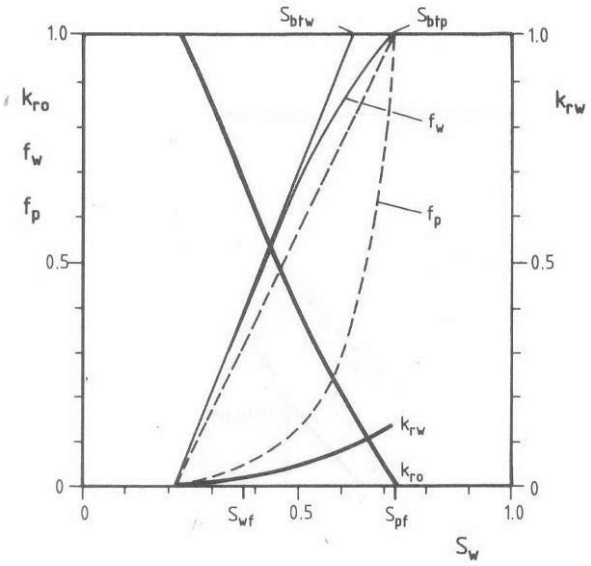

Figure 3: Typical relative permeabilities for oil and water of a water wet sandstone and fractional flow curves for displacement of oil by water and polymer solution (Viscosities oil: 15 cp; water: 1 cp; polymer solution: 15cp) [8]

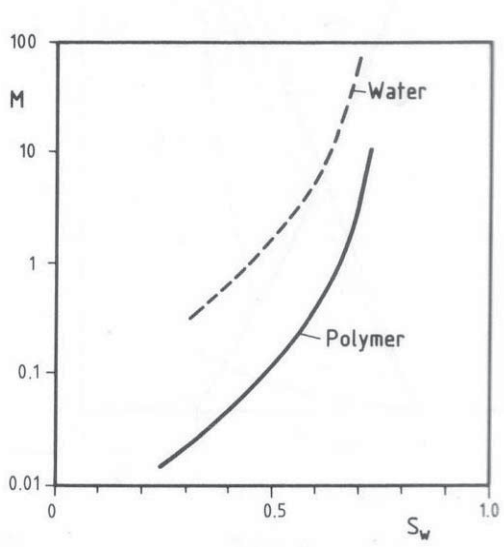

Figure 4: Mobility ratio for the displacement of oil by water and polymer solution as a function of the saturation of the displacing phase[8].

The mobility ratio of a flood is the primary determinant of areal sweep efficiency for a given well spacing and pattern and is defined for water floods in Eq. 2 as:

$$M = \frac{k_{rw}\mu_o}{k_{ro}\mu_w}$$

No real reservoir can be swept uniformly and even in a homogenous reservoir a 100 % areal sweep at water breakthrough and an economically water/oil ratio cannot be achieved. For any given reservoir, the recovery till breakthrough will decrease with increasing mobility ratio. Also, the later recovery will be less for a given volume of water injected. Polymer solution may improve the mobility ratio in the same way as mentioned above. They can increase the water viscosity or decrease the water relative permeability. It must be considered that at low mobile oil saturations there is only small potential for improvement. From this point of view, a secondary over a tertiary application for a polymer flood is favourable. Another example of the effect of different mobility ratios is given below in Fig 5. This figure clearly demonstrates the improvement in recovery related to a decreasing mobility ratio. The irreducible oil saturation should be the same for all cases, but the period of time and therefore the volume injected can vary slightly. The improvement shown below is that the oil can be recovered earlier at a lower water cut and thus in practice at lower lifting costs.

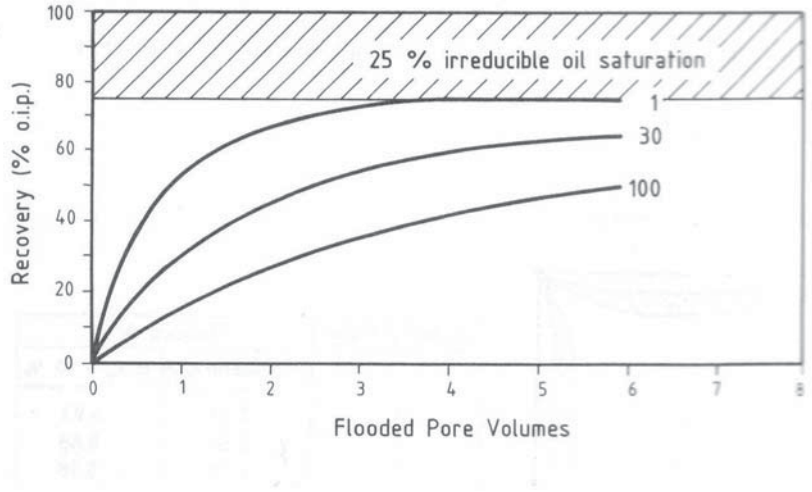

Figure 5: Influence of mobility ratio on oil recovery process [8]

So far two profitable effects of polymer flooding have been shown:

a.) a more rapid oil displacement through improved fractional flow characteristics and
b.) an improved areal sweep efficiency through the improved mobility ratio.

Both these effects mainly work in homogenous reservoirs and on mobile oil saturations on polymer flooded zones. Unfortunately, no uniform homogenous reservoir exists. The majority of the reservoirs have significant heterogeneities in the areal and particularly in the vertical direction. As a result, water preferentially flows and penetrates the high permeable zones and sweeps out those areas more rapidly. Therefore, areas which are contacted by the flood water are swept very efficiently. Areas with lower permeability and higher flow resistance in which water does not flow, stay untouched and have poor to zero recovery. When injecting a polymer solution into the already contacted areas, the reservoir may recover very little oil out of this zone. But such polymer solution floods can get very beneficial because of the fluid diversion. The polymer will build up flow resistance through permeability reduction in the penetrated portions of the reservoir. This increased resistance to flow will divert subsequently injected water into unswept or poorly swept areas.
It is assumed that for most of the polymer floods initiated at high water oil ratios, fluid diversion contributes much more to recovery than fractional flow or mobility ratio effects. Best results should be obtained when physical properties of the polymers can be sustained over a long period during the flooding project. This tends to place a premium on permeability reduction as opposed to straight viscosity improvement

because permeability reduction can be very long-lasting. Optimized permeability reduction may make cross linking of the polymer desirable. Cross linking polymers has been done successfully for a long time and can be achieved in a number of ways, including the use of multivalent cations and organic compounds. A network of linked polymers that results in a long lasting permeability reduction and a greater reduction in water permeability is caused by the cross linking of the polymers. The resultant permeability reduction causes subsequently injected water to be directed into zones that have not been completely flooded.

At high water oil ratios, the fluid diversion effect reported above would be the most important effect. Because of the prevailing low values of k_{ro} in the swept zones, fluid diversion will contribute to high recoveries in areas in which it is already too late for fractional flow and mobility ratio improvements.

Figure 6 below shows the results of a flood experiment by Sandiford, which discribe a system of two parallel flooded cores of different permeabilities. The oil recovery due to the polymer flooding is significantly higher than during a flood in one core of uniform permeability [8].

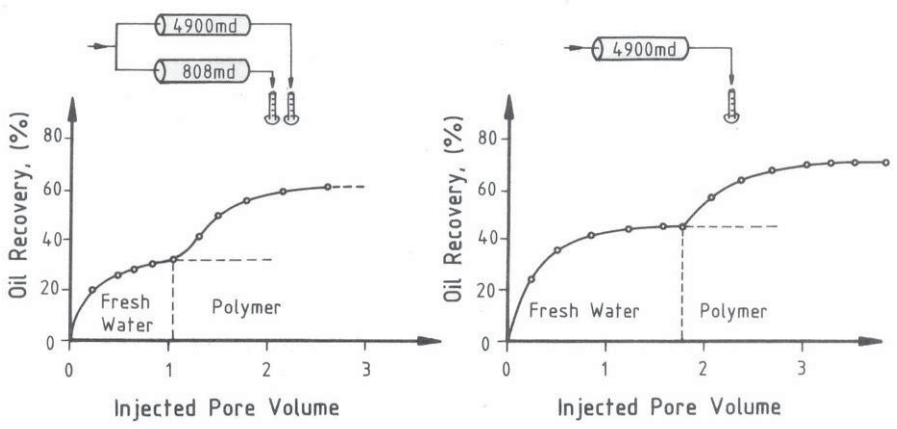

Figure 6: Possible effect of polymer solution when dealing with a heterogeneous reservoir [8]

Screening of an EOR Polymer Flooding Project

Because not every EOR methodology is suitable for every reservoir, different parameters and characteristics of a reservoir fit different enhanced recoveries. Before planning any details of a polymer flood, it has to be evaluated if it is possible at all or whether it will be successful in respect to technical performance and profitability. Typical situations are high water cut reservoirs with poor recovery and a bad economic efficiency. Mobility ratio, permeability and its variation, porosity, formation temperature and pressure, formation type, fluid saturation, rock minerals and the properties of the water are such characteristics which decide whether a polymer flood is successful or a failure. So the purpose of the next chapter is to show some of the important parameters which have to be taken into account to perform a successful polymer flooding.

Permeability

The order of permeability and the variation within the reservoir are of major importance in a polymer flooding project. The water injectivity which also defines the well spacing and the project life, is determined by the reservoir permeability. In other words, a 5 acre well spacing in a high permeable reservoir will perform better than a 2 acre spacing with a very low permeability. Polymer injectivity is normally lower than the brine injectivity because of the difference in fluid viscosity. This might be a particular problem under pressure limited conditions in very shallow reservoirs. The range of permeability, in which successful polymerflooding projects have been performed, is from 20 md to 2,300 md.

Mobility

Mobility ratio is defined here as the mobility at residual oil saturation to the irreducible water saturation. To be on the safe side at a polymerflood water-oil mobility ratios should be in the range of 1 to 42. Speaking about oil viscosities, projects with a oil viscosity up to 500 cp has been tested for polymerfloods so far.

Effective Porosity

Effective porosity only counts pores which are connected and can be divided into three groups: a) intercrystalline, b) intergranular and c) fracture matrix porosity. Pore surface and space have a major influence on adsorption and retention characteristics

of the polymers. In addition porosity also determines the amount of polymer solution which has to be provided for injection. A useful tool to determine the porosity is the Scanning Electron Microscope (SEM).

Mobile Oil Saturation

In general, the higher the oil saturation the higher the economic success in polymer flooding as well as in water flooding projects. Good candidates for polymer flooding projects are heterogeneous reservoirs with significant volumes of mobile oil, which can be produced at high water oil ratios (WOR). As a rule of thumb, the mobile oil saturation should be in the range of 0.15 to 0.46.

Initial water saturation

Despite some literature that high initial water saturations can be deleterious for polymer flooding projects with initial water saturations of 0.47 were successful.

Depth – Temperature and Pressure

Temperature and pressure are usually controlled by the depth of the reservoir in a normal pressured system. Lower temperatures protect the polymer solution from degradation. The temperature limit for polymers is in the range of 250°F (121°C) . Exceeding this temperature will lead to degradation, even with a zero oxygen concentration.

Depletion Stage

Polymer flooding with technical and financial success has been reported for secondary and tertiary recovery. Comparing published results, polymer flooding projects initiated at the secondary recovery stage produced more oil with less used polymer than comparable projects initiated after an intensive water flooding period as a tertiary recovery method. Projects started at WOR $>$ 10 showed less success than others. All in all the earlier the polymer flooding is initiated the better.

Formation Type

Field applications conducted on both sandstone and oolitic limestone formations showed technical success. Whereas grossly vugular limestones were avoided due to the missing appreciable resistance factor.

Rock Minerals

The efficiency of the polymer solution may be affected by the presence of different rock minerals. The contact of clay with water leads to a swelling of the clay and results in a reduced injectivity. Another negative effect of clay is the adsorption of the polymer solution and the surfactant during a miceller-polymer flood. Gypsum ($CaSO_4*2H_2O$) in a high enough concentration causes precipitation of petroleum sulphonate which reacts with polyacrylamide and reduces its viscosity significantly.

Water salinity

Increased salinity in reservoir brines is usually a problem for most polymer and miceller polymer solutions. Brines containing high concentrations of magnesium and calcium ions may accelerate the degradation process by precipitation of petroleum sulphonates. This can cause the break-up of the miceller solution into an oil rich and a water phase or the precipitation of surfactants. The most sensitive polymer to brine and multivalent ions is hydrolysed polyacrylamide. This sensitivity results in a loss of viscosity and thus increasing mobility. By running a pre-flush and displacing the reservoir brine, this effect can be avoided. The usage of fresh water will therefore result in lower polymer costs [8] [9].

Development and Evaluation of a Polymer Flooding Project

After the evaluation of the suitability of a polymer flood, the design variables such as polymer type, polymer slug size and polymer concentration need to be discussed and chosen. The simulation process of a polymer flood involves more complex physics than a conventional waterflood and therefore is more complex. Parameters like changing viscosities with different concentrations, shear thinning and thicking behaviour of polymer solution, in situ mixing thermal degradation, changes in relative permeabilities due to adsorption and inaccessible pore volume have to be modelled. The next section will give a short guideline of laboratory work, reservoir simulation, field testing, field piloting and finally commercial application.

A staged summary of a polymer flooding workflow is presented in Figure 7. This process consists of six major parts: 1) preliminary screening (discussed in the previous chapter), 2a) preliminary analysis, 2b) detailed analyses, 3a) field testing, 3b) field piloting, 4) commercial application.

Stage 2a) requires laboratory experiments to determine fluid rheology and polymer-reservoir compatibility. Additionally, basic reservoir simulation models have to be worked out. Stage 2b) continues with core flood experiments to gain more data for simulation, which will be the basis of the economical estimate. After passing stage 2 field plans have to be developed to exclude uncertainties in a potential polymer flood. 3a include more detailed and optimized field application plans and a practical demonstration of polymer injectivity and quality. If 3a is satisfying, a piloting project on a scaled version will be performed and assessed in stage 3b. Depending on the success of this pilot project, the application will evolve to a full scale commercial project or not. Each stage above involves a couple of small activities which all have to be passed in order to reach the next step of the workflow. The matrix in Figure 8 is a useful document to manage those small activities. The most common subjects for EOR projects can be found in the first column and are also listed below:

- Analogs
- Reservoir modelling
- Polymer Selection
- Solution Rheology
- Polymer Retention
- Polymer Stability

- Injectant Preparation
- Injectivity
- Facilities
- Quality Assurance
- Economics

Analogs consist of specific case studies as well as general screening workflows based on history of former polymer floods. General guidelines, which for example present the key challenges for low permeable sands or high in situ temperatures, may be used. Specific case studies should give positive and negative views of comparable projects.

Reservoir simulation is the key methodology to estimate the economic success and to compare the polymer flood with alternative EOR techniques. Laboratory, geological and field data are required to scale the physical phenomena and identify uncertainties.

Polymer selection starts at a very early stage of the planning. Different types of polymers should be evaluated in terms of the molecular weight and degree of hydrolysis when dealing with HPAM. Reservoirs with very high salinity may require Xanthan polymer because of its better resistance against water hardness.

Polymer solution rheology depends on the polymer type, concentration, brine composition and reservoir temperature. Since all of them are Non-Newtonian fluids, they have different behaviour according to different shear rates. An important parameter is the flow velocity near the wellbore and in the reservoir to get an estimate of the later behaviour of the polymer solution.

Polymer retention has a major influence on flooding efficiency. It can reduce the solution concentration and retard the transport through the reservoir by adsorbing the polymer molecules on the rock surface and by trapping particles in small pores. Lower permeable reservoirs are more likely to have polymer retention due to increasing rock surface per unit mass and reducing pore throat size.

Polymer stability is usually connected to high temperatures. As a rule of thumb, 60°C should be the limit but depending on the polymer and other reservoir conditions, there are always exceptions. Thermal degradation is accelerated by adding oxygen or iron

into the brine. As it can take up to one year to test those behaviours, such experiments should be initiated at a very early stage.

Injectant preparation stands with the mixing of the right polymer solution. An over-mixing shears polymers too much and results in degradation whereas an insufficient mixing often includes non dissolved gel particles.

Injectivity depends on the injectant quality as well as on the polymer chemistry. Some polymers can show a shear thickening behaviour at high velocities near the wellbore and therefore reduce injectivity significantly. Another negative effect is that even a well prepared polymer solution with high molecular weight can be trapped by narrow pore throats and decrease injectivity slowly. Pilots to prove the required injectivity to be technically and economically successful, are of major importance.

Facilities to generate and deliver the polymer solution have to be tested and certified during the pilot project. To be on the safe side, any fitting valves and pumps which produce high shear rates should be avoided in order to protect the polymer solution from mechanical degradation.

Quality assurance of a polymer flood faces the following threats. Impurities in the polymer powder caused during the transport, presence of oil or small amounts of oxygen in the mixing water from the reservoir, poorly mixing or over-shearing the polymers can degrade the polymer performance seriously. Defining quality checks at different points and corrective actions in case of failure prevent any misleadings.

Economic assessments have to be done after each planning and performance stage to make sure that the project is still worth being financed. Reservoir simulations, laboratory and field studies should give a risk analyses in the early as well as in the later stage of the project. The closer the end of the planning comes, the more accurate and detailed should be the risk scenarios and possible uncertainties worked out and identified [10].

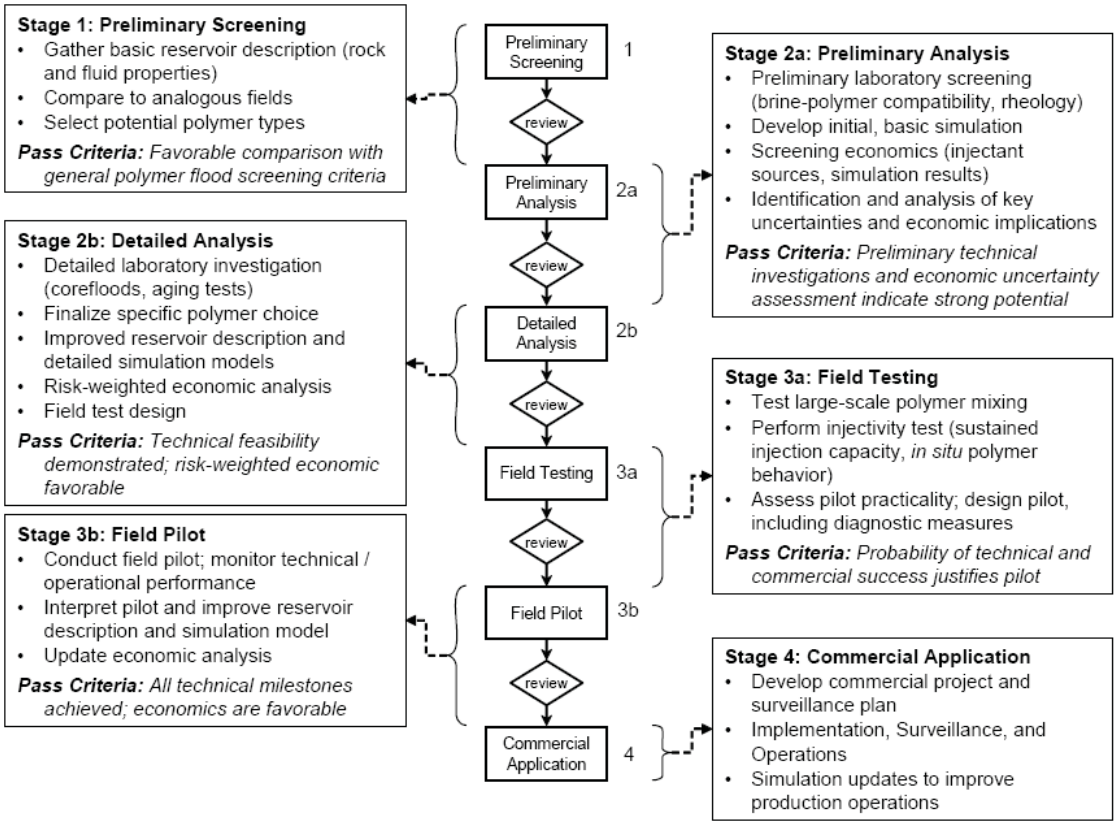

Figure 7: Staged process for polymer flood project evaluation and development [10]

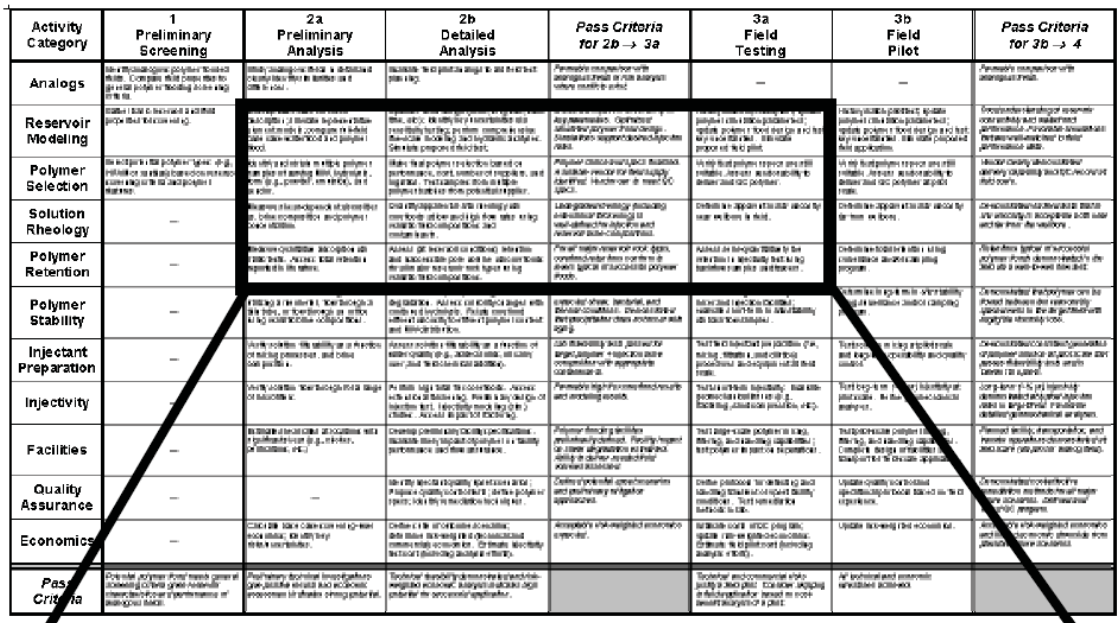

Activity Category	1 Preliminary Screening	2a Preliminary Analysis	2b Detailed Analysis	*Pass Criteria for 2b → 3a*	3a Field Testing	3b Field Pilot	*Pass Criteria for 3b → 4*
Analogs					–	–	
Reservoir Modeling							
Polymer Selection							
Solution Rheology	–						
Polymer Retention	–						
Polymer Stability	–						
Injectant Preparation	–						
Injectivity							
Facilities	–						
Quality Assurance	–	–					
Economics	–						
Pass Criteria							

Activity Category	2a Preliminary Analysis	2b Detailed Analysis	*Pass Criteria for 2b → 3a*	3a Field Testing
Reservoir Modeling	Develop base case reservoir description; simulate representative element models; compare full-field base case waterflood and polymer flood.	Optimize flood design (conc., slug size, start time, *etc.*); identify key uncertainties via sensitivity testing; perform comprehensive fine-scale modeling and hydraulic analyses. Simulate proposed field test.	*Evaluated impact of uncertainty on key parameters. Optimized simulated polymer flood design. Simulations support desired injection rates.*	History match injectivity test; update polymer simulation parameters; update polymer flood design and test key uncertainties. Simulate proposed field pilot.
Polymer Selection	Identify and obtain multiple polymer samples of varying MW, hydrolysis, form (*e.g.*, powder, emulsion), and vendor.	Make final polymer selection based on performance, cost, number of suppliers, and logistics. Test samples from multiple polymer batches from potential supplier.	*Polymer choice and specs finalized. A suitable vendor for field supply identified. Vendor can to meet QC specs.*	Verify that polymer specs are still suitable. Assess vendor ability to deliver and QC polymer.
Solution Rheology	Measure shear-dependent viscosities vs. brine composition and polymer concentration.	Quantify apparent *in situ* rheology via corefloods at low and high flow rates using realistic fluid compositions and contaminants.	*Un-degraded rheology (including extensional thickening) is well-defined for injection and reservoir brine compositions.*	Determine apparent *in situ* viscosity near wellbore in field.
Polymer Retention	Measure qualitative adsorption via static tests. Assess total retention reported in literature.	Assess (at reservoir conditions) retention and inaccessible pore volume via corefloods for all major reservoir rock types using realistic fluid compositions.	*For all major reservoir rock types, coreflood retentions conform to levels typical of successful polymer floods.*	Assess semi-quantitatively the retention in injectivity test using backflow samples and tracers.

Figure 8: Representative Portion of polymer flood project evaluation and development matrix [10]

Chemistry of EOR Polymers

EOR techniques basically use two types of water soluble polymers, which can be divided into: polysaccharides produced from natural sources like wood, seeds or bacteria and fungi, and polymers which are synthetically produced. At the moment the most commonly used polymers are hydrolysed polyacrylamides (HPAM), which belong the latter ones.

Polysaccharide

Carbohydrates are generally described with $C_m(H_20)_n$. Saccharides are carbohydrates with the formula $C_nH_{2n}0_n$ and can be divided into three groups: a) Monosaccharides, b) Oligosaccharides, c) Polysaccharides. Polysaccharides are present as cellulose building materials for cell walls, starch etc., it is a most abundant organic matter. The chemical structure of hydroxyethyl cellulose is given below in Fig. 9, to have a better chemical understanding. The basic unit is the cellulose. Within the ring there are three positions which can be connected to different functional groups without destroying the character of the ring. Those three positions are the CH_2OH and the two hydroxyl groups[11].

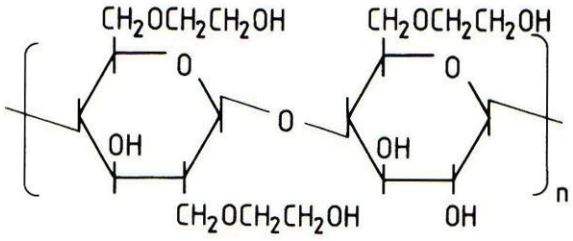

Figure 9: Molecular structure of hydroxyethyl cellulose [8]

For the hydroxyethyl cellulose, three CH_2CHOH (hydroxyethyl) groups were added to the possible positions. Other polymers can be obtained by adding different functional groups like ethyl or carboxyl which would result in carboxylmethyl cellulose or ethylhydroxylethyl cellulose.

Xanthan

Xanthan, a polysaccharide, is produced by a bacterium called xanthomas campestris. In order to protect the bacteria themselves from dehydration they produce the polymer.

"*The backbone of the molecule is a cellulose chain having two different sides at every second glucose ring (ß-L glucose) like seen in Fig. 10. The side chains also have saccharide rings as basic elements. Every side chain is made up of three monosaccharides. The end of the first side chain begins with a mannose, followed by gluceron acid, and then by a mannose having an acethyl group at the sixth carbon atom. The second side chain is similar to the first one, but it contains a pyruvate unit at the rear mannose. The distribution of the pyruvate within the molecule is not exactly known. The pyruvate group and the two gluceron acids lend the molecule an anionic character. Though like polyacrylamide this molecule also carries electrical charges at its side chain, its behaviour is totally different in high salinity waters. The xanthan molecule shows practically no decrease of viscosity yield as a function of rising salinity. The reason for this is that the molecule, because of the side chain structure, essentially stiffer than the polyacrylamide molecules. This may also be the reason for its good shear stability. But if the pyruvate content becomes too high, the molecule may behave similar to polyacrylamide with respect to its chemical stability (precipitation, gel formation), and the adsorption may increase*." [8]

Other important polysaccharides for EOR are alginate, which reduces the water cut in production wells and scleroglucan, which is produced by fungis and was tested for polymer flooding as well. As the miceller may not be correctly removed from the high viscous broth and thus plugging the formation in the wellbore, it has not been tested in any further field applications.

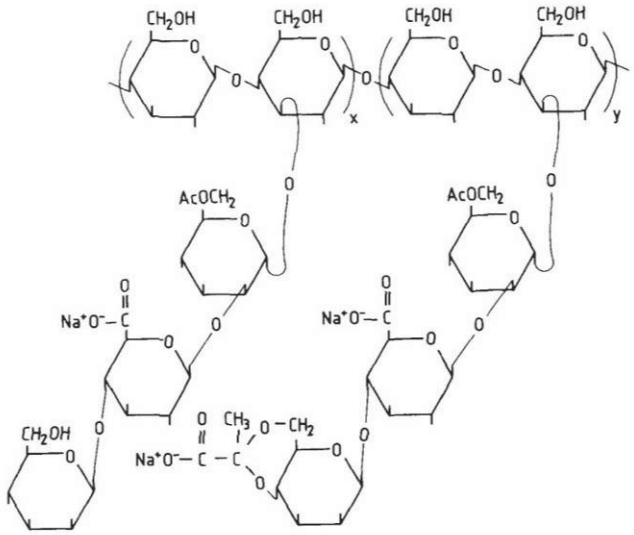

Figure 10: Molecular structure of xanthan[8]

Synthetic Polymers

Polyacrylamide

Polyacrylamides are water soluble polymers which are produced for many different purposes. Deriving the acryl acid leads to the monomer acrylamide, which can be seen in Figure 11.

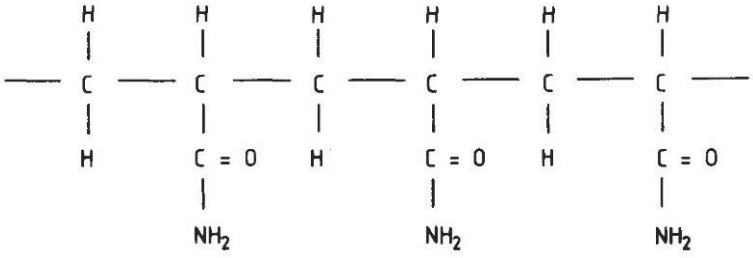

Figure 11: Structure of polyacrylamide (not hydrolized) [8]

The range of the molecular weight is between $1*10^6$-$8*10^6$ with an average particle size between 0.1-0.3 μm.

During the hydrolysis in a water solution some of the $CONH_2$ groups react and form carboxyl groups (COOH), which dissociate in an aqueous solution. The properties of

polyacrylamide in water solution are defined by the degree of hydrolysis and are taken as an important parameter for the enhanced oil recovery. The structure of partially hydrolysed polyacrylamide is shown in Figure 12.

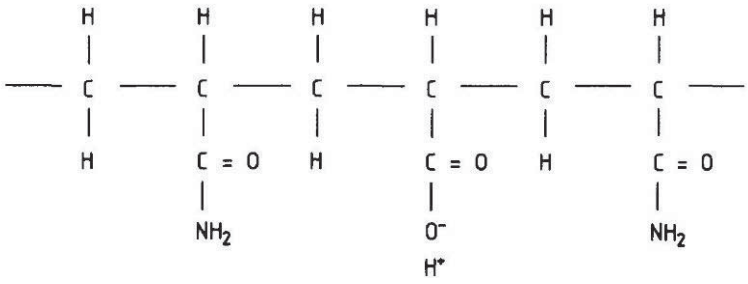

Figure 12: Molecular structure of partially hydrolysed polyacrylamid[8]

The structure above represents a 25 percent hydrolysed polyacrylamide; in a pure distilled water solution. The negative charges of the dissociated carboxyl groups react so that the molecule chain is kept in a more or less stretched form, as the repulsion of the charges have the same polarity. A very high viscosity is gained by the molecule coil which occupies the largest possible volume. Small amounts of cations in the water compensate the negative charges of the oxygen and the molecule coil tends to curl and thus occupy smaller volumes in the aqueous solution. Another interesting mechanism is the cross-linking of the molecules caused by higher amounts of divalent cations. A too high concentration forms a gel like liquid or molecular aggregates, which fall out of solution, are built.

Thus, polyacrylamide is a co-polymer consisting of acrylic acid and acrylamide. The degree of hydrolysis is determined by the amount of acrylic acid in the molecule chain. The usual amount of hydrolysis for enhance oil recovery polymer products is between 25-30%, but there are also products available with a zero degree of hydrolysis. Those products are not as sensitive to salinity as comparable polymers with a higher percentage of hydrolysis. For the purpose of polymer flooding, the latter has to be used with higher concentration and hydrolysis can take place any time during flowing through the reservoirs, which also has to be considered.

Additionally, the shear behaviour of HPAM plays an important role in the reservoir. While shear thinning can be noticed at low to intermediate flow velocities, after exceeding a critical flow velocity it becomes high shear-thickening. This high apparent viscosity is produced when the polymer solution is flowing through a number of pore bodies and throats in the reservoir and flow field elongation and contraction occurs. When exceeding the critical velocity the polymer molecules do not have sufficient time

to stretch and recoil and this elastic strain causes the high apparent viscosity. Higher molecular weight HPAMs have a more shear-thickening behaviour than low molecular weight HPAMs. [11] [12]

Associative Polymer

Associating water-soluble polymer is a relatively new class polymer, which was recently introduced to oil field applications. Essentially, these polymers consist of a hydrophilic long-chain backbone, with a small number of hydrophobic groups localized either randomly along the chain or at the chain ends. When these polymers are dissolved in water, hydrophobic groups aggregate to minimize their water exposure. In aqueous solutions at basic pH, hydrophobic groups form intramolecular and intermolecular associations, which rise to a three-dimensional network. This behaviour increases the viscosity of polymer solution significantly. Another important fact is that the functional groups on this polymer build more and stronger links with increasing salinity which lead to higher viscosities compared to a conventional polymer solution like polyacrylamides which decrease viscosity with increasing salinity. Former experiments showed that they can also have shear thinning behaviour at high flow velocities and shear thickening behaviour at intermediate flow velocities. To have both lower pressure drops at the injection wells in order to achieve enough injectivity with high velocities and higher viscosities in the reservoirs would be a highly preferable on field applications [13]

Polymer Degradation Mechanism

Three different types of polymer degradation have been known so far:

- mechanical degradation
- chemical degradation
- biological degradation

Biological Degradation

Biological degradation is mainly caused by bacteria or by chemical processes governed by enzymes which destroy the polymer molecules. Enzymes catalyse different processes in nature, like the hydrolysis of polysaccharide. These enzymes are also called hydrolases. Such enzymes are used to remove gel plugs after a polymer treatment. In most cases only biopolmyers undergo biological degradation at lower temperatures and salinities.

Xanthan for example is destroyed by fermenting bacteria attacking the glucose units of the molecular backbone under anaerobic conditions. To be on the safe side polymer solutions should be tested under field conditions.

Mechanical Degradation

Mechanical degradation occurs when the polymer solution is exposed to high or very high shear rates. Such conditions arise, during the mixing of polymer solution, flow through chokes, injection through perforations or near well bore area where flow velocity is very high. Polyacrylamide is the most sensitive one to mechanical degradation, but nevertheless it is the most common used polymer for EOR.

Chemical Degradation

The main factor causing chemical degradation in an aqueous polymer solution is the presence of divalent ions, oxygen and temperature. Cations such as Ca^{2+} ,Mg^{2+}, influence its ability to flocculate and the solution stability by disturbing the hydrolysis of polyacrylamides. Besides calcium and magnesium, Fe^{2+} is also present in small amounts in the reservoir water. In combination with oxygen, which may be added

during the mixing and handling process on the surface, iron cations may oxidize to Fe^{3+} which in turn may flocculate polyacrylamides as well as polysaccharides. Increased temperature may accelerate this process. As a rule of thumb polyacrylamide can be used up to 70°C and a calcium concentration of 200 ppm. Corresponding to water hardness this is a degree of 25, where 1 degree of hardness is equal to 10 mg/l of CaO. In Fig. 13 the effect of water hardness on viscosity can be seen.

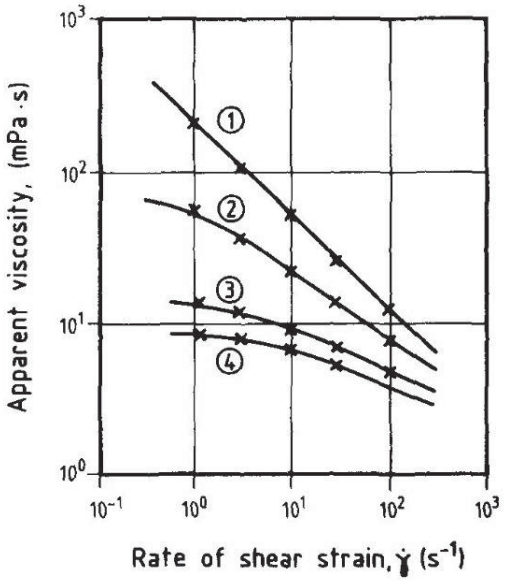

Figure 13: Flow curves of a 1000 ppm polyacrylamide solution at different hardness of mixing water: 1.) 1.6°dH; 2.) 5°dH; 3.) 15°dH; 4.) 25°dH. (1°dH =10 mg CaO/l) [8]

To observe the sensitivity of the associative polymers to salinity, 3 different mixtures of Superpusher 255 with 2000 ppm with increasing salinities were prepared and their viscosity measured. Only light changes in their viscosity were observed as can be seen in Fig. 14 [8]

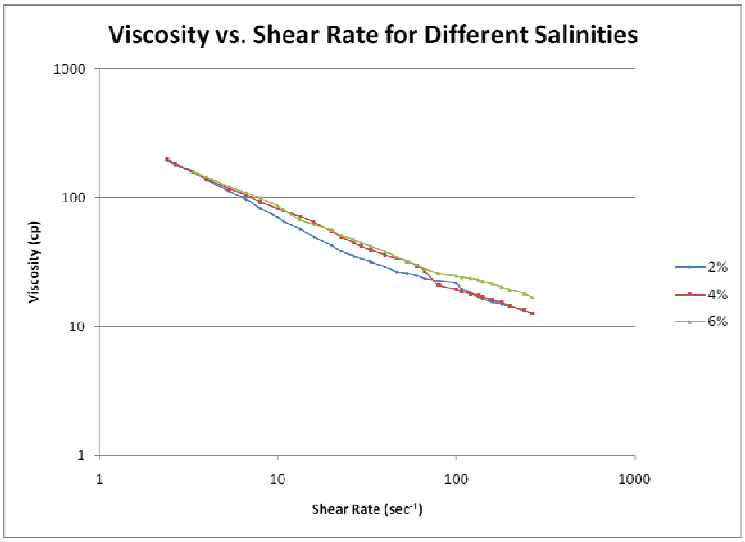

Figure 14: Influence of salinity on viscosity

Rheological Behaviour of Polymers

Viscosity

The basic measurement for any fluids such as liquids, semisolids or gases is their viscosity. To understand the behaviour of the fluids and to force them according to the needs in the reservoirs, it is essential to know their rheological relationship.

The definition of viscosity according to the Webster dictionary is the property of resistance to flow in a fluid or semifluid[14]. Furthermore viscosity is defined as:

the ratio of the tangential frictional force per unit area to the velocity gradient perpendicular to the direction of flow of a liquid [14].

The internal friction of a fluid is called viscosity. Friction occurs when a fluid layer is moved in relation to another layer. The greater the force to initiate this movement, which is called shear, the greater is the friction. Any movement of a fluid e.g.: spraying, pouring, flowing is connected to a shearing. Therefore, high viscous fluids require more force or shear to move than less viscous fluids. The figure below, Fig. 15, shows the schematic definition according to Isaac Newton, where two parallel planes of fluid with the same size and the distance dx are moving in the same direction with a different velocities, v_1 and v_2.

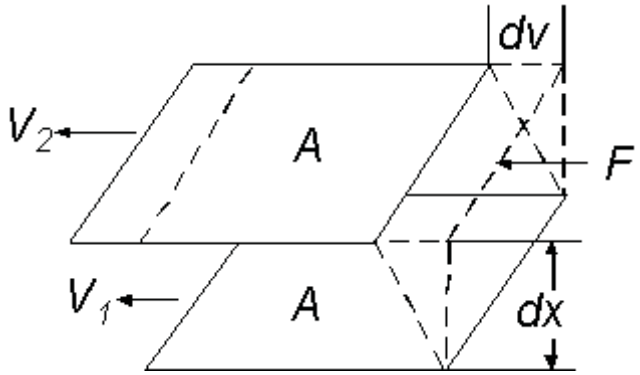

Figure 15: Schematic picture of two planes moving in the same direction for shear rate calculation

The force to maintain the difference in speed was proportional to the velocity gradient. The change in speed at which the intermediate layers move in respect to each other is the velocity gradient. It is a measurement of shearing on the liquid and is called shear rate. Below it is be symbolized as S and its unit is the reciprocal second (sec^{-1}). The second force is the shear stress, F´, which is defined by Eq.3 and has the unit of dynes per square centimetre ($dynes/cm^2$)

$$F' = \frac{F}{A}$$

After defining these two forces, viscosity, μ, can by defined as the ratio between shear stress and shear rate see Eq. 4

$$\mu = \frac{F'}{S}$$

The fundamental unit of viscosity measurement is the *poise*. A material requiring a shear stress of one dyne per square centimetre to produce a shear rate of one reciprocal second has a viscosity of one poise, or 100 centipoises. Newton assumed that all materials have, at a given temperature, a viscosity that is independent of the shear rate. In other words, twice the force would move the fluid twice as fast.

According to the rheological behaviour the fluids can be divided into two major groups of fluids: a) Newtonian fluids, b) Non-Newtonian fluids

Newtonian Fluids

The characteristic graphical representation below in Fig. 16 shows the linear relationship between shear stress and shear rate of a Newtonian fluid. The second graph shows that there is no change in viscosity by changing the shear rate. The majority of the fluids belong to the more complex Non-Newtonian fluids, but typically Newtonian fluids are water or thin motor oil.

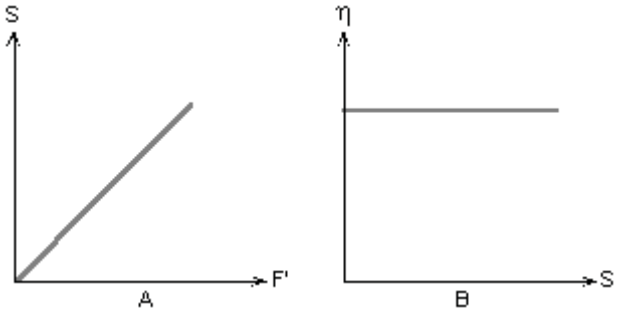

Figure 16: Characteristic rheological behaviour of Newtonian fluids[15]

Non-Newtonian Fluids

A common definition of Non-Newtonian fluids is that the relationship between F´/S is not a constant. By changing the shear rate the shear stress will not vary in the same portion or even in the same direction. Therefore, viscosity will also change with increasing or decreasing shear rate. Viscosity measured that way is also called apparent viscosity.

Among the Non-Newtonian fluids there are several other groups of fluids which are characterized by the way of changing their viscosity but for the purpose of this work only the pseudoplastic and dilatants fluids are mentioned.

Pseudoplastic Fluids

This type of fluid will display a decreasing viscosity with an increasing shear rate, as shown in Figure 17. Probably the most common of the non-Newtonian pseudo-plastics fluids include paints, emulsions, and dispersions of many types. This type of flow behaviour is sometimes called shear-thinning.

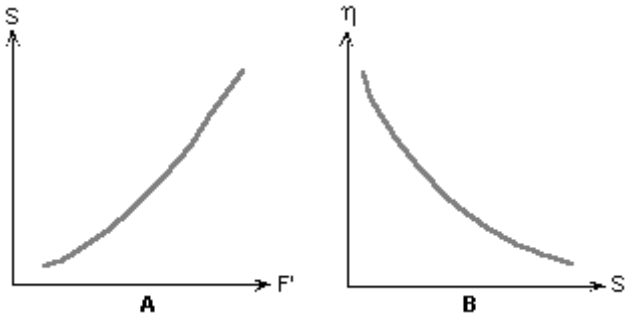

Figure 17: Shear rate determines viscosity in pseudoplastic fluids [15]

Dilatant

Increasing viscosity with an increase in shear rate characterizes the dilatant fluid; see Figure 18. Although rarer than pseudo plasticity, dilatancy is frequently observed in fluids containing high levels of deflocculated solids, such as clay slurries, candy compounds, corn starch in water, and sand/water mixtures. Dilatancy is also referred to as shear-thickening flow behaviour [15].

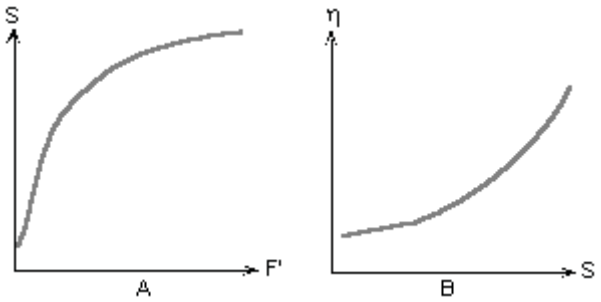

Figure 18: Shear thicking viscosity graphs [15]

The previous chapters were presented to get a better overview of polymer flooding and to understand the physical properties of polymer solutions. The following part will deal with the experimental apparatus and procedure in more detail.

Experimental Apparatus

This chapter will list up all equipment used for the experiment and for gathering the supporting data. The equipment consists of two parts: the injection system and the data gathering system.

Injection System

Two main parts build up the injection system:
1. Syringe pump (only for pumping water)
2. Vessels for gas (CO2), water, brine, polymer, oil

Syringe Pump

The syringe pump is a Teledyne Isco Model 100 DM (Fig. 19). The capacity of the pump is 103 mL. The pump was only used to pump water. To avoid any damage of the pump by pumping other fluids like brine or oil the vessel system is used.
The limit set up for the experiments are the following:

- The minimum flow rate: 0.0001 mL/min
- The maximum flow rate: 25.0 mL/min
- The minimum pressure: 10 psi
- The maximum pressure: 60 psi

Vessel

Vessels were equipped with a gauge at the top or bottom to control the fluid flow. To fill up a vessel, it was connected with one end to the vacuum pump and with the other end to the fluid which was sucked in. In Fig. 20 the vessel system for a brine injection can be seen. Vessels were fixed to a holder in the vertical direction before the start of an experiment.

To connect vessels with the pump and to the micromodel, a 1/16" plastic tubing was used. The advantage of plastic tubings is that with a visual control, bubbles in the flowing system can be noticed early enough and in case of an eventual failure action can be taken.

Figure 19: Teledyne Isco Model 100 DM syringe pump

Figure 20: Vessel system with decane and brine for water

Data Gathering Equipment

Microscope

A Nikon Eclipse ME 600 (Fig. 22) with a metal halide lamp is used for this study. An adapter mounted on the microscope allows the surveillance of the pore spaces via a camera. Both videos and pictures are taken through this adapter. Three different magnifications were used to observe the micromodel: 40X, 100X and 200X. Optical properties of these lenses can be seen in Tab. 1.

Magnification	Working Distance (mm)	Aperture	Viewable Diameter(µm)
4X	17.1	13	5500
10X	16.0	0.3	2200
40X	7.4	0.45	1100

Table 1: Optical properties of microscope lenses [16]

Camera

A Nikon Coolpix P5100 is used to collect pictures at micro and meso scale. High magnification micro images are taken with support of the microscope, whereas meso scale photographs are taken with a diffusion box.

Viscometer:

A digital Brookfield DV-II-Pro+© viscometer, Fig 21, was used for the viscosity measurements of oil and polymer solution. Calibration of the viscometer was done by using Brookfield calibration fluids of 10 cp and 100cp. The measurements were done with a spindle adapter. The viscometer allows a measurement range from 0.1cp to 10000 cP. Additionally a water bath can be used to measure fluids at a specific temperature.

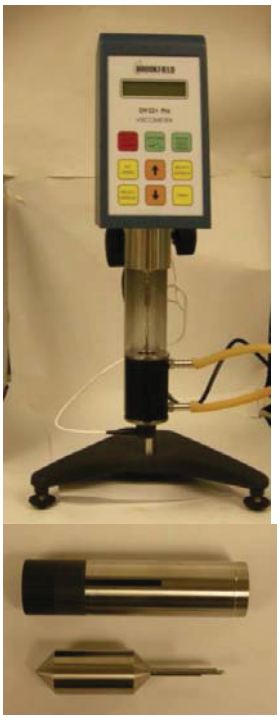

Figure 21: Brookfield viscometer with example beaker and spindle for measurements

Figure 22: Nikkon Eclipse microscope

Micromodel

Early micromodel experiments simply used capillary tubes with different diameters and lengths to study the miscibility or displacing process of different fluids or phases. Those models where followed by Hell Shaw models which consist of two glass plates with a narrow space in between to allow fluid flow. Later on this space was filled with glass beads in order to build a kind of artificial porosity and permeability. They were simple models and could not count for real rock and pore geometries or properties.

"Micromodels can be used to study the flow behaviour on a pore scale. They are patterns of a porous medium etched on a silicon or glass surface and hence are representative of the two dimensional structure of the porous medium. Micromodels have been extensively used to study the flow behaviour in multiphase flow, oil-foam interaction studies, solution gas drive, contaminant hydrogeology, etc. The patterns used in the construction of the porous medium may be prepared from thin sections of the porous medium to actually represent the medium or in several cases are geometrically constructed as series of repeatable simple or complex geometric figure aggregates. However as the micromodels represent a two dimensional porous medium, flow problem, extrapolation of results to the three dimensional flow problem occurring in the real porous medium needs to be done with certain amount of caution. It has also been observed that a non uniform etch depth in the micromodels may lead to snap-off situations not consistently predictable with the flow behaviour (Rossen, 1999). Another constraint of the micromodels regarding dimensionality is the lower macroscopic connectivity and co-ordination number (Nguyen, et al., 2000). Though both etched glass and silicon micromodels have been used, glass micromodels because of the nature of their fabrications have pores whose sizes are several times larger than the actual size." [17]

A brief summary of the use of micromodels for various applications is listed below.

The first etched-glass micromodel was developed by Mattex and Kyte. Straight interconnected flow channels built up the network. It was a very good approach to observe and visualize flow behaviour. [18]

A further development of the micromodel was achieved by Davis and Jones[19]. They worked on the drawbacks and limitations of the micromodel and came up with a new fabrication technique. A photosensitive fluid, which was resistant to several solvents after beeing exposing to ultraviolet light, was coated on glass. Hence, they were able

to produce more complex pore structures, which met the requirements for more realistic experiments.

In 1987 Owete and Brigham [20] used silicon-wafer micromodels for further development. Their special material characteristics allowed a better control of the etching process and therefore also the etching depth. With this new technique a more detailed and complex artificial pore network was etched in the micromodel. Because the silicon wafer is initially not water wet, they also worked on a technique to coat the surface of the silicon wafer with a thin dioxide film to create water wet conditions. The etched flow channels in the micromodel were sealed with a pyrex glass by an anodic bonding process to allow visual observation. Drilled inlet and outlet ports at the corners of the micromodel allowed the fluid communication.

Hornbrook [21] produced the first micromodels, which were almost identical to original Berea sandstone. Geometrical and topological properties as well as wettability and pore roughness were close to an original core sample. Micromodel pore structure was based on a thin section of a Berea sandstone. With a scanning electron microscope a high resolution photograph was taken and digitally processed. The drawback of this technique is that the SEM captures only a very little portion of the thin section. Hence the edges of the photograph had to be processed to loop this unit cell image together and to provide connectivity between the edges to fill a 5cm x 5 cm area.

In 1996 Keller [22] used the micromodel to observe the flow behaviour of three phases. The pressure limitations allowed not more than 35 psi. Exceeding this limit led to a material failure and to an abortion of the experiment. For higher pressures special experimental equipment had to be used.

Campbell and Orr [24] performed the first high pressure experiments for the displacement of oil by CO_2. To handle these elevated pressures the micromodel was housed in a pressure vessel[23] .
A more detailed description of high pressure micromodel applications can be found in the work of Gorge (1999). [17]

In this study the micromodel structure and design is almost identical to Berea sandstone in terms of pore geometry and topology.

Micromodel Fabrication

A simple micromodel holder for low pressure systems was used, fabricated from aluminium for the experiments in this case. Basically the micromodel represents a two dimensional network of a porous medium on a silicon wafer. First attempts used etched glass wafers to provide the artificial pore structure, but because of the limitations and disadvantages reported above, glass wafers were replaced by silicon wafers involving the visualization of the flow behaviour on pore scale.

A scanning electron microscope (SEM) image of a reservoir rock thin section acts as the basis of a typical micromodel, see Fig 23. However such a pattern needs some digital modification at the edges to ensure continuity in the porous medium. The pattern etched on the micromodels for these experiments was taken from a random hand drawn pattern, which represents the two dimensional structure of the porous medium. The grains of this pattern are range from 50 to 100 µm. Small and large pores, channels and very narrow throats build up the artificial network in the unit cell and made it similar to a real reservoir rock.

Figure 24 represents the unit cell which was repeated several times to fill up an area with the dimensions of 5cm x 5cm. In Fig. 25 the looped unit cell is presented.

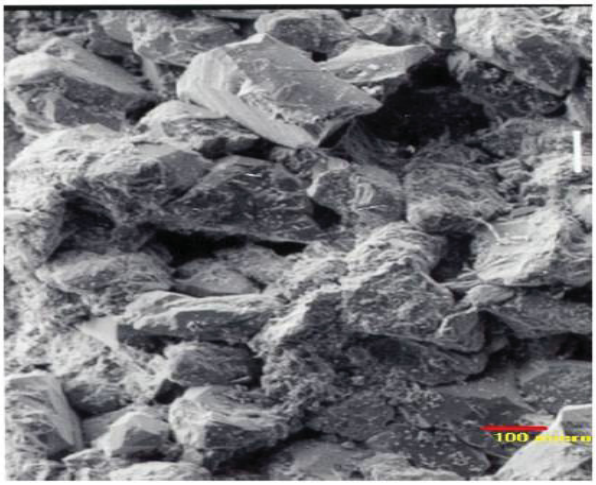

Figure 23: SEM image of a thin section of a Berea Sandstone [25]

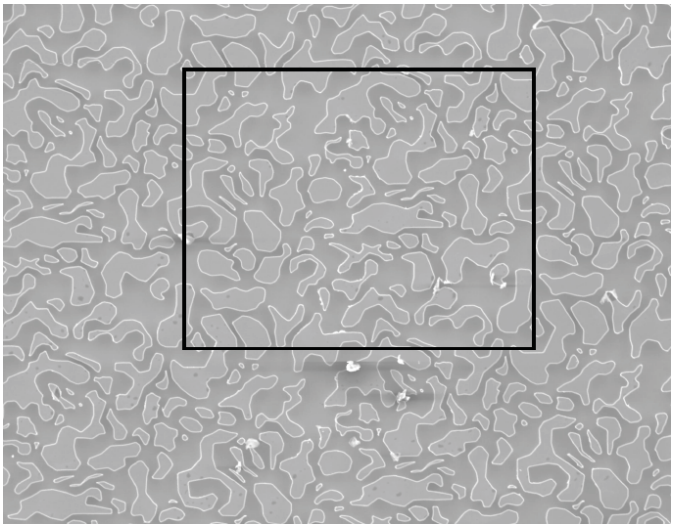

Figure 24: Unit cell of the micromodel [17]

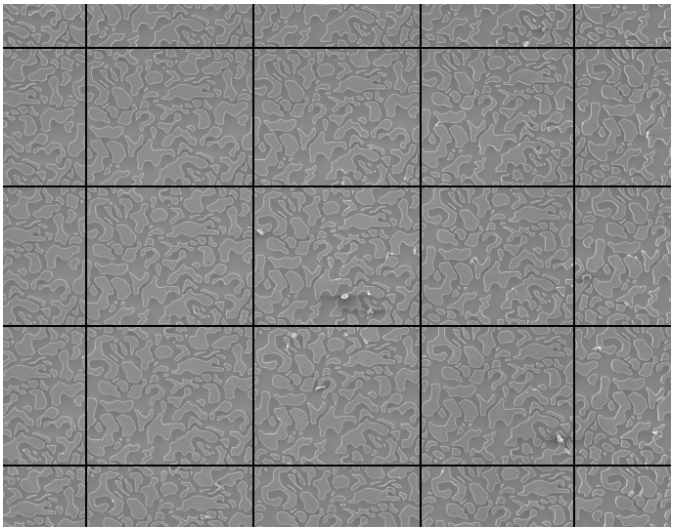

Figure 25: Repeating units of the micromodel[17]

To guarantee that the pattern is continuous, the edges had to be arranged, to sit together like a jigsaw puzzle. But the key features of the micromodel are the inlet and outlet channels or fractures and ports. They enable the displacement process to work in a linear way along the edges and not like a radial displacement which can be observed in a five spot pattern. A schema of the model with the features described above can be seen in Fig. 26

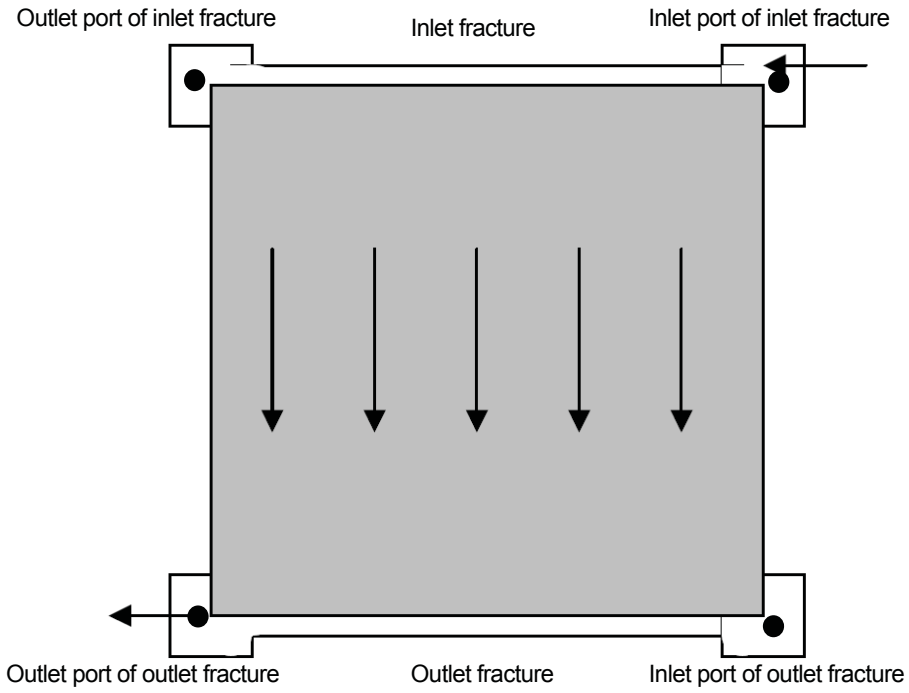

Figure 26: Schematic picture of the micromodel with inlet and outlet fracture and ports [17]

The construction of the micromodel incorporates several stages until it can be used for an experiment. The micromodels were produced at the Stanford Nanofabrication Facility (SNF). The SNF is a clean room facility for Micro Electronics Research Scientific, where structures up to a range and resolution of 5 Angstrom can be etched. Each of these models had to run the same procedure and should be a replica of the basic lithography mask image model. Micromodels cannot be bought, they have to be produced manually. As the production of these high-tech models was a major part in the experiments and works, it is mentioned in more detail in the following chapter.

As reported above, a 2D etched network forms the basis of the micromodel and represents the porous medium. To seal those silicon channels, another plate with the same size and with transparent characteristics is added on the top. The transparency of this top plate enables the visual observation through a microscope or an attached camera and gives the required high resolution micro scale pictures of the pore scale displacement.
Once the thin section of a Berea sandstone is taken and the structure put on a chrome mask, also called lithography mask, the manufacturing process for micromodels can start as listed below:

Imaging : A photosensitive chemical is sprayed on the silicon wafer, which is then exposed to ultraviolet light through the mask on top. After exposing the photoresist is selectively removed during the developing step.

Etching: The developed wafer is then etched with hydrofluoric acid to produce a micromodel with an etch depth of around 25-30 µm on the silicon wafer.

Cleaning and Bonding: The silicon wafer with the etched pattern is first cleaned in a sulphuric acid cleaning and then bonded to a glass plate to create a flow medium.

The schematic of the steps described above can be seen in Fig. 27

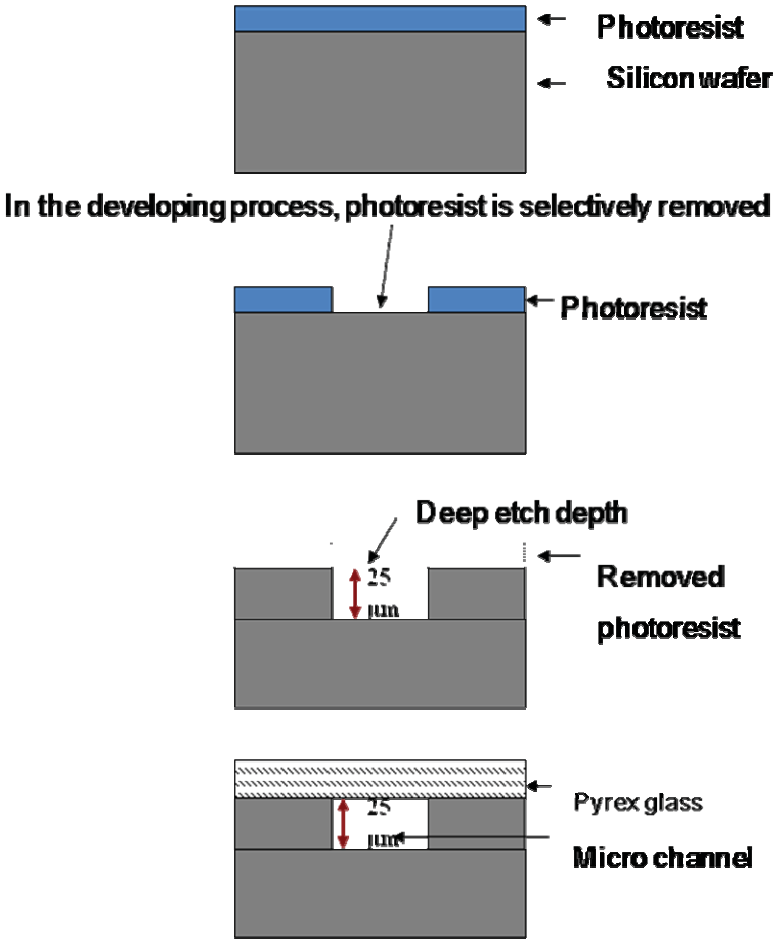

Figure 27: Micromodel fabrication: a) Coating with photoresist; b) Exposing and developing; c) Etching; d) Bonding

The next chapter will describe the above steps in more detail and show where precautions have to be taken in order to produce a perfect micromodel.

Micromodel Pattern Preparation

The structure of the repeated unit cell is a handmade drawn pattern and incorporates the entire feature of a real reservoir rock with comparable dimensions. The software, L-EDIT is required to do the preparation of the pattern, which is available at the SNF lab. A file which is compatible and needed for the mask-making machine is produced. The major tasks, which have to be done when preparing the mask with the software are:

- Design of the repeatable unit cell having the features of the porous medium
- Design of the inlet and outlet ports and channels of the entire micromodel assembly.

To enable the communication with fluids through the micromodel, inlet and outlet ports are required. These ports can be seen in Fig. 26 and are in the middle of the squared boxes at the four corners of the micromodel. For polymer or water floods, all four ports are necessary to clean the inlet fracture in order to achieve a linear displacement. When the software work is done, the pattern can be reproduced on a glass chrome plate, which is called mask. The mask making is not done in SNF since it is very complicated. Only one mask is required and can be used to produce thousands of micromodels. Fig. 28 shows the mask used to produce the pore pattern for these experiments.

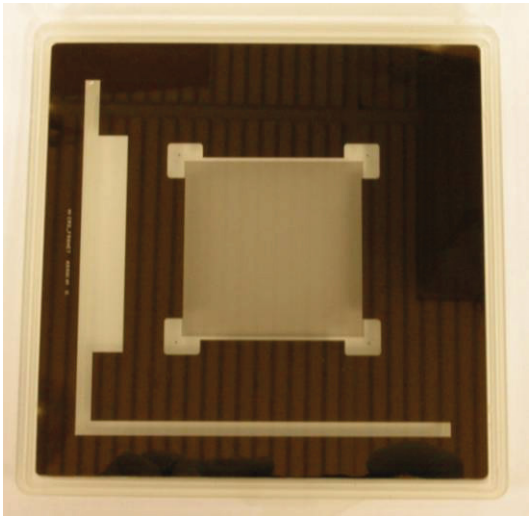

Figure 28: Lithography mask, coated with chrome

Wafer Imaging

There are a lot of manufactures selling silicon wafers which differ in surface roughness size, resistivity and price. For manufacturing the micromodels a doubled polished silicon wafer of the type K-Test is used. Starting the processing of the micromodel, the wafer is coated with a 2 µm thick layer of Shipley 3612 photoresist (Fig. 27 a), without edgebead removal (edgebead removal is the process in which a small ring of photoresist is removed around the wafer).

It is of crucial importance that the wafers are not wet and do not contain any moisture on the surface before being coated with the photoresist. New wafers which are sealed in a box, can be directly processed and coated. If the sealing of a box is already broken and the wafers are old or have been exposed to air, they need to be baked in a singe oven at a temperature of 150°C for 20 minutes before being coated with photoresist. When using the sing oven a special cartridge is required, this has a very high thermal resistance and is made of Teflon to prevent melting.

Once the coating process is over the wafers should be exposed to ultra violet light within 2 to 3 hours to guarantee the best possible result. The coating, exposing and developing steps are all done in a special yellow light area in the SNF lab. Any other light would destroy the characteristics of the photoresist. So at no time during these processes the wafer has to be taken out of this area. The mask used in the process of exposing the wafer to the ultraviolet light needs to be cleaned every time before use, to prevent exposing dirt marks and dust particles. The cleaning is done at a wet bench in the following strict order: acetone, methanol and isopropanol.

A final wash with de-ionized water and N_2 jet makes the lithography mask ready to be used. While exposing the resist coated wafer to ultraviolet light, it is important to make sure that the mask and the wafer are aligned, to prevent the pattern from being off centre on the wafer. During this process parts of the wafers which represent the pore channels of the micromodel at the end, are hit by the ultraviolet light. At this part the photoresist is getting unstable. Areas which are protected by the chrome of the mask do not have any contact to ultraviolet light and stay stable. An exposure of 3 to 4 seconds to the ultraviolet light is sufficient to make the photoresist unstable. During the

developing step, which is a chemical wash, the unstable parts of the photoresist are selectively removed (Fig. 27 b)

Wafer Etching and Finishing

The developed wafers are taken out of the yellow light area and can be further processed in the SNF lab. The etching process utilizes hydrofluoric acid gases to etch a depth of approximately 25 µm ± 3 µm.
In the figure below (Fig. 29) a SEM image of a the etched pattern can be seen.

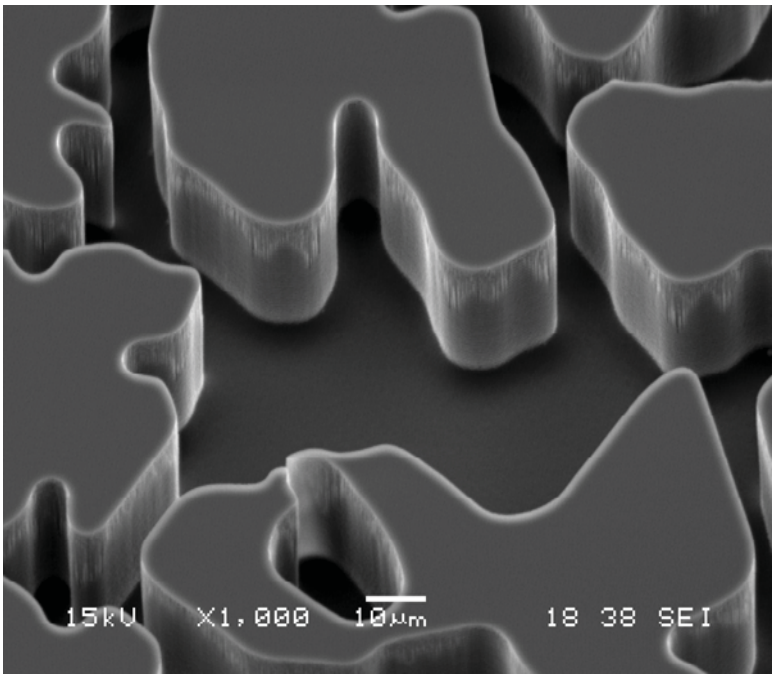

Figure 29: SEM image of etched micromodel. Pore diameters between 10 µm -150 µm [25]

After the etching the wafers have to be cleaned in a sulphuric acid/ hydrogen peroxide piranha solution (9:1 H_2SO_4:H_2O_2) to remove any residual photoresist or precipitation product from the etching process.

The drilling of the four holes which later allows the communication of the fluids with the micromodel is made at a different lab. After drilling the wafers are taken back to the SNF where a 15 min intensive cleaning procedure with a sulphuric acid/ hydrogen peroxide, piranha solution, (9:1 H_2SO_4:H_2O_2) removes any residual moister. The last

step is done outside the SNF where the wafer is heated on a hot plate at 700°F for 30 minutes.

This is done to oxidize the silicon to form a thin film of silicon dioxide on the surface. As a consequence the surface gets water wet. As a final step the wafer is bonded with an anodic bonding to a glass plate to complete the flow system. During the bonding a wire gauze with a weight is placed on the top of the silicon wafer and a potential of 1000 volts is applied for 1 hour. The elevated temperature causes the sodium ions on the glass plate to move and to attract the negative electrode on the glass surface, where they are neutralized to form a bond. Pyrex is used because of its similar thermal expansion coefficient to silicon: pyrex: 3.25 x 10-6 / °C; silicon: 2.56 x 10-6 /°C. Figure 30 shows a bonded micromodel ready to use.

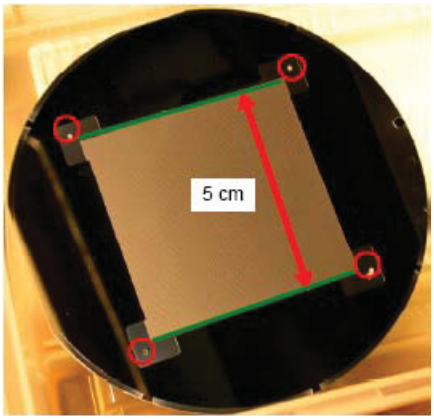

Figure 30: Bonded micromodel [16]

Micromodel Holder

The micromodel is placed in a holder which has conduits connected to the plumbing of the setup as shown in Fig. 33. This holder is fabricated from aluminium and consists of two inlet and two outlet ports, which communicate with the micromodel at the drilled holes. The ports are sealed with viton O-rings, Fig. 34. These rings need replacement after a few runs. Figure 31 shows a schema of the micromodel holder

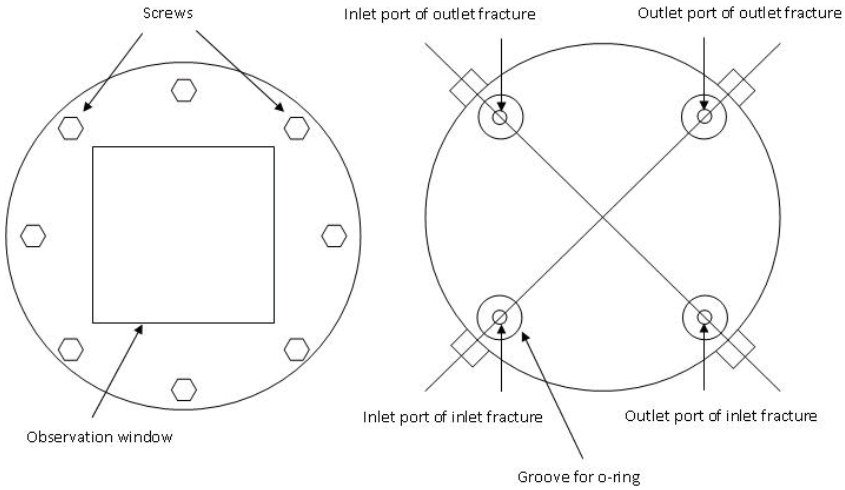

Figure 31: Micromodel holder sketch

Figure 32: Micromodel with O-rings graving

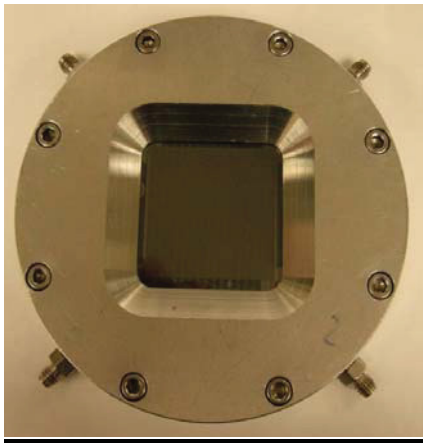

Figure 33: Micromodel holder with fixed micromodel

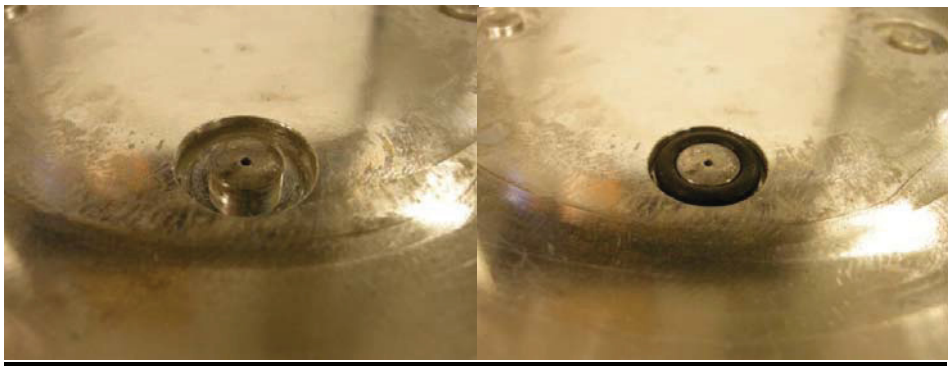

Figure 34: O-ring graving without and with o-ring

Experimental Procedure

The aim of the experimental procedure and preparation was to have exactly the same or at least very similar initial conditions for every experiment. Therefore, each experiment had the same workflow:

- Clean micromodel holder and micromodel
- Saturate micromodel with brine (calculate permeability)
- Saturate micromodel with oil (take pictures to determine S_{wi})
- Dismantle the micromodel holder and clean holder as well as micromodel. Reassemble holder and micromodel
- Start the flood with polymer solution or brine and take meso scale pictures during the flood and micro scale pictures after breakthrough and after 22 hours

This section of the thesis will report the specific work steps of the experiment

Clean Micromodel Holder and Micromodel

The cleaning of the micromodel holder is the first step of an experiment. When pumping polymer solution through the micromodel, small polymer precipitations form at the inlet ports of the holder. These small particles can get loose during the next experiment when saturating with water or oil and cause a plugging of the pores, which would result in changed initial conditions. By using a vacuum pump, toluene, isopropyl alcohol (IPA) and water the four entry ports of the holder and the o-rings can be freed from oil and polymer solution.
During the first water flood experiments, the micromodel could be cleaned and reused for the next experiment. Because of the irreducible plugging of the pores, the micromodels could not be cleaned when using a polymer solution. When cleaning micromodels, the following procedure is used.

"*Flush with isopropanol (IPA) to remove some residual oil and flush with IPA at constant pressure (P=50psi). In this set-up water pushes IPA into the micromodel/micromodel holder assembly. Once IPA begins to flow out of the outlet*

port of the inlet fracture, cap this port. Continue to pump IPA for 1mL, or until there is only immobile oil in the micromodel.

Pump with toluene to remove the remaining residual oil: Pump toluene into the micromodel at pressure <50psi; once toluene is noted at the outlet port of inlet fracture, cap this port. Continue pumping at P<50psi until micromodel appears to be clean. At this point, there should be no visible oil, or at the most a few immobile patches of residual oil.

Pump with carbon dioxide to remove the toluene: Disassemble micromodel holder. Use vacuum and heat lamp to remove and vaporize residual toluene in the holder. A heat lamp is positioned about 8 inches above the micromodel/micromodel holder assembly while CO_2 floods the micromodel at constant pressure. Carbon dioxide is pumped until toluene is removed. If streaky spots persist, check under microscope to ensure that there is no visible toluene in the micromodel; the streaks are due to toluene adhering to pore grain surface. If any residual oil remains in micromodel, repeat steps three and four as necessary.

Pump with IPA: Repeat step 2, except that the end point is achieved 1 mL after the micromodel is 100% saturated with IPA. Any streaks noted in step four should be removed by the IPA. The micromodel is clean and is ready to be fully saturated with water"[16]

Saturate Micromodel with Brine

After cleaning the micromodel or using a new one, it has to be saturated with brine. After oil saturation small amounts of brine stay in the model and act as the initial water saturation. In Fig. 35 the setup for this step is presented.

The water pump provides water through a 1/16 inch plastic tubing with a constant pressure of 40 psi into the bottom of a decan vessel. The lighter decan is forced out at the top of the vessel and flows into the top of the brine vessel. The heavier brine is pushed towards the vessel and goes from the bottom of the brine vessel into the inlet port of the micromodel inlet fracture. As soon as brine comes out of the outlet port of the inlet fracture, the outlet port is closed. About 5-10 ml of brine has to be flushed

before all CO_2 bubbles are gone. To make sure that no CO_2 is left in the micromodel, it has to be checked with the microscope. When increasing the pump pressure from 40 psi to 55 psi or 60psi trapped CO_2 is usually dissolved in the brine. Any CO_2, which cannot be removed during brine saturation will stay till the end of the experiment and can falsify results. In Fig. 36, CO_2 trapped in a brine saturated micromodel can be seen.

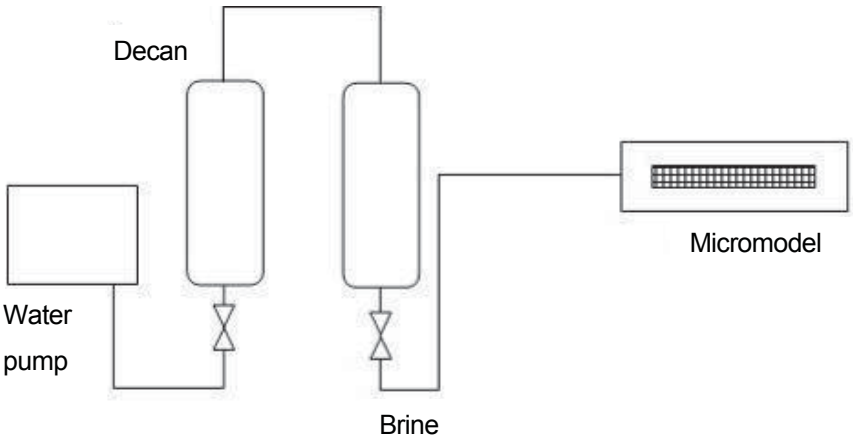

Figure 35: Experimental setup for brine saturation

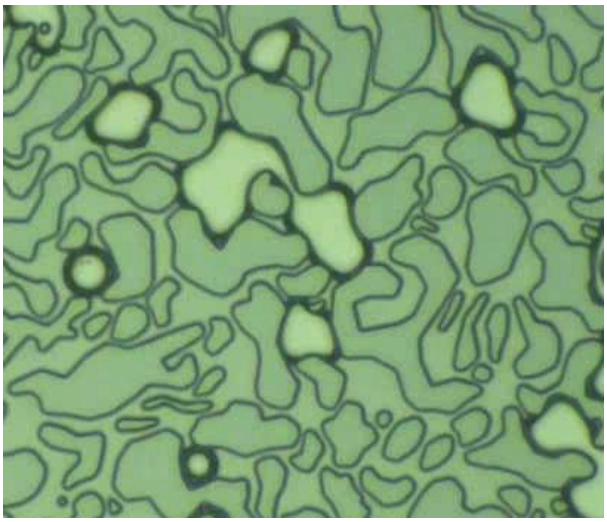

Figure 36: Brine saturated micromodel with trapped CO2 (white bubbles)

If the micromodel is 100% water saturated, the permeability can be measured like reported below.

Permeability Measurement

Permeability measurements before each experiment were part of the quality control and should ensure that the initial conditions for all experiments are the same. Because of discrepancies during the last experiments permeability measurements were performed in two different ways to have a quality check.

1. The micromodel is flooded with water with 4 different flow rates and pressures and their corresponding pressure drops and flow rates are measured. Permeability is calculated according to Darcy´s Law.

2. The micromodel is flooded with CO_2 at different pressures. With a bubble flow meter which is connected to the outlet of the micromodel flow rates are measured (Fig. 37) and the permeability can be calculated with Darcy´s Law.
The working principle of a bubble flowmeter is the following:
A soapy solution can be found at the bottom of the bubble flow meter. CO_2 from the micromodel frees single bubbles and forces them upwards the glass column.
The time that a bubble (CO_2) needs to flow from point x_1 to x_2 (see Fig. 37) is measured. The distance from x_1 to x_2 marks a defined volume of 1 cm³. With these data the flow rate can be calculated which is used for Darcy´s calculations.

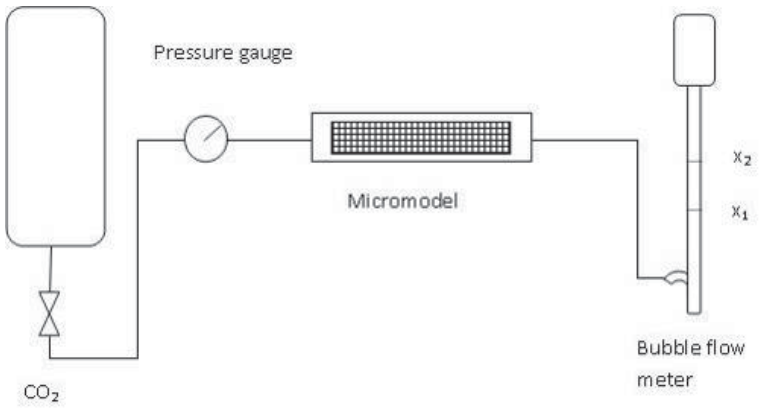

Figure 37: Schematic view of permeability measurement with a bubble flow meter

The three different results of a measurement are presented below: constant pressure (Tab.2), constant flow rate (Tab. 3) and bubble flow meter (Tab.4). In practice all the

measurements are averaged and a final average value out of three values is calculated. In the example below this would result in 918 md.

			INPUT					**OUTPUT**
P2 (psig)	P2 (atm)	P1 (atm)	Q (mL/min)	Q (mL/s)	Area (cm^2)	L (cm)	viscosity (cP)	k (darcy)
40	3.72	1.00	0.378	0.0063	0.0125	5	1.0	0.92
30	3.04	1.00	0.277	0.0046	0.0125	5	1.0	0.90
20	2.36	1.00	0.179	0.0029	0.0125	5	1.0	0.87
10	1.68	1.00	0.088	0.0014	0.0125	5	1.0	0.86
							average	0.89

Table 2: Permeability measurements with constant pressure

			INPUT					**OUTPUT**
P2 (psig)	P2 (atm)	P1 (atm) >	Q (mL/min)	Q (mL/s)	Area (cm^2)	L (cm)	viscosity (cP)	k (darcy)
37	3.52	1.00	0.35	0.0058	0.0125	5	1.0	0.92
32	3.18	1.00	0.3	0.005	0.0125	5	1.0	0.91
21	2.43	1.00	0.2	0.0033	0.0125	5	1.0	0.93
11	1.75	1.00	0.1	0.0016	0.0125	5	1.0	0.89
							average	0.91

Table 3: Permeability measurements with constant flow rate

	40 psi	**30 psi**	**20 psi**	**15 psi**	**10psi**
	time (sec)	time (sec)	time (sec)	time (sec)	time (sec)
1	0.81	1.25	2.4	3.65	6.13
2	0.85	1.3	2.38	3.64	6.06
3	0.87	1.27	2.44	3.66	6.22
4	0.88	1.31	2.47	3.66	6.15
5	0.84	1.24	2.44	3.62	6.1
					940 md

Table 4: Permeability measurement with bubble flow meter

Saturate Micromodel with Oil

After being saturated with water, the micromodel is ready to get oil saturated. For oil saturation, the same apparatus as in Fig. 38 is used. Water from the pump flows into the bottom of the oil vessel and pushes the oil towards the top of the vessel from where it goes through the tubing into the inlet port of the inlet fracture. The whole process is run with a constant pressure of 55 psi.

It is not required to cap the outlet port of the inlet fracture when oil is dropping out of the port, since the oil acts as a plug in the very narrow outlet port. The oil saturation is one of the critical parameters during an experiment. Final oil saturations can vary between 90-98% although no changes in pore structure or etching depth is observed or measured. Even extended oil saturation periods with abnormal high pump pressures do not increase the oil saturation for the micromodels with 90% saturation. Depending on the micromodel, connate water saturation was reached after 2 to 8 hours.

According to Fig. 41 saturation does not change a lot with time. Meso scale pictures often indicate a uniform and fully saturated micromodel, but by having a closer look at micro scale pictures, changes in oil saturation can be significant. Fig. 39 and Fig. 40 show two different pictures after eight hours of oil saturation.

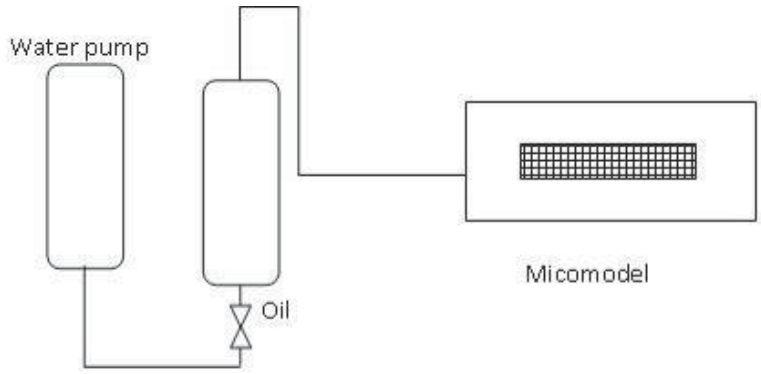

Figure 38: Setup for oil saturation with water pump and oil vessel

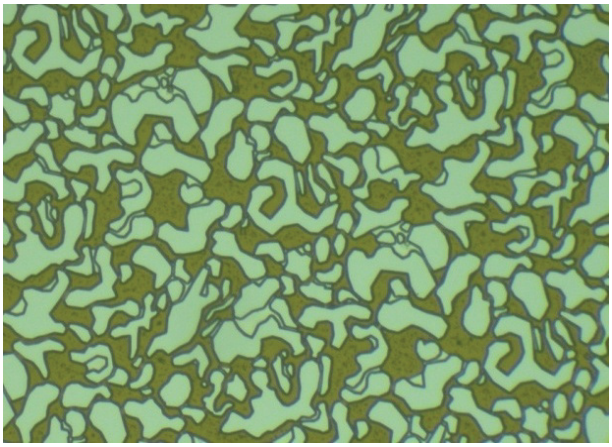

Figure 39: Well oil saturated micromodel (brown: oil; white: grains and water)

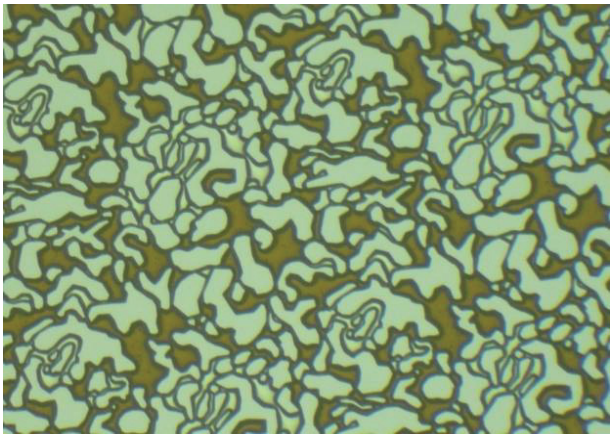

Figure 40: Poor oil saturated micromodel

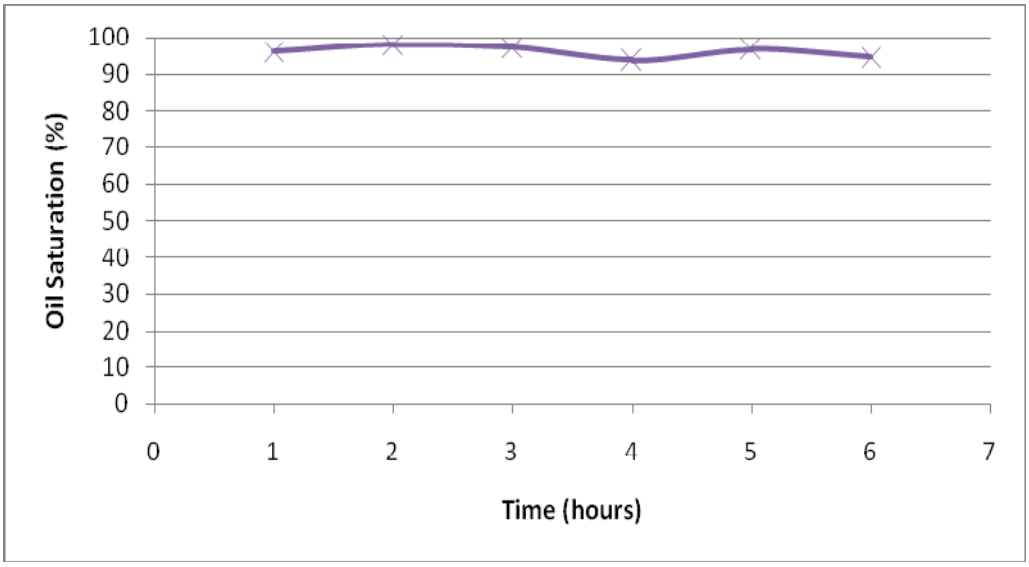

Figure 41: Oil saturation in relation to time

After checking the process on micro and meso scale, micro scale pictures are taken and initial water saturation S_{wi} can be calculated. In case of a not satisfying oil saturation, even after a long time, the model has to be cleaned and the process repeated. A typical sequence of meso scale pictures after periods of time can be seen below in Fig. 42. Picture a.) demonstrates oil entering the micromodel matrix and filling up the inlet fracture towards the end of the outlet port.

The saturation propagations follows a radial way as long as the fracture is not fully oil saturated. After the oil has reached the outlet port, saturation continues in a more linear way. In picture d.) the outlet fracture starts being saturated. The last photograph f) represents a perfect uniform oil saturated micomodel which is ready for a polymer flood. Fig. 43 represents a sequence of oil saturation at micro scale. In former experiments, a heat lamp was used to lower viscosity of the oil and to reach saturation faster. Because of several broken wafers, caused by thermal cracking during this process, the heat lamp was avoided for this series of experiments.

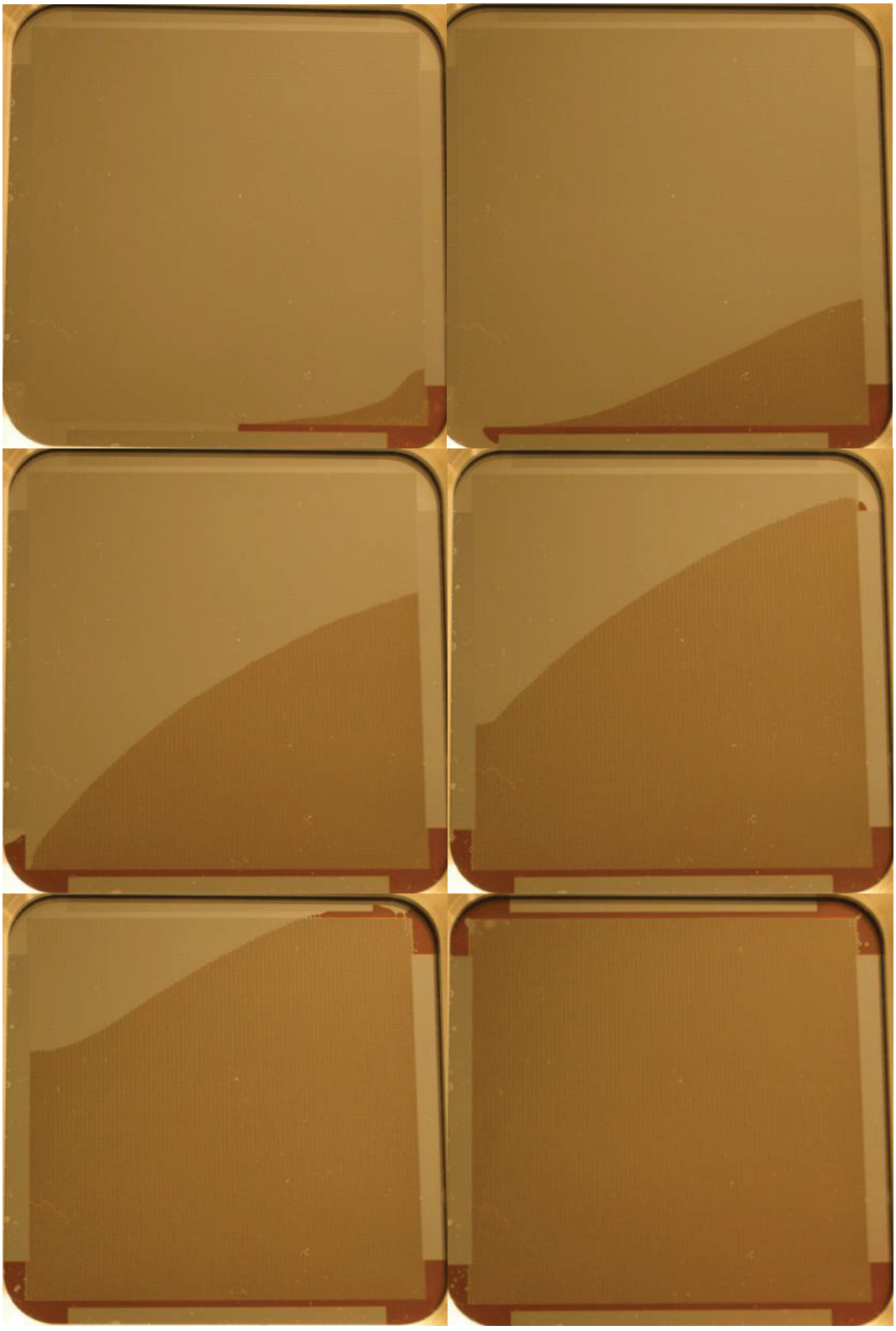

Figure 42: Meso scale oil saturation after time (from the left top to the right bottom: a,b,c,d,e,f)

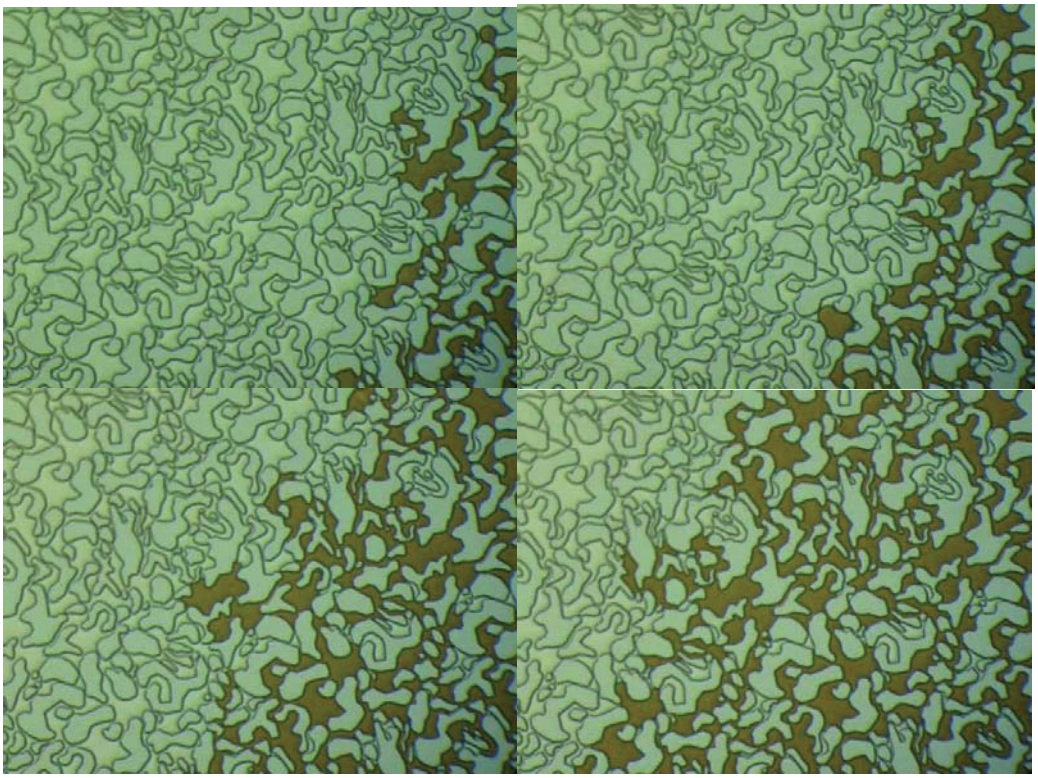

Figure 43: Micro scale oil saturation after time

Leaking O-rings at the inlet ports, trapped CO2 bubbles, which suddenly become free and get into micromodel during oil saturation and cracked wafers due to too high pressure are the main problems arising during saturation. The most frequent problem was the leaking at the O-rings. Therefore another micromodel holder, which had a better fit to the O-rings, was used for the later experiments. Below in Fig. 44 a leaking micromodel after oil saturation can be seen. As a result not the fully applied pressure could act on the micromodel and oil saturation was not appropriate.

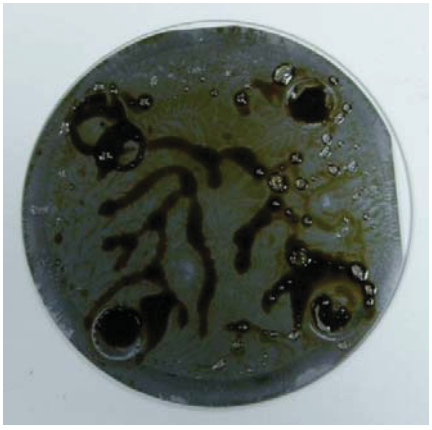

Figure 44: Micromodel reverse side after oil saturation with a leaking O-ring

Cleaning After Oil Saturation

The most critical part of the experiment is the start of the flood, where the inlet fracture has to be cleared in order to achieve linear displacement. In former times, the flooding fluid was directly connected after completing the oil saturation. As a result the cleaning of the inlet fracture of the oil took several hours and was insufficient for a perfect displacement most of the time. In other words, the displacing fluid started to get into the micromodel before the complete fracture was cleared and the outlet port at the inlet fracture capped.

Different cases of cleared fractures when capping the outlet port of the inlet fracture can be seen in Fig. 45. As a consequence the micromodel was taken apart after oil saturation since February 2008. Micromodel, micromodel holder, entry ports and the backside of the micromodel are cleaned with toluen and water and then re-assembled. To avoid any air bubbles between entry ports and micromodel, the micromodel entry ports are filled with water or polymer solution before re-assembling the holder. This procedure enabl a very fast and improved cleaning of the inlet fracture and guarante a better linear displacement.

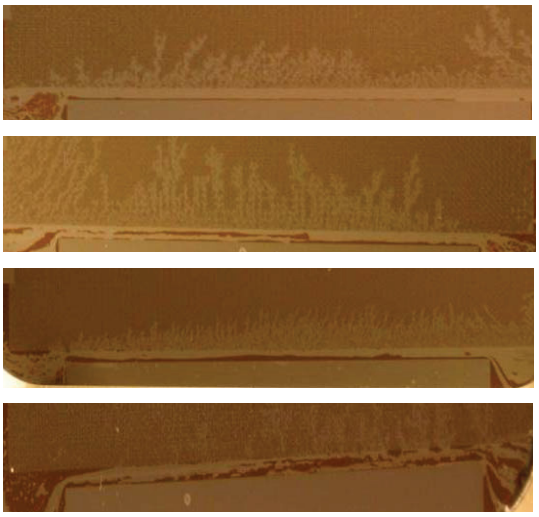

Figure 45: Inlet fractures from different experiments with different stages of clearness. From top to bottom decreasing clearness.

Starting the Flood

After the holder has been cleaned and re-assembled the displacing fluid (water, or polymer solution) can be connected to the oil saturated micromodel. The setup can be seen in Fig. 46. Water pushes the polymer solution towards the bottom of the vessel and enters the micromodel.

At the beginning of the flood the polymer solution is injected at a constant pressure of 10 psi to clean the fracture from oil. Once the fracture is free and the polymer solution is dropping out of the outlet of the inlet fracture the outlet port is capped. Then the pump is switched from a constant pressure to a constant flow rate of 0.0001 ml/min.

The micromodel is put into the diffusion box for meso scale pictures to be taken. Once the polymer solution reaches the outlet fracture the micromodel is placed under the microscope where micro scale pictures are taken. Then, the flood is continued for 22 hours which represent 10 pore volumes. After that period, micro scale pictures are taken to determine the ultimate recovery. A typical series of pictures at the front of a polymer displacement can be seen in Fig. 47.

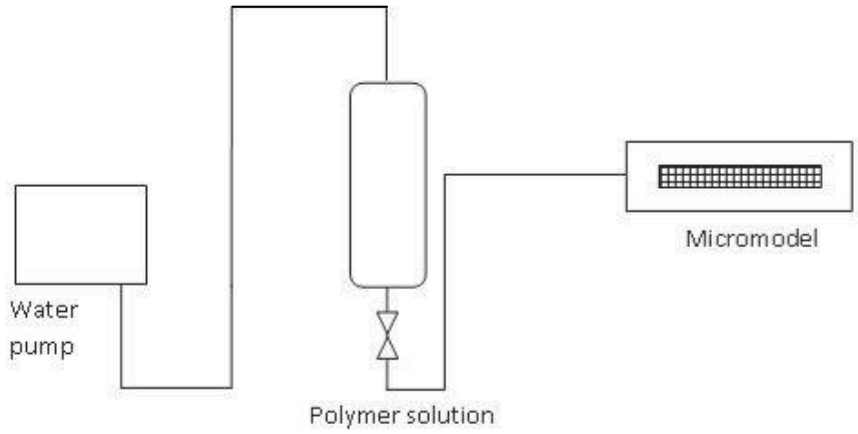

Figure 46: Polymer flooding set up with water pump and polymer vessel

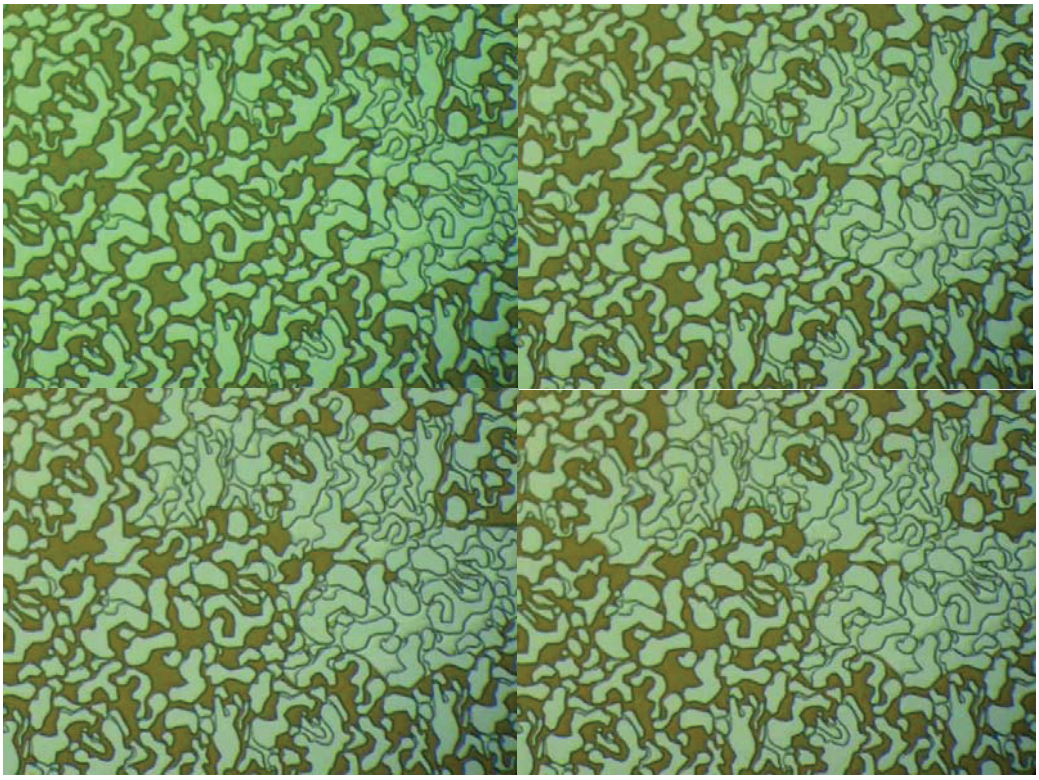

Figure 47: Micro scale pictures at the displacing front after different time intervals (5 sec: 10 sec; 15sec; 20 sec)

Image Analysis

Results of recovery and swept area are necessary to evaluate the experimental success. A major drawback of the micromodel is the missing possibility to perform any material balance.

Inlet ports and O-ring cravings occupy 10 times greater volume than the micromodel matrix. This huge dead volume is a serious problem in measuring the volume of the displacing or displaced phases. Additionally, the amount of liquid used for a whole experiment is so small that it does not reach the outlet port of the outlet fracture and therefore it cannot even be collected for measurement. Several other attempts to reach a material balance with weighting and using finer injection ports were not successful.

So, as a consequence, 25 high resolution photographs of the pore structure in the micromodel are taken to determine irreducible water saturation (S_{wi}), water saturation at breakthrough (S_{btp}) and residual oil saturation (S_{or}). To make sure that the whole area of the model is captured the micromodel is subdivided into 25 equally sized rectangles, Fig 48. At specific times, one single photograph of each rectangle is taken. These moments are first after oil saturation to determine S_{wi}, secondly after breakthrough of the polymer solution at the outlet fraction to determine the S_{btp}, and finally, after 22 hours which refers to 10 swept pore volumes of the micromodel to determine S_{or}. The pictures are taken with a Nikon Coolpix P5100 and with a Nikon Eclipse ME 600

.

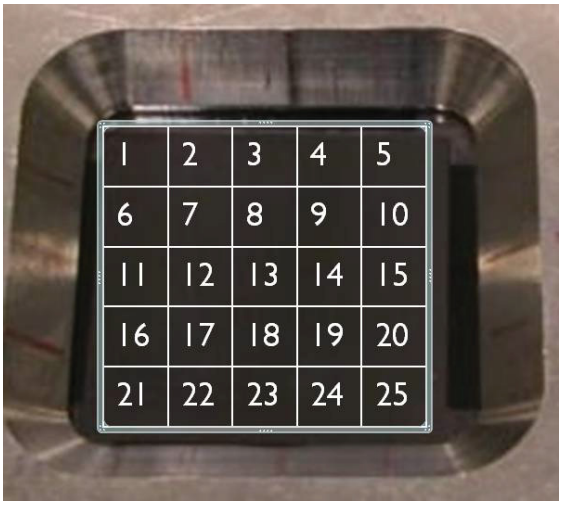

Figure 48: Micromodel grid for taking micro scale photographs

Figure 49 represents a photograph of a micromodel at S_{wi} at a 10X magnification, which is ready for a polymer flood at this point. These photographs are manipulated and analysed digitally in MATLAB or G.I.M.P. to calculate the saturations mentioned before. This post experimental procedure is imprecise due to the shadow of the pore grain/space interface, and therefore yields relative saturation values.

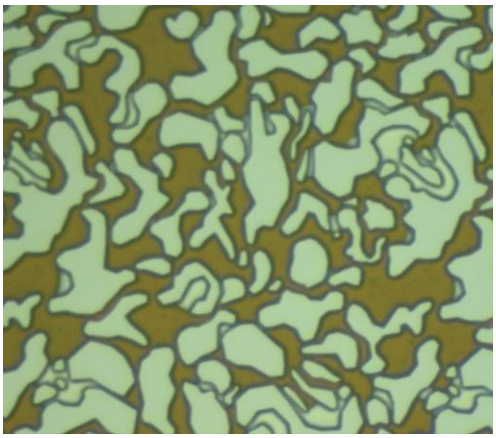

Figure 49: Saturated micromodel ready for a polymer flood

Image Analyse in G.I.M.P.

The very first experiments were post processed with the photostudio program G.I.M.P. To obtain values for saturation, the colour histograms for each single picture had to be analysed. In Fig. 50, the RGB histogram of the picture above is shown.

The three humps represent the three different colours, brown for the oil, black for the grain edges and white for water, polymer solution and grains. The further processing of the pictures required a manually determination of the threshold values. In other words to define a limit, at which everything more colour intensive or brighter is white and everything less intensive or darker is black. As shown in Fig. 51, the blue area marks the parts which are white after processing.

As a result of this threshold procedure, a black and white picture is obtained. In this picture the black and white pixels are counted automatically and give the saturation values.

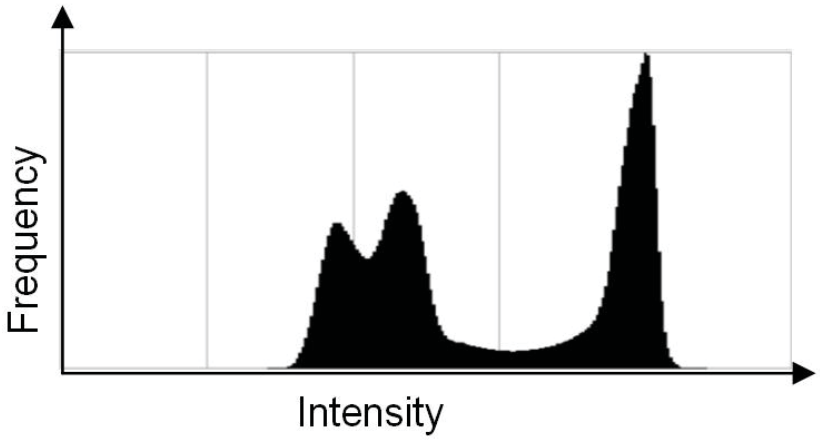

Figure 50: Typical micromodel histogram of a micro scale picture. Three humps represent oil, polymer or water saturation, grain edges and grains from the left to the right

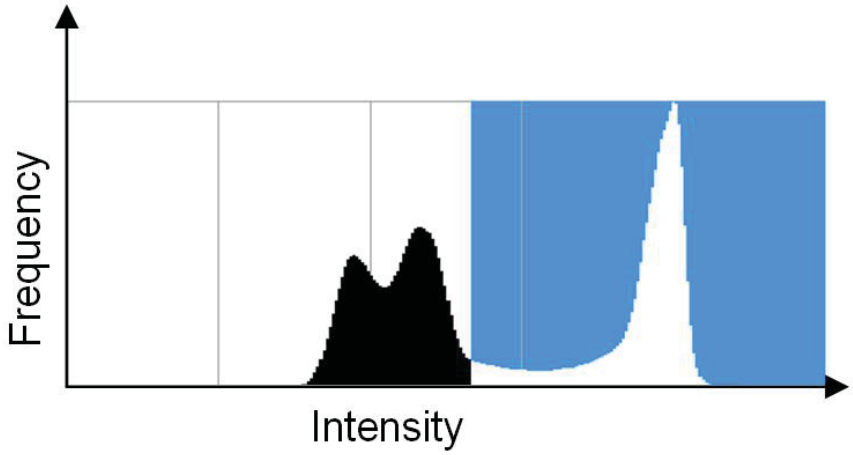

Figure 51: Histogram with threshold limit (blue area)

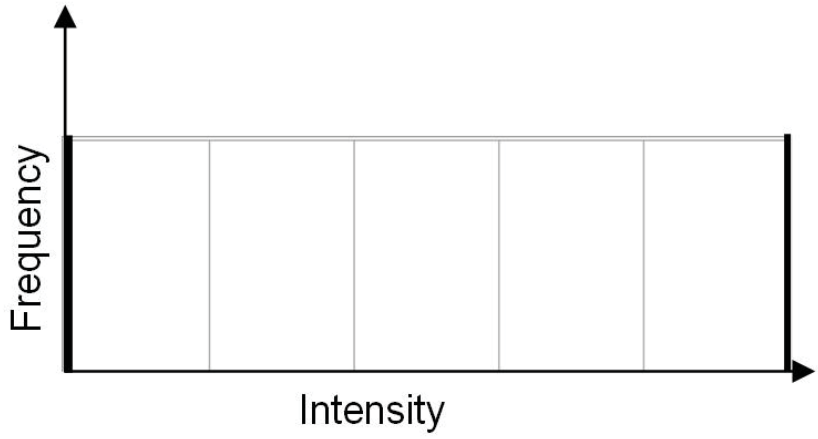

Figure 52: Histogram after setting a threshold value and converting into a binary picture. The bars at the beginning and the end of the diagram represent the frequency of black and white.

Figure 53: Processed binary image of Figure 49

The problem of this procedure was that it was not possible to automize the procedure. Therefore every single threshold value had to be defined manually which in fact is not very precise either. So, another method was found to make the image analyses in a more precise and faster way.

Image Analysis in MATLAB

The primary hindrance in accurately calculating the saturation values is that a significant minority of the pore space is obscured by the shadow cast, by the pore grains and the shadow at the oil-water interfaces. Figure 54 shows an unetched micromodel, meaning that the wafer was only exposed and the photoresist was selectively removed. Whereas Fig. 55 presents an etched (to 25 μm) and bonded model. When comparing the two pictures a lack of a gap between the grains is obvious. In the etched wafer, the grains appear to be touching each other and seem to be closer together. This shadow makes it impossible to determine which fluid occupies this space when calculating saturations. As a consequence, only the space which can be seen is considered as pore space for the image analyses. About 20-30 % of the pore volume is lost because of these shadows.

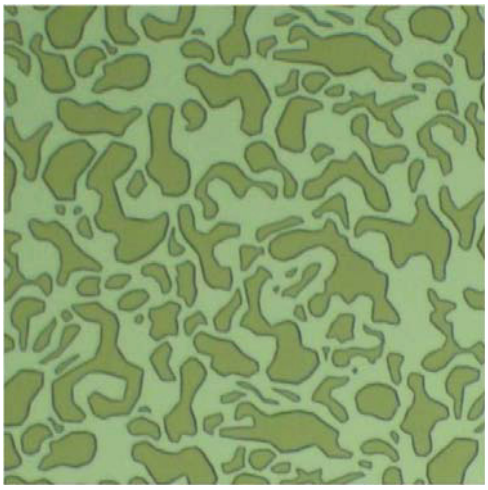

Figure 54: Only coated and exposed micromodel (not etched)

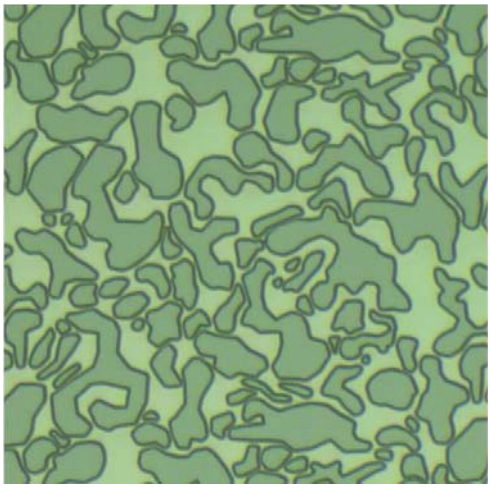

Figure 55: Etched empty micromodel

A 100% water saturated micromodel can be seen in Fig.56 and Fig. 57 before and after being processed with image software. The black lines cover about 25% of the total picture and contribute to 26% of the pore space. When having a closer look at Fig. 58, it can be seen that the lines are getting thicker towards the edges of the photograph. The developed MATLAB routine (Appendix A) automatically crops and removes the portion of the image which is unevenly illuminated. This distorting effect is caused by the adapter which is not 100 % centred adapter. The RGB (red, green, blue) colour ranges for oil in the photographs are determined by manually sampling the values for oil in a few of the 25 pore scale photographs. During the further processing, MATLAB converts the colour images to binary images, which black represents oil and grain shadows and white indicates grains, water and polymer solution. The RGB vales have to re-sampled a couple of times in order to obtain a very precious binary image which captures all the visible oil and the pore edges. Once the range is determined MATLAB counts all the black and white pixels. The pore shadow which has been determined as 26 % as an average value for all pictures is subtracted to get the oil saturation.

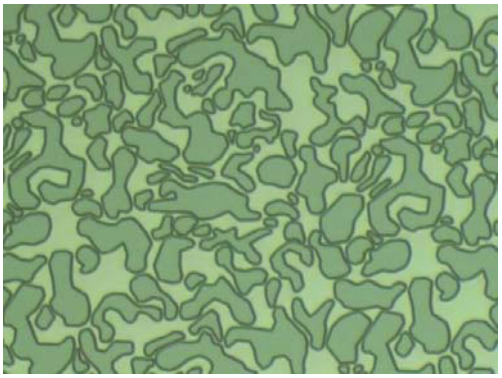

Figure 56: 100% water saturated micromodel

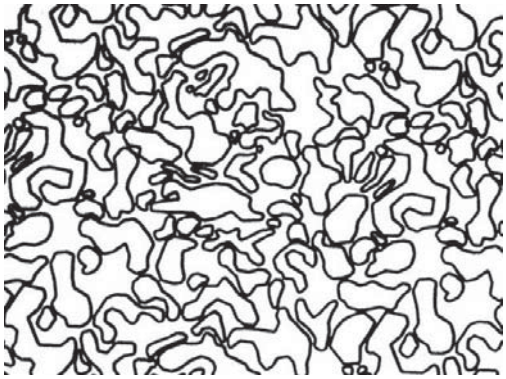

Figure 57: Pore edges after digital processing

Sensitivity Analysis of RGB Values

To understand the sensitivity of the processed pictures on RGB values, a series of tests was done with changing RGBs. RGB values were adjusted individually and in succession on a series of initial water saturated photographs. Table 5 shows the range in which the pictures change their oil saturation according to different RGB values. In Fig. 58 and Fig. 59, the base case and the case with the most significant change in oil saturation can be seen. The maximum change in black pixels was 0.76 % which corresponds to a change in oil saturation of 3.43%.

Although the photographs look at first sight similar the changes in oil saturation can be very delicate and therefore easily lead to misassumptions. The conclusion is that the best RGB range can be found when comparing the pictures of the processed images in the same experiment. As a rule of thumb, visual inspection shows deviations in the scale of ±4 %. So by changing RGB values, similar looking pictures are obtained, but with a variability up to almost 3.5 %. Varying the RGB values more than done during the sensitivity study, leads to different appearance and percentage change bigger than 3.5%.

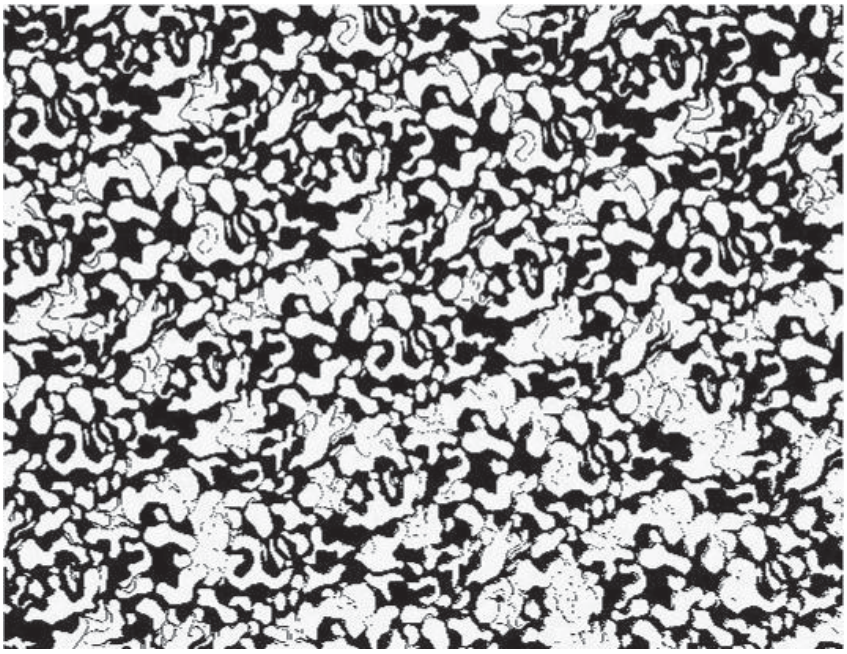

Figure 58: Modified binary image from the base case

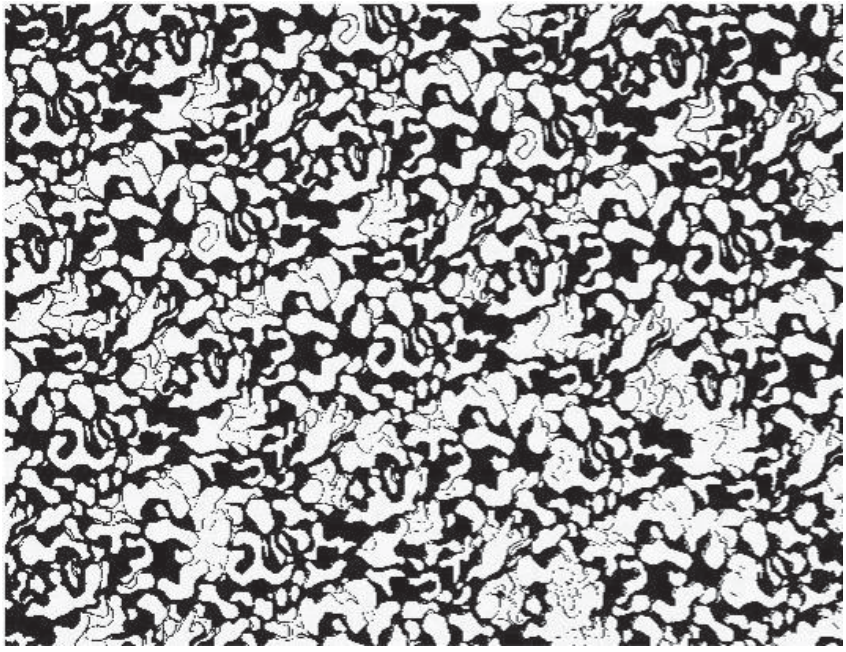

Figure 59: Modified picture with the largest deviation from the base case

	Base	Case1		Case 2		Case 3		Case 4		Case 5		Case 6	
	R>79	R>82		R>76		R>79		R>79		R>79		R>79	
	G>108	G>108		G>108		G>111		G>105		G>108		G>108	
Picnr.	B>80	B>80	diff	B>80	diff	B>80	diff	B>80	diff	B>83	diff	B>77	diff
1	22.51	23.03	0.52	22.11	0.40	23.14	0.63	21.85	0.66	23.13	0.62	21.92	0.59
2	21.97	22.48	0.51	21.58	0.39	22.54	0.56	21.41	0.56	22.54	0.57	21.45	0.52
3	23.47	23.86	0.40	23.17	0.29	24.04	0.58	22.87	0.59	23.98	0.52	22.98	0.49
4	22.22	22.60	0.38	21.95	0.27	22.83	0.60	21.58	0.64	22.72	0.49	21.77	0.45
5	22.13	22.43	0.30	21.92	0.21	22.73	0.60	21.48	0.65	22.59	0.46	21.72	0.41
6	20.83	21.11	0.28	20.65	0.18	21.51	0.67	20.08	0.76	21.28	0.45	20.43	0.41
7	22.55	22.97	0.41	22.26	0.29	23.15	0.60	21.93	0.62	23.11	0.56	22.03	0.52
8	21.97	22.36	0.39	21.71	0.26	22.68	0.71	21.23	0.74	22.54	0.56	21.44	0.54
9	22.78	23.14	0.36	22.52	0.26	23.35	0.58	22.17	0.61	23.29	0.51	22.30	0.47
10	23.57	23.89	0.32	23.33	0.24	24.02	0.44	23.12	0.46	24.04	0.47	23.16	0.41
11	21.94	22.29	0.35	21.71	0.24	22.64	0.69	21.22	0.73	22.45	0.51	21.46	0.48
12	23.14	23.47	0.33	22.91	0.23	23.75	0.61	22.51	0.63	23.66	0.52	22.65	0.49
13	22.66	22.90	0.25	22.49	0.17	23.26	0.61	22.00	0.66	23.13	0.47	22.21	0.44
14	22.05	22.37	0.32	21.82	0.23	22.58	0.53	21.48	0.57	22.51	0.46	21.64	0.41
15	19.52	19.89	0.37	19.27	0.24	20.19	0.67	18.83	0.68	20.08	0.57	19.00	0.52
16	20.98	21.39	0.41	20.70	0.29	21.56	0.58	20.40	0.58	21.53	0.55	20.48	0.50
17	20.73	21.01	0.28	20.56	0.18	21.39	0.65	20.06	0.67	21.32	0.58	20.19	0.54
18	22.74	23.04	0.30	22.54	0.20	23.30	0.56	22.16	0.58	23.34	0.60	22.19	0.55
19	22.43	22.71	0.28	22.25	0.18	23.05	0.61	21.79	0.65	23.01	0.58	21.90	0.54
20	21.72	22.03	0.30	21.53	0.20	22.38	0.66	21.06	0.67	22.32	0.60	21.16	0.56
21	20.93	21.23	0.30	20.75	0.19	21.59	0.65	20.27	0.66	21.55	0.61	20.39	0.54
22	20.15	20.45	0.31	19.94	0.20	20.79	0.64	19.48	0.67	20.77	0.63	19.58	0.57
23	20.33	20.64	0.31	20.12	0.21	20.95	0.62	19.68	0.65	20.87	0.54	19.84	0.49
24	21.41	21.65	0.25	21.25	0.16	22.03	0.63	20.74	0.67	21.98	0.57	20.88	0.52
25	21.94	22.22	0.28	21.76	0.19	22.46	0.52	21.41	0.53	22.52	0.57	21.42	0.52
Aver.	**21.87**	**22.21**	**0.34**	**21.63**	**0.24**	**22.48**	**0.61**	**21.23**	**0.63**	**22.41**	**0.54**	**21.37**	**0.50**
Max.			**0.52**		**0.40**		**0.71**		**0.76**		**0.63**		**0.59**
Oil %			**2.34**		**1.81**		**3.20**		**3.43**		**2.83**		**2.66**

Table 5: RGB-Sensitivity analysis

Meso Scale Image Analysis

As mentioned above during the flooding process, not only micro scale pictures are taken at certain intervals, but also meso scale pictures. Depending on the speed and progress of the flood, pictures are taken after every minute or three minutes till breakthrough. In former times, meso scale pictures suffered from reflections and bad picture qualities. Since a new diffusion box, which is illuminated from outside, is used, quality has improved significantly.

The setup for the meso scale pictures is shown in Fig. 60. These pictures show whether a polymer or water flood is stable or not and moreover the area swept at breakthrough can roughly be determined. The photograph at breakthrough time is manually processed. Swept areas are painted black and are further processed into a binary image in MATLAB to determine the percentage of swept area. Because the contrast between the swept and unswept areas is very subtile, the dying of the areas concerned cannot be done automatically. Figure 61 to Fig. 63 present the way from an unprocessed to a manually processed and to the final binary image.

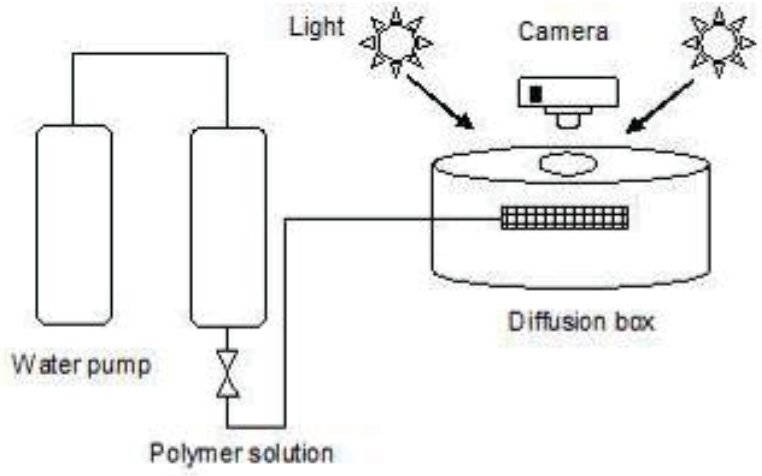

Figure 60: Polymer injection set up with camera, lights and diffusion box

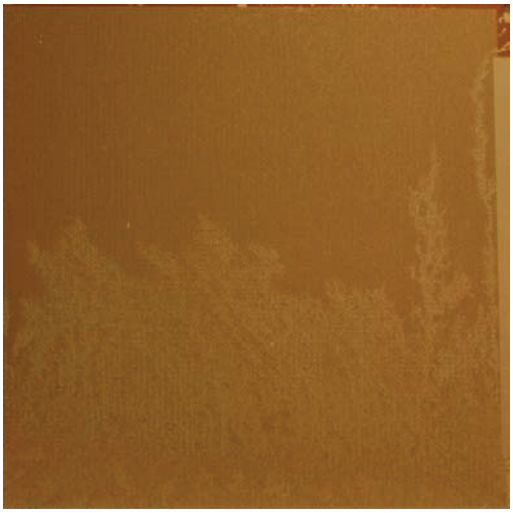

Figure 61: Unprocessed meso scale photo

Figure 62: Manually marked swept area (black)

Figure 63: Digitally converted binary image

Brine Mixing

Brine instead of fresh water was used for mixing the polymer solution to create realistic conditions. The brine composition was measured in the Hochleiten field in Austria. To prepare the brine, an OHAUS Explorer Pro scale and Thermoline stirrer are used. Both can be seen in Fig. 64 and Fig. 65. 1000 ml deionised water is filled in the beaker and stirred at a sufficient rate to create a strong vortex with a magnetic bone. Stepwise, each component was added to the water in small portions. Particles which could not be dissolved were removed with a 15 μm cartridge filter before filling up the brine vessel. The composition can be seen in Tab. 6

Figure 64: Ohaus digital scale

Figure 65: Stirrer with beaker and stirring bone

Name	Formula	g/1000 ml
Sodium Chloride	NaCl	19.75
Potassium Chloride	KCl	0.193
Calcium Chloride 2-Hydrate	$CaCl_2$-$2H_20$	0.6615
Magnesium Chloride 6-Hydrate	$MgCl_2$-$6H_20$	0.586
Sodium Sulfide 10-Hydrate	Na_2SO_4-$10H_2O$	0.015
Sodium Bicarbonat	$NaHCO_3$	0.92

Figure 66: Table 6: Chemical composition for brine mixing[26]

Polymer Mixing

The apparatus for the preparation of the polymer solution was the same as for the brine preparation process: mechanical stirrer, scale and a beaker. Careful preparation of the polymer solution should avoid precipitation and guarantee a perfect flooding fluid.

For each experiment different concentration and, therefore, different amounts of polymer were used. Two different types of polymer an associative polymer Superpusher 255 and a conventional polymer Flopaam 3630 S, Fig. 66, were prepared for solution.

Table 7 represents some technical details of the polymers according to the technical data sheet from SNF FLOEGER s.a.s.. For these experiments, brine was used to mix the solution but it is also possible to use deionised water. For an appropriate mixing, the stirrer has to be set up at a speed fast enough to build a very strong vortex, which is approximately 500-600 RPM. Then, the weighted polymer is added slowly by sprinkling it into the wall of the vortex. After 2-5 minutes of stirring, the RPMs are reduced to 300-400 RPM and with this rate the solution is stirred for 4 more hours. The mechanical stirrer also heats up the plate to improve the dissolution process. Most often, some particles do not dissolve and the solution is filtered with a cartridge filter with a mesh size of 15 μm Fig. 67 and Fig. 68. [27]

	FP 3630	**S 255**
Molecular weight	20 Million Dalton	8 Million Dalton
Temperature limit	85°C	71°C
Ionic character	Anionic	Anionic
Charge density	Medium	Medium
Mesh size	% > 10 mesh: 2	% > 10 mesh: 2
	% < 100 mesh: 6	% < 100 mesh: 6
approximate bulk density	0.67 kg/m³	0.8 kg/m³
Viscosity Measurements	@ 5.0 g/l 1800cp	@ 5.0 g/l 2000cp
	@ 2.5 g/l 700cp	@ 2.5 g/l 550cp
	@ 1.0 g/l 260cp	@ 1.0 g/l 190cp
Dissolution time	90 min	120 min
Stability of solution	1day	1day

Table 6: Technical dates for used polymers [27]

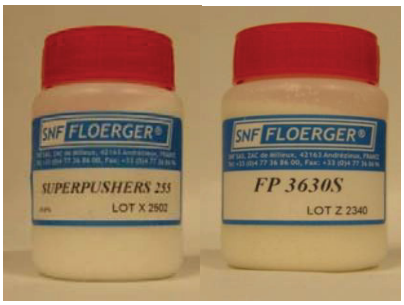

Figure 67: Polymer sample beakers

Figure 68: Cartridge filter with 15 microns average filter size

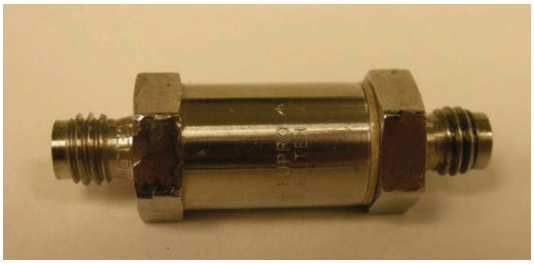

Figure 69: Cartridge filter holder

Viscosity Measurement Experiments

The polymer solution, as mentioned before, is a Non-Newtonian fluid. It changes its viscosity properties with changing shear rates. The reservoir consists of different areas, like near wellbore area, perforation zone or the outer reservoir. Those areas are characterized by different permeabilities, flow velocities and therefore also different shear rates.

The polymer solution reacts to these changing surroundings and also changes its viscosity. Each polymer solution was observed with a DV-II-Pro+ Brookfield © viscometer to understand the change of viscosity with increasing or decreasing shear rate with regard to direction and magnitude. All the measurements were done at constant room temperature (22.2°C) to have the same conditions as during the experiment.

The only drawback was that this viscometer was only able to measure viscosities down to shear rates of 2 sec^{-1} and the micromodel used for the experiments has shear rates two orders smaller than that in the range of 0.09 sec^{-1}. So the measurements performed in the lab cover only a small range of the possible shear rates. More accurate data would have been obtained by a cone plate viscometer or a rheometer.

In addition to the measurements done at Stanford University, accurate data from the Alberta Research Council for the associative polymer S255 were available, see Fig. 71. Figure 69 and Fig. 70 below show the behaviour of viscosity versus shear rate for the associative polymer solution Superpusher 255 (S255) and the conventional Flopam 3630 S (FP3630).

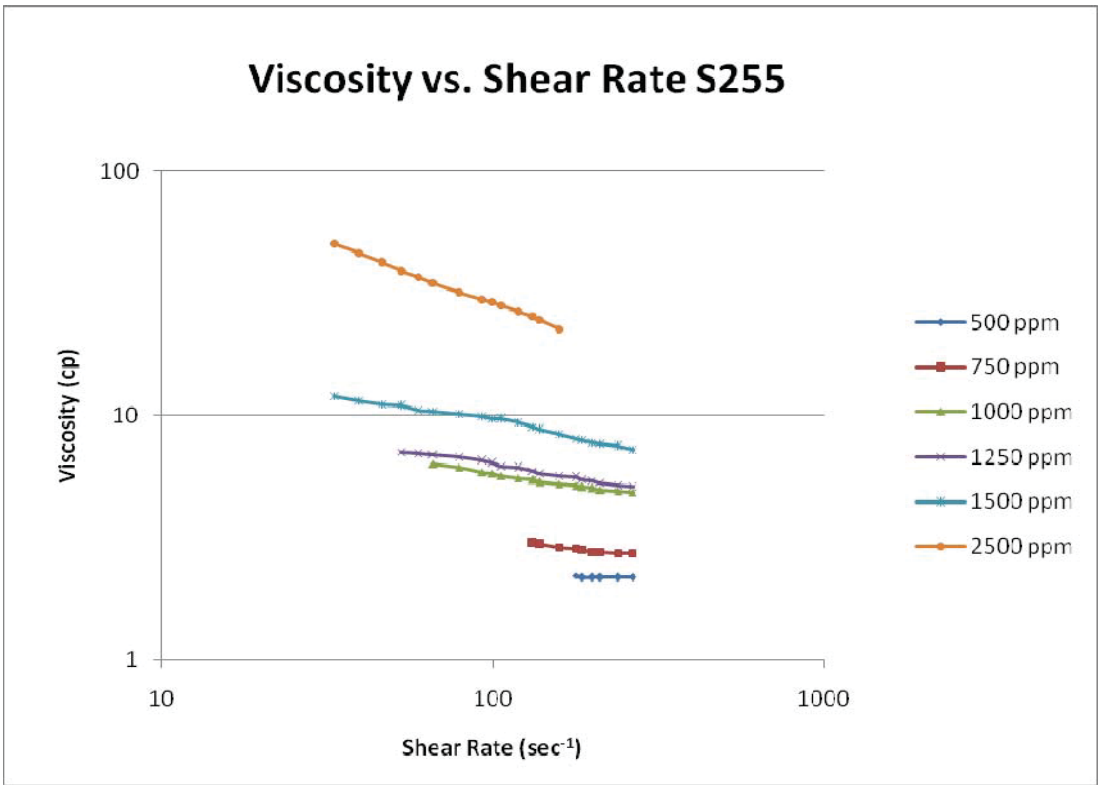

Figure 70: Associative polymer solution viscosity measurement

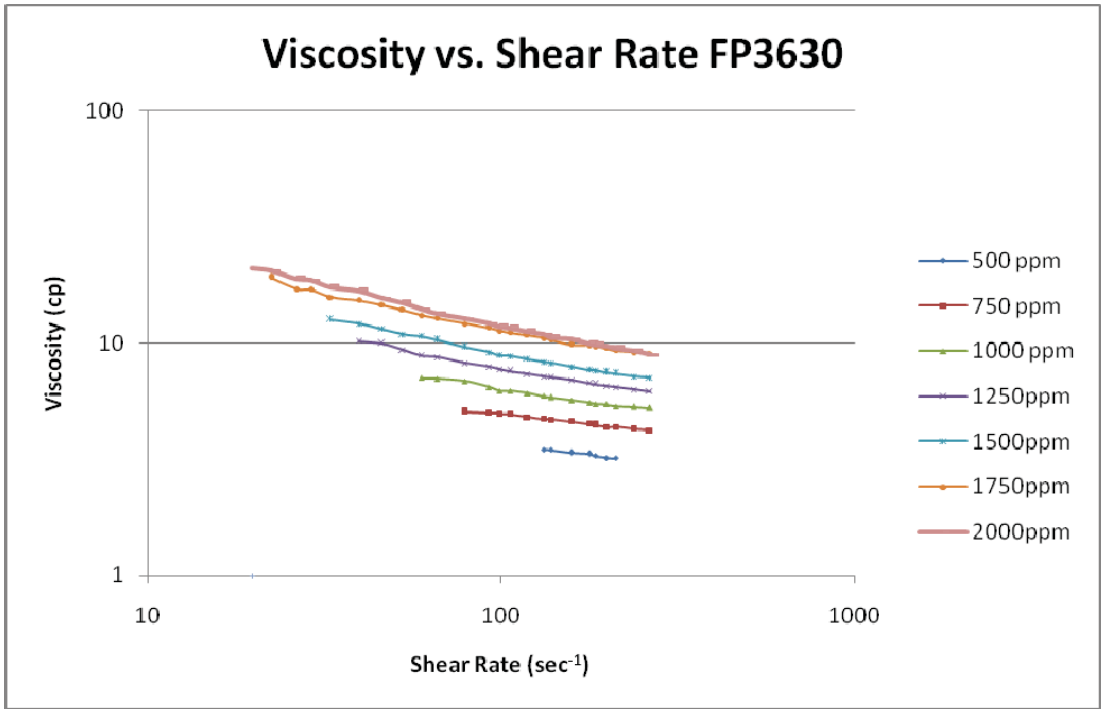

Figure 71: Conventional polymer solution viscosity measurement

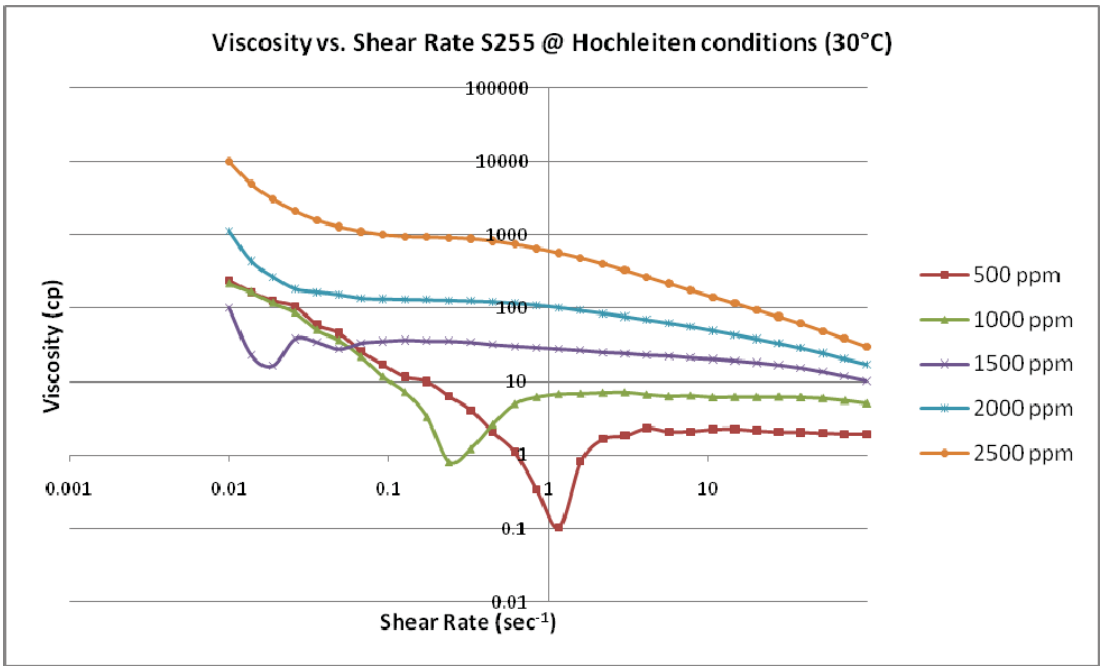

Figure 72: Viscosity measurements for associative polymer solution from Alberta research council [26]

The figures above prove that the polymer solution has lower viscosities at higher shear rates and higher viscosities at lower shear rates. In the near wellbore case with lower permeabilities and higher flow rates and, therefore, also higher shear rates viscosity is lower. This is positive because injection pressure therefore is lower as well. An important effect of the polymer solution is the reversible behaviour, which means after being exposed to very high shear rates the polymer is not destroyed and keeps its characteristics.

In other words, later in its lifetime when flow velocities are very low, e.g. between injector and producers, and shear rates are low, viscosity will increase and contribute to a better mobility ratio. To prove that the polymer solution does not change its thinning and thickening characteristics the solution was flooded through a cartridge filter with a pore diameter of 4μm at very high flow rates, which leads to very high shear rates. The polymer solution was measured before and after the filter in order to see any alteration or damage of the polymer solution. As can be seen in Fig.72 the solution did not change seriously after the filtration.

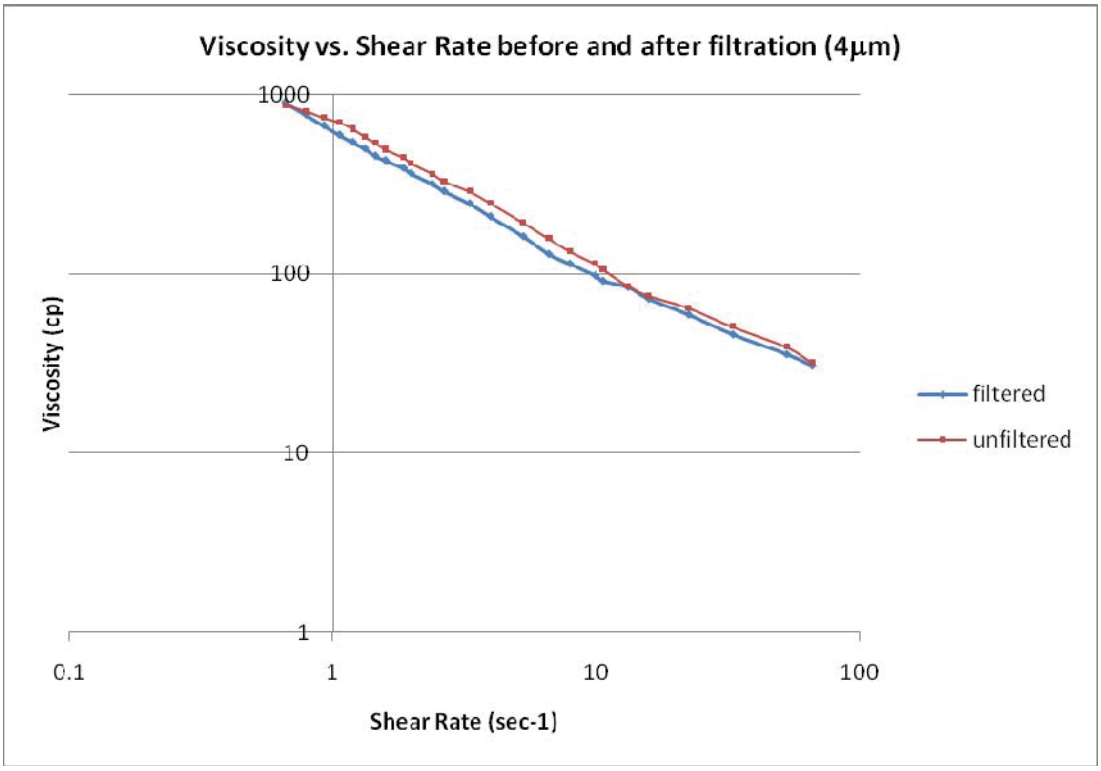

Figure 73: Viscosity measurement before and after filtering with a cartridge filter

Shear Rate Experiment

Understanding the rheological behaviour of the polymer is essential in order to estimate and observe the displacement process during a polymer solution flood. As mentioned in the chapter above, polymers are Non-Newtonian fluids and therefore have changing properties with different shear rates. The property which is most important in reservoir applications is viscosity with respect to shear rate. Viscosities determine whether an experiment will have a high tendency for a stable or unstable displacement depending on the mobility ratio. In order to get an idea of the magnitude of shear rate in the micromodel, the following experiment was conducted:

- Flood MM with water to determine absolute permeability (Darcy´s Law)
- Flood with polymer and wait till MM is completely saturated with polymer solution
- Measure pressure drop at a constant rate
- Calculate apparent viscosity from polymer solution (Darcy´s Law)
- Determine shear rate with values from Table 9

For this experiment, an associative polymer solution, S255 with 2500 ppm, was used. Taking the measurements at the right time was the only problem for this experiment. It will be reported in one of the following chapters that the polymers tend to plug the pores and therefore reduce permeability significantly. Since it is impossible to determine whether pores are plugged or free, the measurement was taken when pressure drop first stabilized. Values obtained from the measurement and calculations can be seen below in Tab. 8:

Time (min)	4	20	40	56	70	90	101	120
Pressure(psi)	8	7	7	6	6	6	6	6

Table 7: Pressure recordings during polymer flooding in a water saturated micromodel

q(ml/min)	1.6667E-06
k (md)	1770
A (cm²)	0.0125
dl (cm)	5
dp (psi)	6

Table 8: Input data for viscosity calculation

$$\mu = -\frac{k}{q} A \frac{dp}{dl}$$

μ =1089 cp

With the value calculated above, a shear rate of 0.09 sec^{-1} can be read up from Fig. 71.

In addition to the experiment above, several empirical formulations exist to calculate the shear rate at an apparent fluid viscosity. One of these formulations are from Hirasaki and Pope in Eq. 5 [11]

$$\gamma = \left(\frac{1 + 3n_{pl}}{n_{pl}}\right) \frac{u}{\sqrt{8 k_i \phi_i}}$$

With u, the superficial velocity, which is the volumetric flow rate divided by the macroscopic cross sectional area normal to the flow, k_i is the aqueous phase permeability, which is the product of absolute permeability and the relative phase permeability and the aqueous phase porosity ϕ_l ,defined as $S_i\phi_l$. n_{pl} is defined as the power law coefficient or exponent and for shear thinning fluids it is in the range of $0 < n_{pl} < 1$. As n_{pl} is not defined for the used polymer solution in this experiment, three different values for n_{pl} were assumed, 0.9, 0.5, 0.1. Values used for calculations can be seen in Tab. 10, results in Tab.11

n_{pl}	0.9; 0.5; 0.1
q (cm^3/min)	0.0001
v (cm/sec)	$1.33\ 10^{-4}$
A (cm^2)	0.0125
ϕ	0.46
S_i	1
k (m^2)	$1.78\ 10^{-11}$
k_{ri}	1

Table 9: Input data for shear rate calculation

n_{pl}	γ (sec^{-1})
0.9	67.5
0.5	82.1
0.1	213.62

Table 10: Results for different fluid coefficients, n_{pl}

The calculated values do not fit to the measured ones. Because several former experiments reported shear rate values in the order of the measured ones, they will be taken for further assumptions.

Relative Permeabilities

In most cases of EOR projects relative permeability curves and their associative parameters are the most relevant petro-physical parameters. Phase saturations, S_j, are the by far most influencing factors for the relative permeability curves, k_{rj}. Rock properties and wettabilities are also conditions influencing the functionality of the k_{rj} and S_j relation. Although it is a rock fluid property, fluid properties only contribute in some rare cases (e.g. interfacial tensions), in which drastically changes can alter relative permeability curves. Relative permeabilities can be used to determine mobilities, relative mobilities and phase permeabilities[11].

In this work relative permeability has been measured to understand the mobility ratios and mobilities of different phases. Although it is only a 2D model and therefore permeabilities are difficult to determine and obtained values have be taken with care for further calculations it gives a better understanding of the range and magnitude of mobilities, in which the experiments were conducted.

The measurement of the relative permeabilities for oil is as following:

- Saturate with brine and determine permeability of micromodel (Darcy)
- Saturate MM with oil long enough to reduce to S_{wr}
- Measure flow rate at a constant pressure
- Calculate relative permeability (Darcy)

As the micromodel is strongly water wet, a more intensive flooding procedure was required to get S_{or} and measure the water relative permeability. The oil saturated model was flooded for more than 22 hours from each side of the inlet ports with pressures above 60 psi. After no change in saturation has been observed, the flow rate at a constant pressure was measured, like in the procedure above. Micro scale pictures with residual oil saturation and connate water saturations can be seen below in Fig. 73 and Fig. 74.

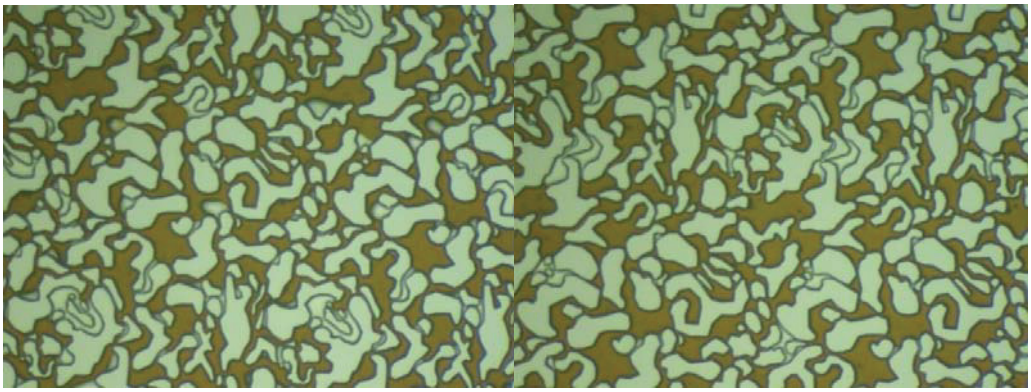

Figure 74: Oil saturation at relative permeability measurement

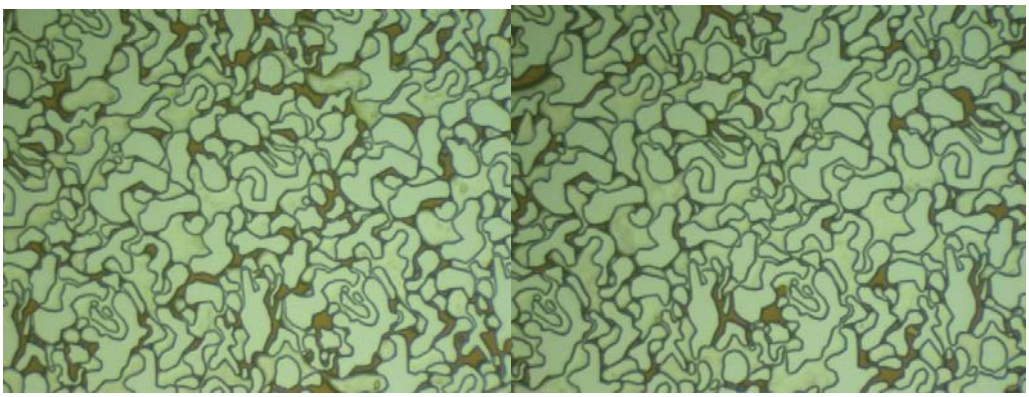

Figure 75: Oil saturation when measuring water relative permeability

The values obtained from the measurements can be seen in Tab. 12 and Tab. 13. The relative permeability was calculated according to Darcy´s law

$$k_{rf} = \frac{q_f \mu_f \Delta l}{A k \Delta p}$$

These relative permeabilities represent the endpoint permeabilities, k_{ro}* and k_{rw}* because they were measured at residual oil saturation and at connate water saturation, respectively.

Water	
Δp	50 psi
q	0.006 ml/min
k	1220 md
S_{orw}	83.25%
k_{rw}^*	0.09804

Table 11: Input data for water relative permeability curve calculation

Oil	
Δp	28 psi
q	0.0001 ml/min
k	1220 md
S_{wr}	5%
k_{ro}^*	0.129

Table 12: Input data for oil relative permeability curve calculatio

The exponential form below in Eq. 5 [11] is used to show the relative permeability urves of water and oil. For calculations n_o is assumed to be 3.0 and n_w 2.0, S_{wr} is the connate water saturation and S_{wor} the water saturation at the residual oil saturation.

$$k_{rw} = k_{rw}^{*}\left(\frac{S_w - S_{wr}}{1 - S_{wr} - S_{wor}}\right)^{n_w}$$

$$k_{ro} = k_{ro}^{*}\left(\frac{1 - S_w - S_{wor}}{1 - S_{wr} - S_{wor}}\right)^{n_o}$$

Figure 75 shows the relative permeabilities of water and oil, only a small range of the vertical axis is plotted for better visualization.

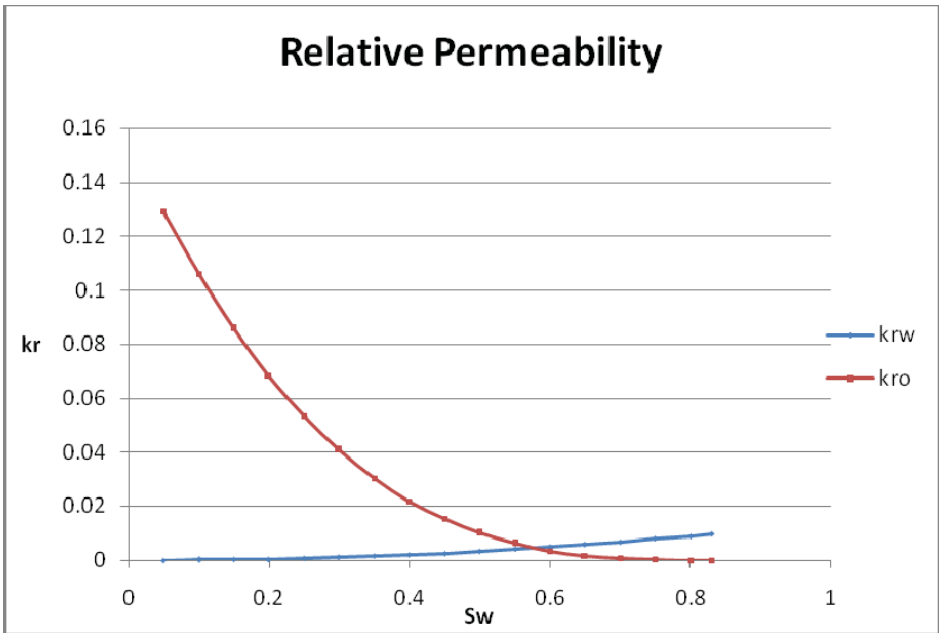

Figure 76: Relative permeability curves of oil and water according to the measurements

Mobility Ratios

To describe and understand the two-phase flow of water or polymer solution and oil relative permeability curves can be helpful for the displacement process in this work. The fractional flow equation from Buckley and Leverett (1942) can be used. In 1954 Dyes Caudle and Ericson developed the mobility ratio out of this concept [11]. The mobility ratio in Eq. 7 and its influence on areal sweep efficiency can be seen in Fig. 76.

$$M = \frac{\frac{k_{rw}}{\mu_w}}{\frac{k_{ro}}{\mu_o}} = \frac{\frac{k^*_{rw}}{\mu_w}}{\frac{k^*_{ro}}{\mu_o}}$$

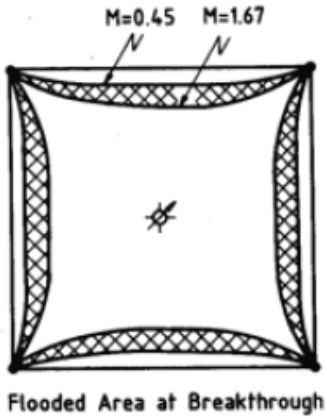

Mobility Ratio	Flooded Area	
	at Breakthrough	at f_w = 90 %
10	0.51	0.83
2	0.60	0.88
1	0.70	0.98
0.5	0.82	0.99
0.25	0.87	0.995

Figure 77: Influence of mobility ratio on breakthrough time and sweep efficiency

As shown above mobility ratios influence the sweep efficiency significantly and thus the success of an enhanced oil recovery project. Mobility ratios in the range of 1 and smaller are referred to as favourable ratios, everything bigger is an unfavourable mobility ratios and should lead to an unstable displacement. A very accurate way of determining the stability of a flood is to compare the shock front mobility ratio, over the endpoint mobility ratio according to Kumar. The shock mobility ratio is defined in Eq. 8:

$$M = \frac{\frac{k_{rwf}}{\mu_w}}{\frac{k_{rof}}{\mu_o}} \Big/ \frac{\frac{k_{ro}}{\mu_o}}{}$$

Due to the instability of the displacement front, the bank behind the front is not at the endpoint mobility ratio[28]. For this work, only endpoint relative permeability values were available and therefore Eq.7 was used to calculate mobility ratios for the different experiments. Viscosity values for polymer solutions were obtained from Fig. 71 with a shear rate of 0.09 sec^{-1}. Mobility ratios for each experiment were calculated, assuming that the relative permeabilities for polymer solution are equal to the water relative permeability. Results are shown in Tab.14. Only ratios of the S255 could be calculated due to missing data from the Alberta Research Council.

	Concentration (ppm)	Viscosity (cp)	Mobility ratio
Brine		1	34.19
S255	500	16.99	2.01
	750	13	2.63
	1000	11.8	2.90
	1250	25.7	1.33
	1500	35.39	0.97
	2000	135	0.25
	2500	1004	0.03

Table 13: Mobility ratios for associative polymer solution and crude oil (450 cp)

Permeability Reduction

Polymer plugging has been reported for a couple of experiments and can be useful as well. In high permeable areas, which are almost completely water saturated, polymer plugging can lead to a reduction of permeability and hence increase the flow resistance so that the polymer slug will contact unswept areas. According to the literature plugging only occurs when the polymer particle diameter is larger than a fifth of the average pore diameter. In former micromodel experiments (Filiz Aktaz 2008) no polymer plugging was reported neither by changed permeability nor by visual observations. During these series of experiments, polymer plugging was observed by incident at very low concentrations at the beginning. In order to determine the shear rate in the MM, it has to be flooded with a polymer solution. The experimental steps of this experiment are listed below:

- Saturate 100% with brine to determine permeability with Darcy´s law
- Saturate 100% with polymer solution
- Measure pressure drop at a constant flow rate
- Calculate viscosity
- Find corresponding shear rate according to Fig. 71
- Clean the micromodel with Toluen, Propanol and Water
- Saturate with brine to determine permeability

During the last step of this experiment a reduction in permeability was calculated according to Darcy´s law, but the visual observation at micro scale did not show any polymer plugging.

To obtain a better understanding of where the polymer particles plug the pores as well as in which spatial distribution, the same experiment was done with a dyed polymer solution. To colour the solution, two drops of conventional red food colour were added to a 200 ml solution, Fig 78.

After the polymer flood, the same order of permeability reduction was observed and additionally, the dyed solution showed its effects. The very first pore throats from the inlet fraction side were obviously plugged with the polymers, as can be seen in Fig. 77. Plugging did not go further into the matrix, it was only within the first 10-15 pores.

Although after the experiment the MM was cleaned intensively with three different cleaning fluids, according to the elutrope row (propanol-ethanol-water) to dissolve the

polymer precipitation, the permeability measurements did not show any significant changes. From Tab. 16 and Tab.17 below a permeability reduction from 1400 md to 933 md, which is almost 35%, can be seen.

As a measure of permeability reduction the residual resistance factor in Eq. 9 [11][8] can be calculated, which is the mobility of a brine solution before(λ_1) and after (λ_{1a}) polymer injection.

$$R_{Rf} = \frac{\lambda_1}{\lambda_{1a}}$$

$$R_{Rf} = \frac{\lambda_1}{\lambda_{1a}} = \frac{\frac{k_1}{\mu_1}}{\frac{k_{1a}}{\mu_{1a}}}$$

R_{Rf} is an indication of the permanence of the mobility reduction caused by the polymer solution. It shows the quantity of channel and pore plugging and blocking of the polymer solution. Another criteria of measurement the permeability reduction are the resistance factor, which gives the ratio of injectivity of brine to that of single-phase polymer solution which can be seen in Eq. 10

$$Rf = \frac{\lambda_1}{\lambda_1'} = \lambda_1 \mu_{app} = \left(\frac{k_1}{\mu_1}\right)\left(\frac{\mu'_1}{k'_1}\right)$$

The fact that the polymer solution plugs pores and thus reduces permeability was of major importance. Otherwise different experiments would have been done with the same micromodel after cleaning without noticing that the permeability has changed. As a logical fact, a new micromodel has to be used for every experiment in order to guarantee repeatability.

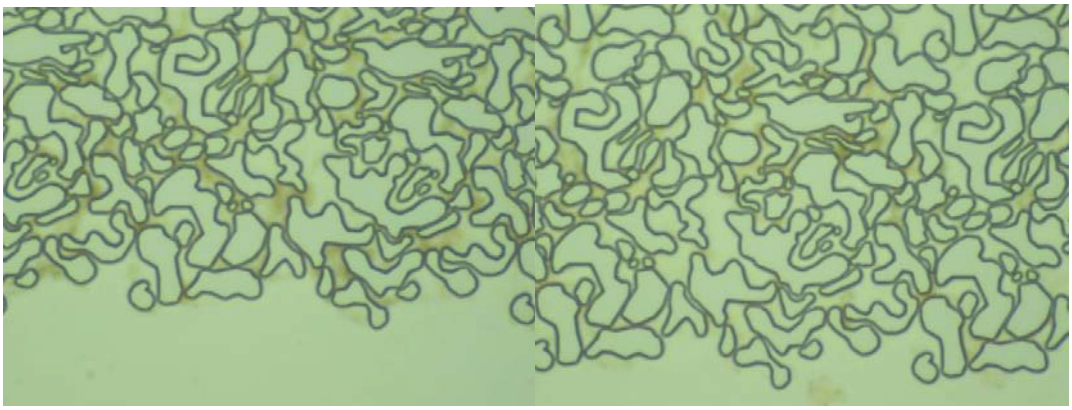

Figure 78: Polymer plugged (red) areas near inlet fracture of the micromodel

Figure 79: Dyed polymer solution with food colour

P2 (psig)	P2 (atm)	P1 (atm) >	Q (mL/min)	Q (mL/s)	Area (cm^2)	L (cm)	viscosity (cP)	k (darcy)
28	2.90	1.00	0.4	0.0066	0.0125	5	1.0	1.4
21	2.43	1.00	0.3	0.005	0.0125	5	1.0	1.4
14	1.95	1.00	0.2	0.0033	0.0125	5	1.0	1.4
7	1.48	1.00	0.1	0.0016	0.0125	5	1.0	1.4
							average	1.4

Table 14: Permeability measurements before injecting the polymer solution (measured with const. flow rate)

			INPUT					**OUTPUT**
P2 (psig)	P2 (atm)	P1 (atm) >	Q (mL/min)	Q (mL/s)	Area (cm^2)	L (cm)	viscosity (cP)	k (darcy)
41	3.79	1.00	0.4	0.0066	0.0125	5	1.0	0.95
31	3.11	1.00	0.3	0.0055	0.0125	5	1.0	0.94
21	2.43	1.00	0.2	0.0033	0.0125	5	1.0	0.93
11	1.75	1.00	0.1	0.0016	0.0125	5	1.0	0.89
							average	0.93

Table 15: Permeability measurement after injecting the polymer solution (measured with const. flow rate)

Polymer Adsorption

Polymer adsorption is a major issue in polymer flooding. The changing polymer characteristics and the concentration when the solution is flowing through the reservoir and contacting rock and brine have to be observed. To determine if the polymer solution changes after flooding through the micromodel, the following experiment was done:

A polymer solution of associative polymer S255 with 2500 ppm was mixed and viscosity versus shear rate was measured. Then, for 30 hours the micromodel was flooded with the polymer solution at a constant pressure of 55 psi and at the outlets, the polymer solution was gathered and measured again. This experiment does not only show if any adsorption happened during the flood, but also if the polymer solution was sheared too much to get damaged. The result can be seen in Fig. 79 and does not indicate any changes in rheology.

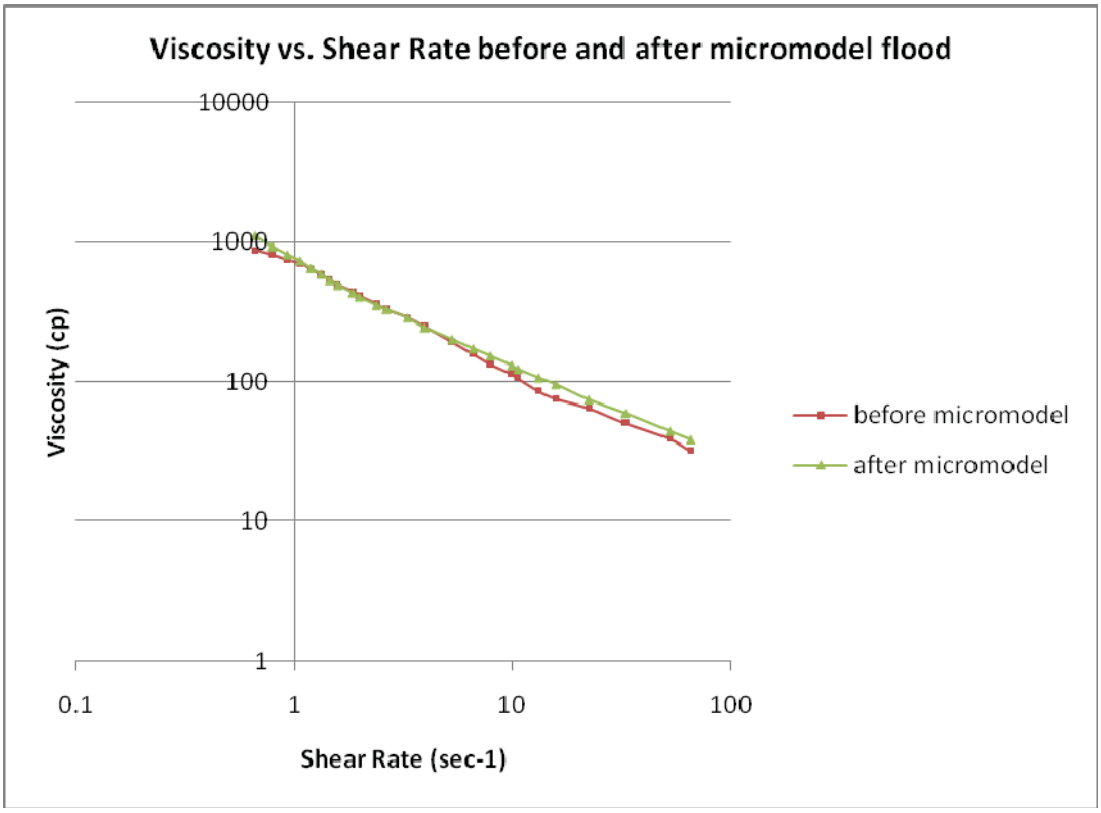

Figure 80: Viscosity measurements before and after flooding the polymer solution through the micromodel

An intensive study of polymer adsorption was performed by Rousseau et al. in 2008. They used silicon carbide granular packs with permeability and porosity of 1000±50

md and 40±1 %. Two types of associative polymer and one conventional polymer solution were tested. Mobility reduction reached a plateau for conventional polymers with equivalent concentration, whereas the associative polymer solution increased the mobility reduction and indicated an internal plugging trend. The determination of the adsorbed layer thickness showed that associative polymer solution has a 7 times higher thickness than conventional ones and corresponds to the amount of polymer injected.

The adsorption phenomenon can either be assumed as a multi-layer adsorption or by the adsorption of multi- chain aggregates already present in the polymer solution.

Further experiments showed that elevated salinities (58.4g/L NaCl) evolve to an over-adsorption. Therefore, optimum salinity conditions have to be found for an associative polymer solution flooding operation[29].

Oil

The oil used for these experiments is dead oil from the Pirawath field in Austria. API gravity and viscosities at reservoir conditions and at room temperature are measured. To calculate API gravity, one litre of dead oil was weighed and the specific density calculated and the index was determined with the API gravity formula as in Eq. 10.

$$API = \frac{141.5}{\gamma_{spec.}} - 131.5$$

$$API = 25.6$$

The viscosity of the oil was measured with the DV-II-Pro+ Brookfield viscometer with a thermal jacket. Measurements at room temperature and reservoir temperature can be seen in Fig. 80 and Fig. 81

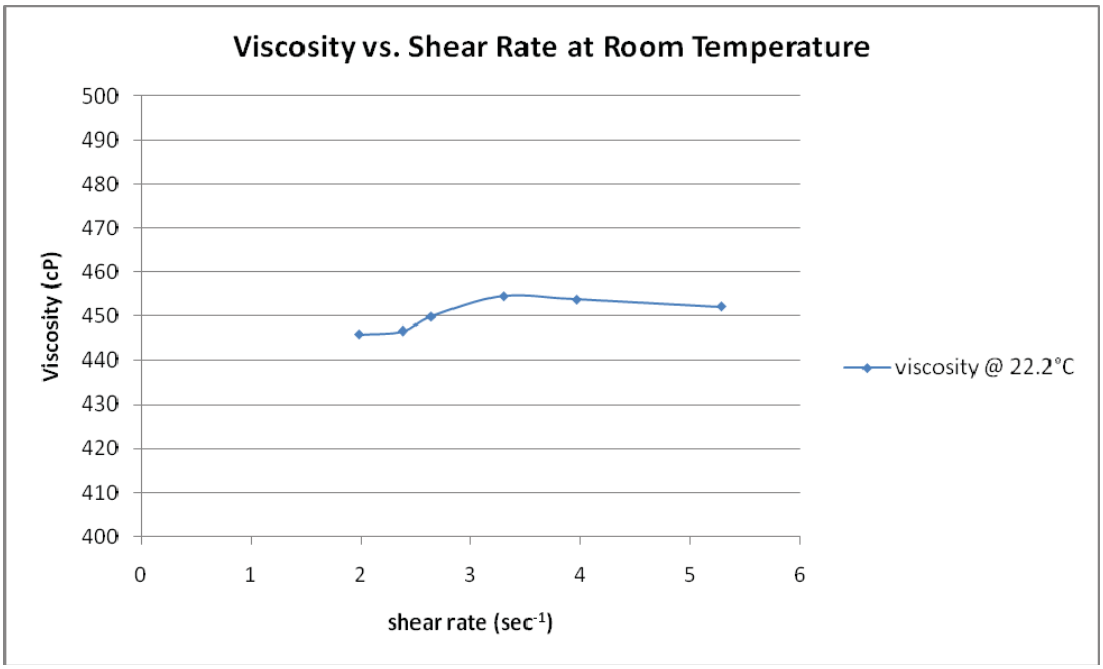

Figure 81: Oil viscosity measurements at room temperature (22.4°C)

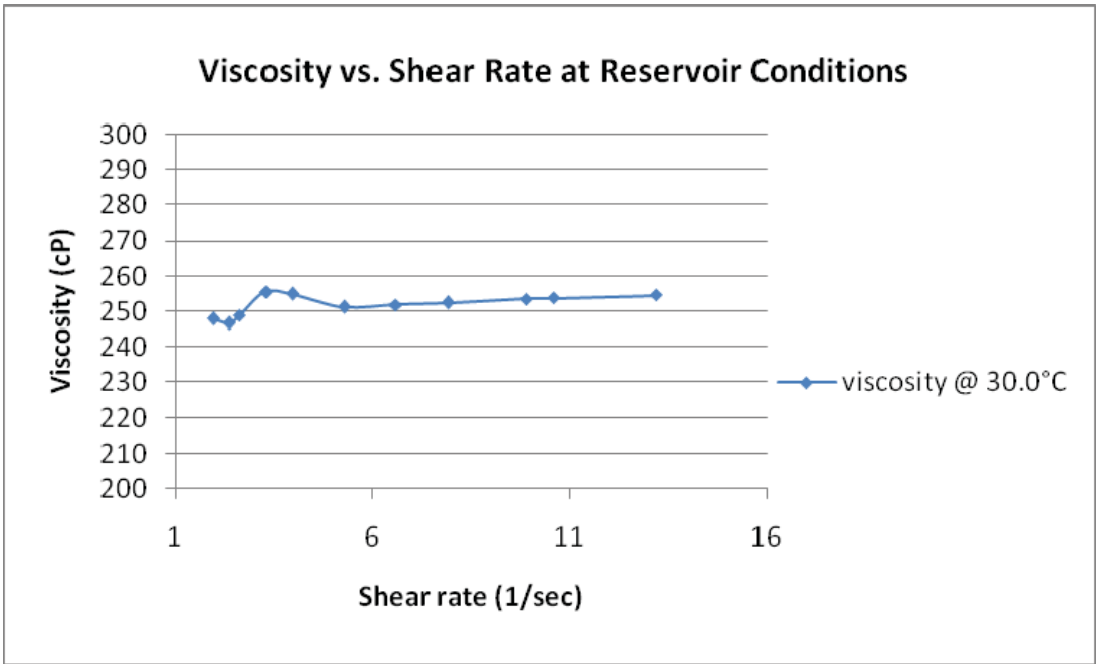

Figure 82: Oil viscosity measurements at reservoir temperature (30.0°C)

Problems

A lot of problems occured before during and even after an experiment. Problems and failures do not only cause only troubles, they also help to improve and show weaknesses in the aperture and work flow of experiments. Accidents and human failure often set back the work for a couple of days. Some of these problems and accidents are reported in the section below to give a better understanding of experimental work. Problems are listed in the chronological orders of an experimental work flow

Drilling the entry and outlet ports

Drilling the holes for the fluid communication is one of the most serious tasks. A damage of the wafer at this time would not only cost a lot of time, but also a lot of money. The wafer has to be fixed with the fingers to drill the holes. Broken wafers most often result from uneven pressure distribution during the fixing. Therefore, a very flat and clean surface is required to drill the holes.

Bonding the wafer

The bonding process, described in one of the sections above is the last step of the micromodel production. While the wafer is heated up for 50 minutes, very fine and tiny particles can settle down on the top of the wafer. These small particles can cause a bad bonding when the wafer is connected with the pyrex glass. The dust can be removed before bonding with an air jet pump. Unfortunately, particles can melt together with the wafer and cannot be removed, which most often makes the wafer unusable.

Tighten micromodel in holder

Broken wafers also occur when tightening the micromodel holder. This happens when the eight screws from the holder are not tightened star-shaped. By tightening them clockwise or counter clockwise, the pressure is not distributed evenly and the wafer may break. Another reason for a damaged wafer while tightening is probably a small particle between holder and micromodel. This particle causes a stress point and breaks the micromodel.

Brine mixing

The brine mixing procedure requires a lot of time to avoid precipitation. Small particles can plug the fine pores of the micromodel later on and give wrong results. Especially Sodium Bicarbonate precipitates easily when mixing the brine. By adding it in small portions within sufficient time intervals, this negative effect is avoided.

Polymer mixing and filtering

The polymer mixing is often insufficient and small undissolved polymer particles are observed, which could result in a pore plugging. Therefore the mixing procedure is usually done at slightly elevated temperatures of 30°C. Sometimes even the elevated temperature is not sufficient in order to guarantee a smooth operation and therefore all polymer solutions are filtered. To filter the solution, a cartridge filter with average filter particle size of 15 μm was used. Viscosity measurements showed that the filter does not change any properties or characteristics of the polymer solution.

Broken and leaking tubings

Broken or leaking tubings when noticed early enough are substituted by new ones and the experiment is continued. But leaking or broken tubing during a flood cannot be repaired or replaced fast enough in order not to falsify the experimental outcome. Reason for a broken or leaking tubing is that the connection is tightened and screwed many times. Leaking tubings can be identified by abnormal pump pressures or rates during the experiment. Also, small drops on the surface of the desk can be a sign for leaking tubings. Therefore, the cleaning of the desk before starting an experiment is part of the workflow.

Air in tubings

Air bubbles in the tubings lead to wrong measurements and results. Most often air was found in between the decane and brine vessel when saturating with brine. When connecting and disconnecting the water pump to the decane vessel, small pockets of air are trapped in the connection and flow into the vessel when pumping is started. Trapped air causes wrong permeability measurements which in consequence lead to the wrong assumption that the micromodel is not useable for the experiment. The problem is solved by connecting a second valve to the decane vessel, where the air is released when pumping starts.

Connect tubings to micromodel

The connection from the oil vessel to the micromodel inlet port has to be tightened very slowly. If tightened to fast, a high volume of oil is pushed into the micromodel in a very short time and result in very high pressure. If the pressure exceeds a certain limit, the micromodel will break. Therefore the connection is screwed very slowly and a very low pressure of 5-10 psi is used to make the connection.

Photographs

The light and diffusion box has to be adjusted so that no shadows are visible when taking meso scale pictures. At breakthrough time the micromodel holder has to be taken to the microscope and micro scale pictures have to be taken in a time window of 2-3 min. Micro scale pictures after 5 or 10 minutes after breakthrough would result in a wrong interpretation.

Image Analyses

Uneven illumination of the pictures makes them very difficult to be analysed. To reduce the effect of illumination, only the middle part of the pictures is cut out and used for further processing.

Experimental Results and Discussions

A couple of experiments were conducted to observe the displacement of associative polymer solution and to compare them with conventional polymer solution and brine flood. An overview of the experiments is listed below.

- **Brine Flood**
- **Associative Superpusher S255 (q=0.0001 ml/min)**
  - 500 ppm
  - 750 ppm
  - 750 ppm (q=0.0004 ml/min)
  - 1000 ppm
  - 1250 ppm
  - 1500 ppm
  - 3x 2500 ppm (to prove the almost complete plugging of pores at this high concentration)
- **Conventional FP3630 (q=0.0001 ml/min)**
  - 500 ppm
  - 750 ppm
  - 750 ppm (q=0.0003 ml/min)
  - 1000 ppm
  - 1250 ppm
  - 1500 ppm

- **Brine- Polymer Combination (Switch to S255 2000 ppm after BT)**
- **Brine- Polymer Combination (Switch to S255 2000 ppm after 2/3 of BT)**
- **Brine- Polymer Combination (Switch to S255 1750 ppm after 1/2 of BT)**
- **Brine- Polymer Combination (Switch to S255 1500 ppm after 22 hours brine flood)**

All experiments except the combination ones, had the same flow rate of 0.0001 ml/min, which refers to 12 cm/day. The oil, which was described before, was intermediate oil from the Pirawath field in Austria. Care had to be taken to have the same initial conditions before starting each experiment. Temperature, mixing time and quality of polymer and permeability variations in the micromodel have to be checked before starting. All experiments had an initial water saturation between 2% and 10%.

A 22.4°C room temperature was measured for all experiments. Experimental data gathering sheets had been laid out for each experiment, which included saturation times for water and oil, permeability measurements and pressure measurements during the flood experiments. An example of such an data sheet from a 500 ppm polymer flood can be seen in Appendix C.

Brine Flood

The baseline for all later experiments was the brine flood done at the very beginning of the study. As expected, the brine flood showed a very serious fingering behaviour in the middle of the micromodel which grew till it reached the outlet fracture and caused the breakthrough after 71 min.

A closer look at Fig. 82 shows another finger at the edge of the micromodel. This effect was observed many times later on. In some cases these edge fingers caused the breakthrough. The origin of the effect is unknown, but it is assumed to be a bonding effect, because the weight is only applied in the middle of the glass plate. So the outer parts may have less bonding and therefore less resistance to flow.

Further flooding also showed that after 22 hours some areas of the micromodel stayed unswept. The result was the same as predicted in literature: early breakthrough, with a lot of bypassed oil and after a long flooding period still un-contacted areas. Another evidence of the unstable displacement was the calculated mobility ratio of Tab. 14. Fig. 82 shows the sequence of the flood till breakthrough and the final picture after 22 hours.

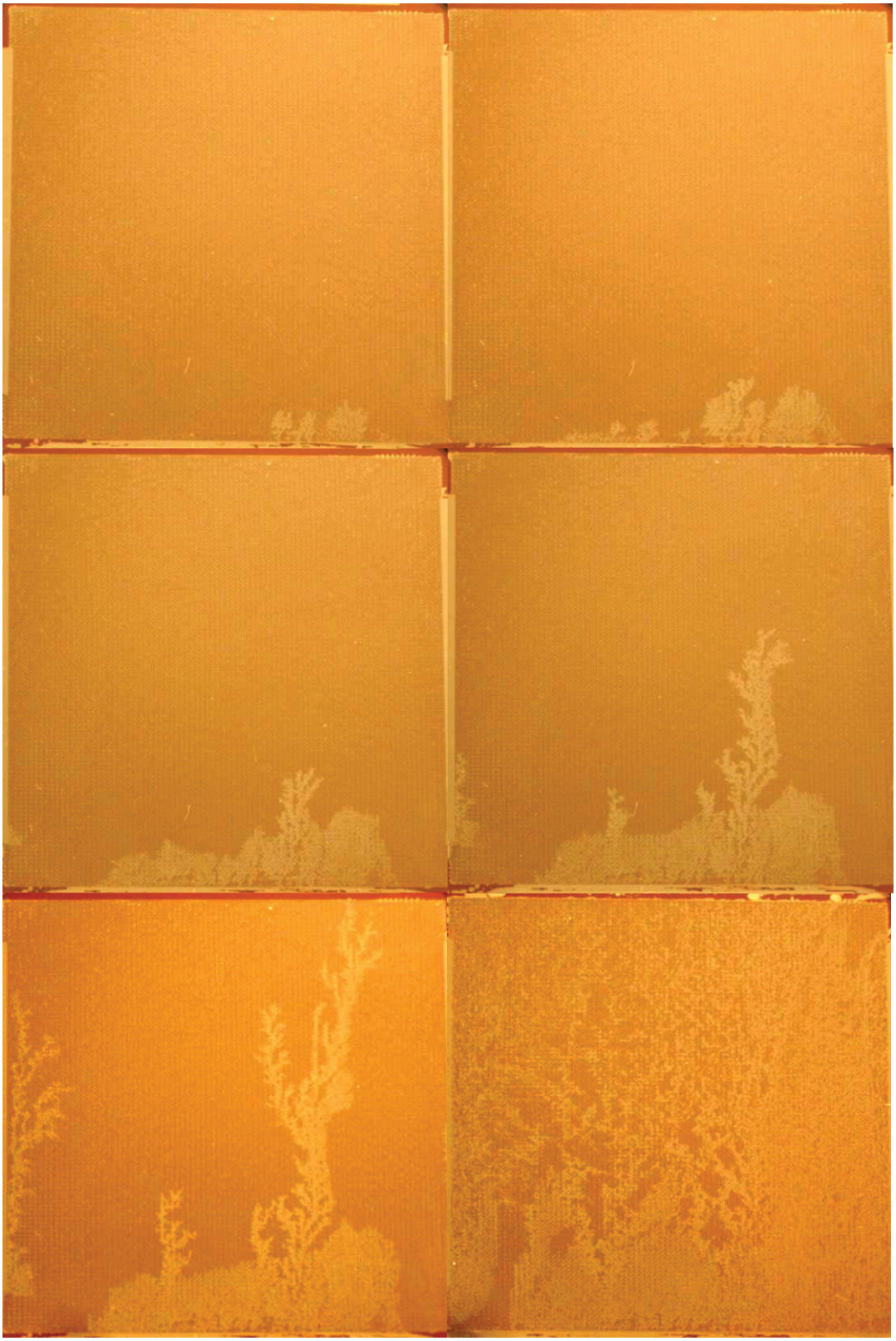

Figure 83: Brine flood meso scale series till breakthrough and till ultimate recovery BT-time: 71 min.

Associative Polymer Floods

All the experiments discribed in this part were made with the associative polymer Superpusher 255. The recovery at breakthrough ranges from 9.4% to 38.8%. Breakthrough times did not show any relation to recovery. The first polymer solution flood was at 500 ppm. The concentration was stepwise increased by 250 ppm till a more or less stable displacement was observed. Better sweep efficiency and therefore recovery at the same concentration as the conventional polymers are the expectations of these new polymers. All the following pictures present the displacement process in meso scale till breakthrough (first picture in third row) and till ultimate recovery (second picture in third row).

The 500 ppm solution shows similar behaviour as the brine displacement. Very early in the flood, two dominant fingers developed, which broke through after 51 min. In contrast to the brine flood, some smaller fingers developed as well which started growing more intensively after the breakthrough. Most of the fingers start merging at half way and build a more cloudy shape of displacement front towards the outlet fracture. After 22 hours of flood, a second front which came up only 10-15 mm into the micromodel matrix can be seen at the beginning of the inlet fracture. This brighter area has a better micro sweep efficiency than the other swept regions. Only very small spots of unswept areas were observed during this flood. No improvement of recovery at breakthrough compared to the brine flood could be achieved. Fig. 83 shows meso scale pictures till breakthrough and after 22 hours.

The 750 ppm polymer solution had a breakthrough after 50 min. Finger development was almost the same as for the 500 ppm solution. The only difference was that the breakthrough fingers were not predominant. At BT a lot of fingers were already merged and swept a large part of the micromodel. The size and shape of the fingers were the same as in the previous experiment. See Fig. 84. In addition, an experiment with the same polymer concentration with a changed flow rate was conducted in order to observe the influence of changed flow rates on displacement. The elevated flow rate of 0.0004 ml/min or 50 cm/day did not show any significant changes in recovery or swept area.

1000 ppm of polymer in solution showed the first slight improvements in stable displacement. No dominant single fingers grew early in flood life. A lot of small short fingers developed at the beginning, followed by a thin stable front of polymer solution. Although fingers became bigger later on, the polymer front behind did not stop, see Fig. 85. A couple of even fingers at almost the same height caused the breakthrough. Recovery factor and swept area at breakthrough could be significantly improved.

The experiment with best recovery and swept area after breakthrough proved to be the one with a 1250 ppm polymer solution. From the beginning, a very continuous stable front moved towards the outlet fracture. Only very small, skeletal and short fingers were visible ahead of the front. Finger number and length also decreased with increasing concentration, as can be seen in Fig.86. The breakthrough was caused by a finger at the edge after 91 min.

To prove whether this stable front was a lucky incident or a success of the polymer solution, the concentration was increased for another 250 ppm to a 1500 ppm polymer solution. The results were even better at the beginning than those at 1250 ppm, as a consequence of the more stable mobility ratio. Unfortunately the breakthrough was caused by a finger at the edge of the micromodel. Till half way, the displacement was perfectly stable as indicated in Fig. 87, even the very small fine fingers ahead of the front can be distinguished. Without the breakthrough at the edge this flood would have been more successful in terms of recovery factor and sweep efficiency.

The last experiment with the associative polymer solution was done at a concentration of 2500 ppm. The aim of this run was to observe if there is a concentration limit, at which the polymer solution plugs the pores too much and hence causes poor recovery and sweep efficiency. In fact the first run showed a perfectly stable displacement till half way of breakthrough. No viscous fingers were seen a head of the front instead a cloudy front developed. Breakthrough was again caused by an edge finger, Fig. 88. After breakthrough the polymer solution was not able to sweep the whole area and left a lot of bypassed oil behind. This could be a consequence of the too high concentration. A second run with the same concentration was conducted to repeat the behaviour. And again the same plugging occurred with a lot of bypassed oil after 22 hours of flooding.

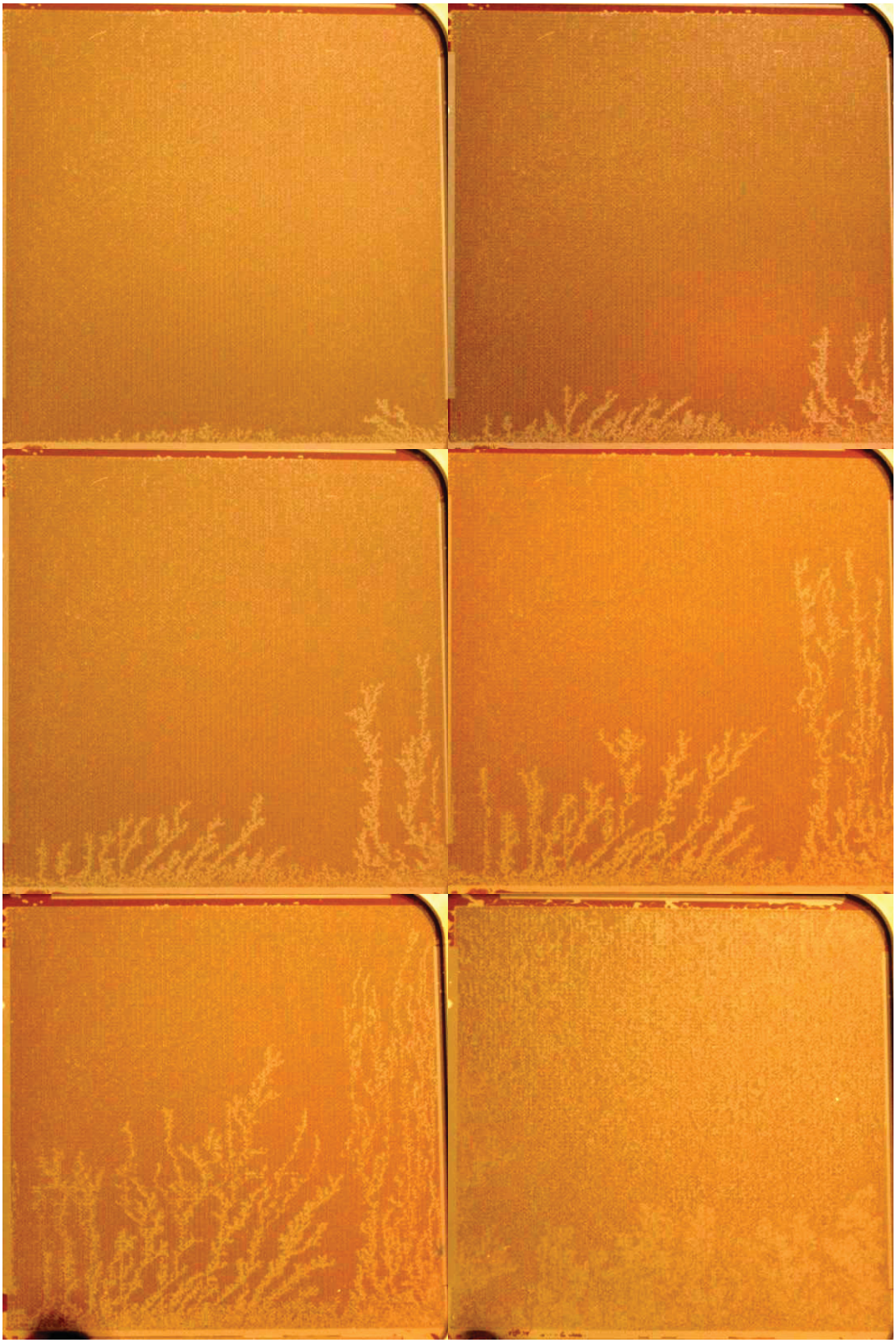

Figure 84: Associative polymer flood S255, 500 ppm; BT-time: 51 min.

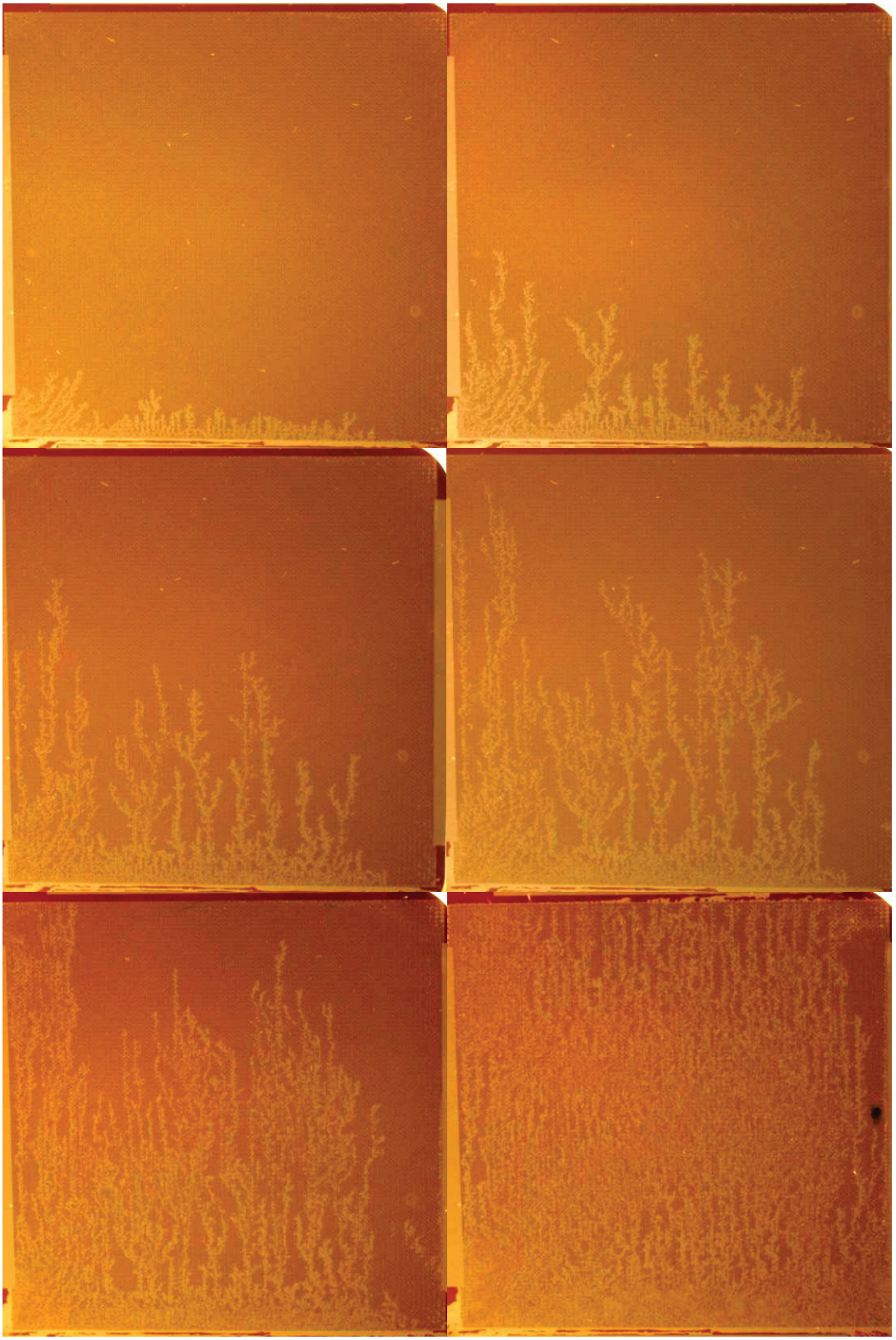

Figure 85: Associative polymer flood S255, 750 ppm; BT-time: 50 min.

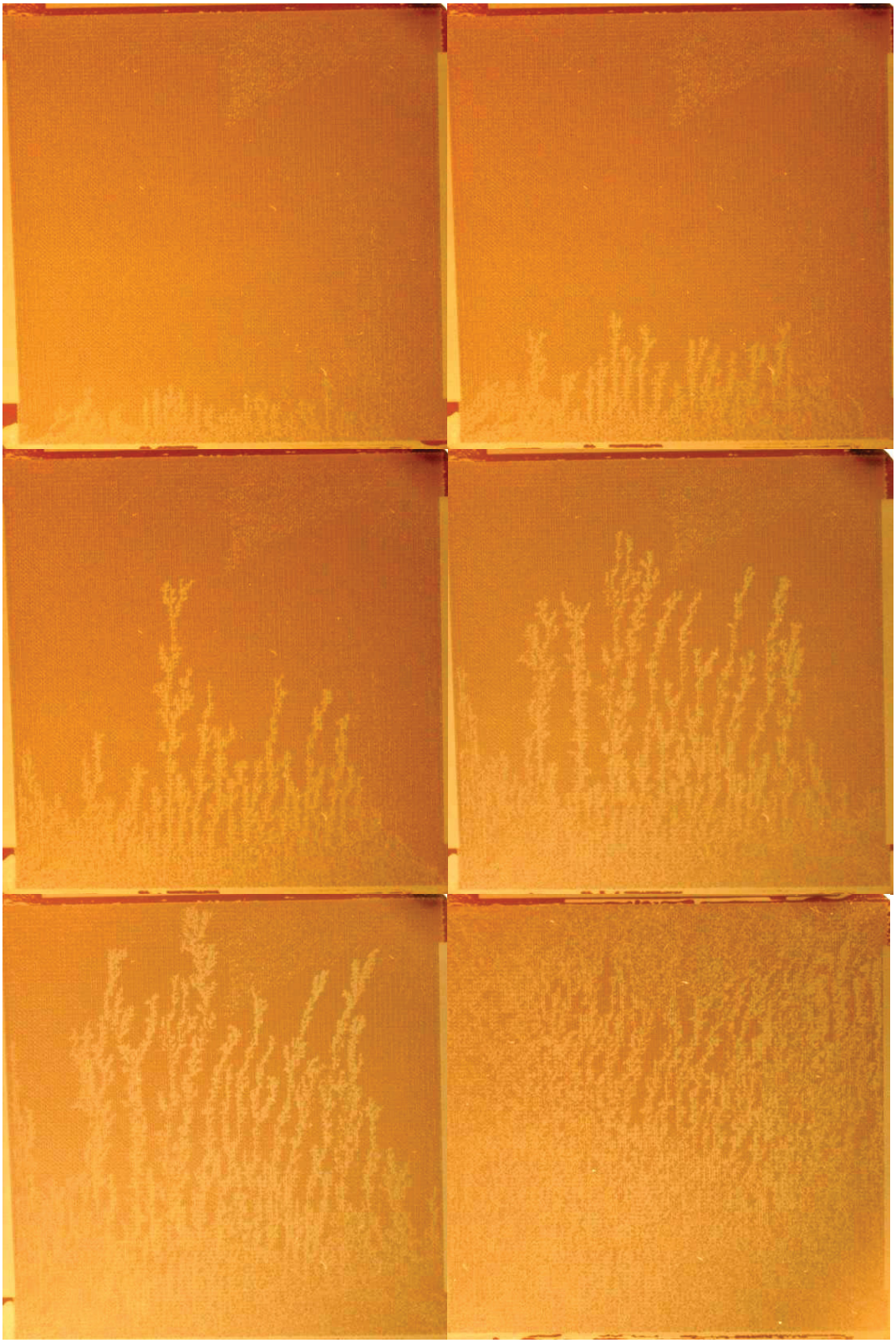

Figure 86: Associative polymer flood S255, 1000 ppm; BT-time: 91 min.

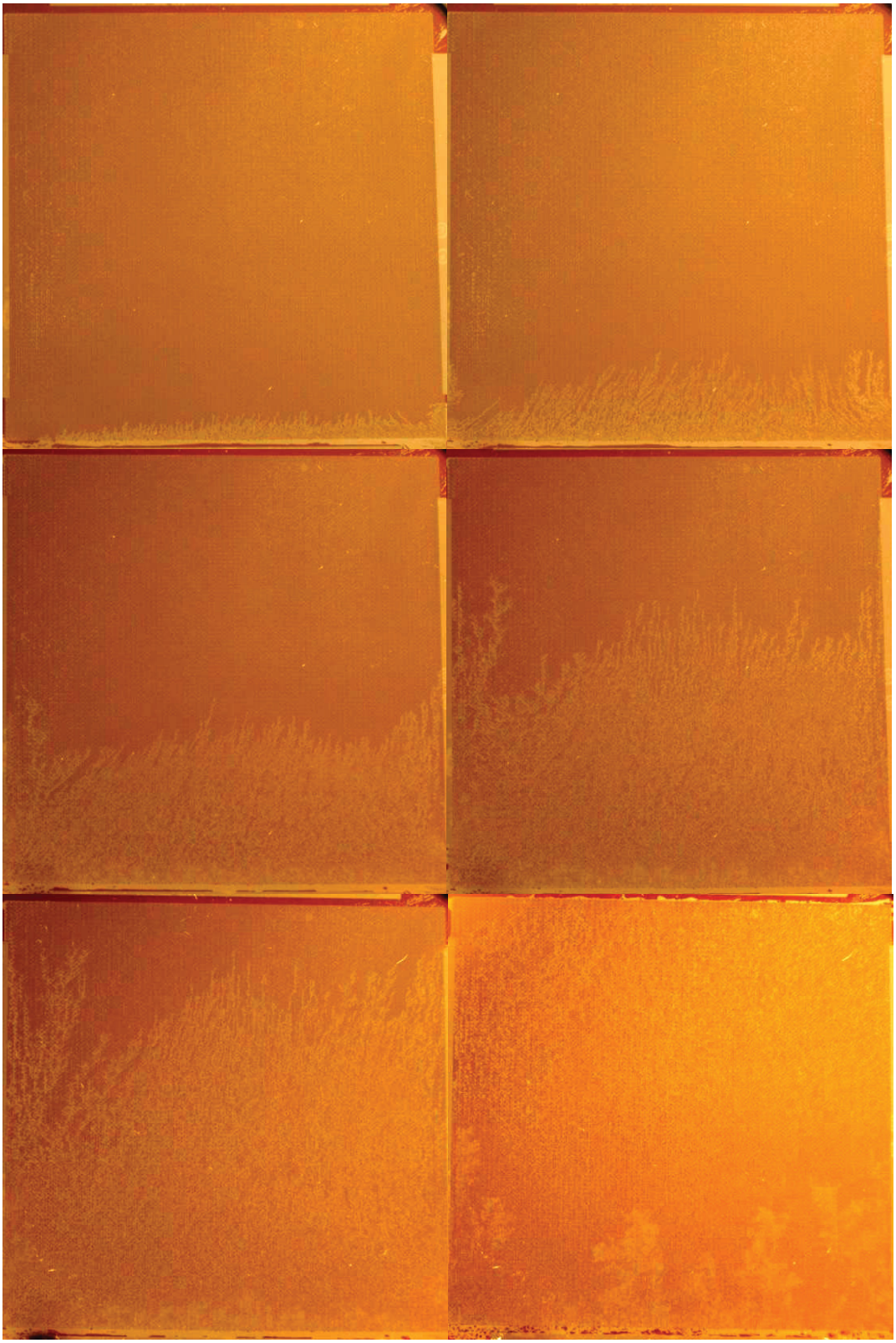

Figure 87: Associative polymer flood S255, 1250 ppm; BT-time: 107 min.

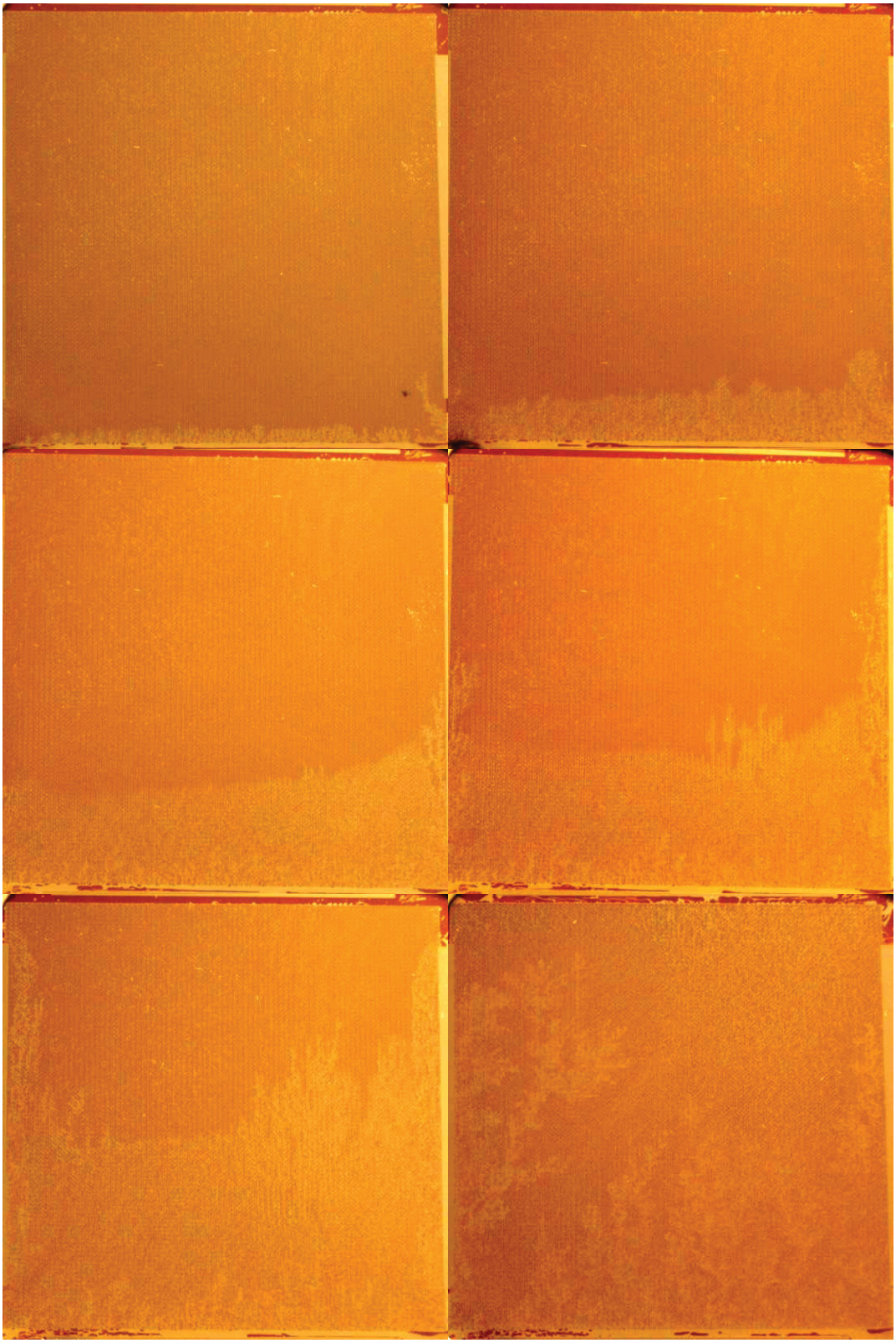

Figure 88: Associative polymer flood S255, 1500 ppm; BT-time: 64 min.

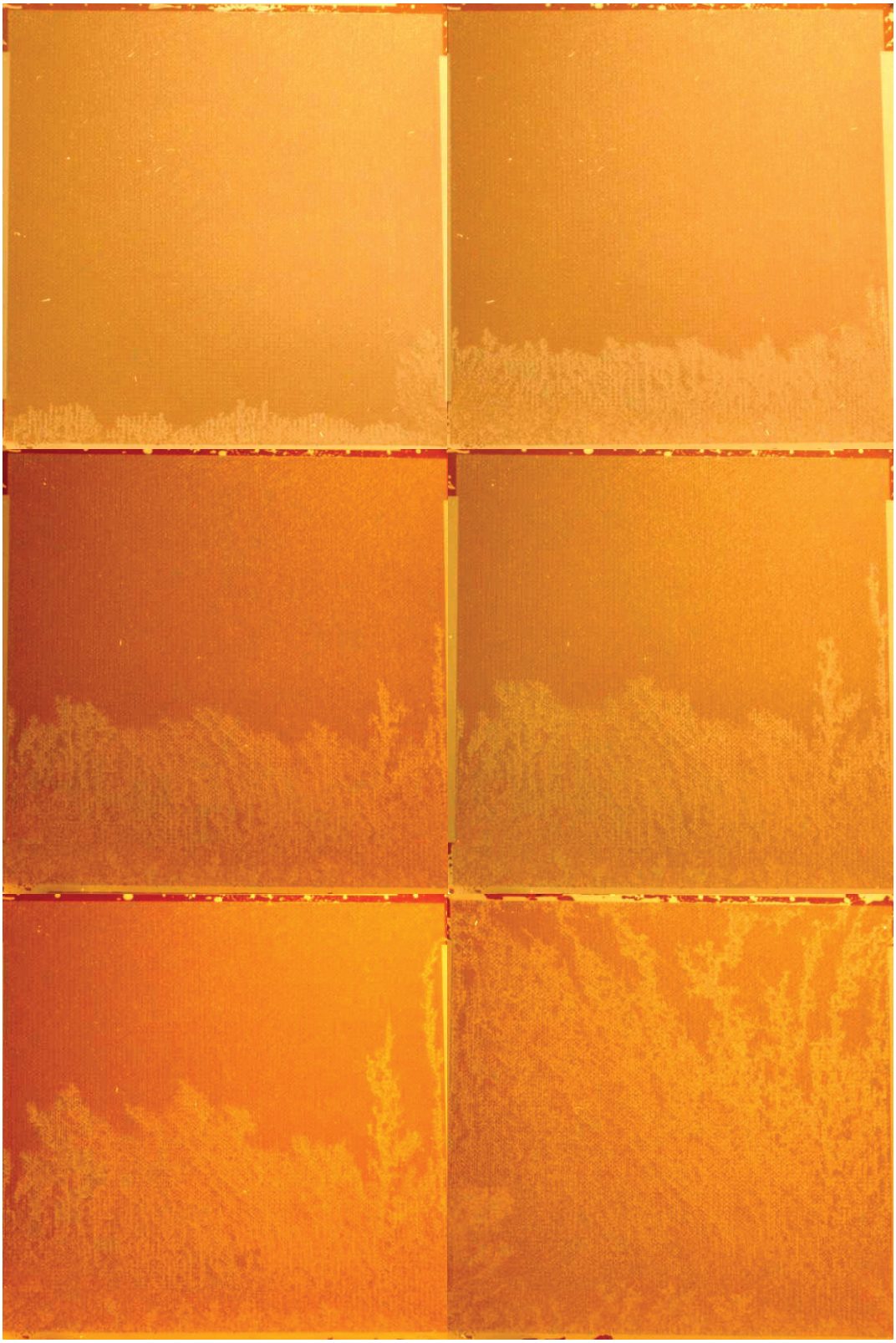

Figure 89: Associative polymer flood S255, 2500 ppm; BT-time: 213 min.

Conventional Polymer Floods

The same series of experiments was performed with the conventional polymer. As a starting concentration a 500 ppm polymer solution was used. Breakthrough times were completely different and allowed no possible relation to recovery or sweep efficiency.
500 ppm solution of the conventional solution showed a similar behaviour as the associative with the only difference that the shape of the fingers had changed. Fingers appeared thinner and finer and merged at an earlier stage, Fig.89.

The 750 ppm solution had several fingers and additionally led to a breakthrough at 25 min. As observed in the earlier experiments the fingers started merging together and building small displacement fronts behind them. Fig. 90 shows the displacement till ultimate recovery of the 750 ppm solution. An elevated flow rate was used to observe the influence on different flow rates. But the 0.0004 ml/min did not show any significant success or failure.

An improved performance could be observed at the 1000 ppm solution. Fingers were at the same height when moving towards the outlet end. The displacement cannot be referred to as stable, but the trend to a stable displacement can be seen in Fig.91.

The best performance again when considering the edge fingers is the 1250 ppm solution. Micro scale saturation pictures and meso scale sweep efficiency were by far the highest at this solution. At breakthrough time the fingers completely merged to a front and showed an almost stable displacement, which can be seen in Fig 92.
The last experiment was conducted with the 1500 ppm solution and did not increase recovery or sweep efficiency from the 1250 ppm solution (Fig. 93).

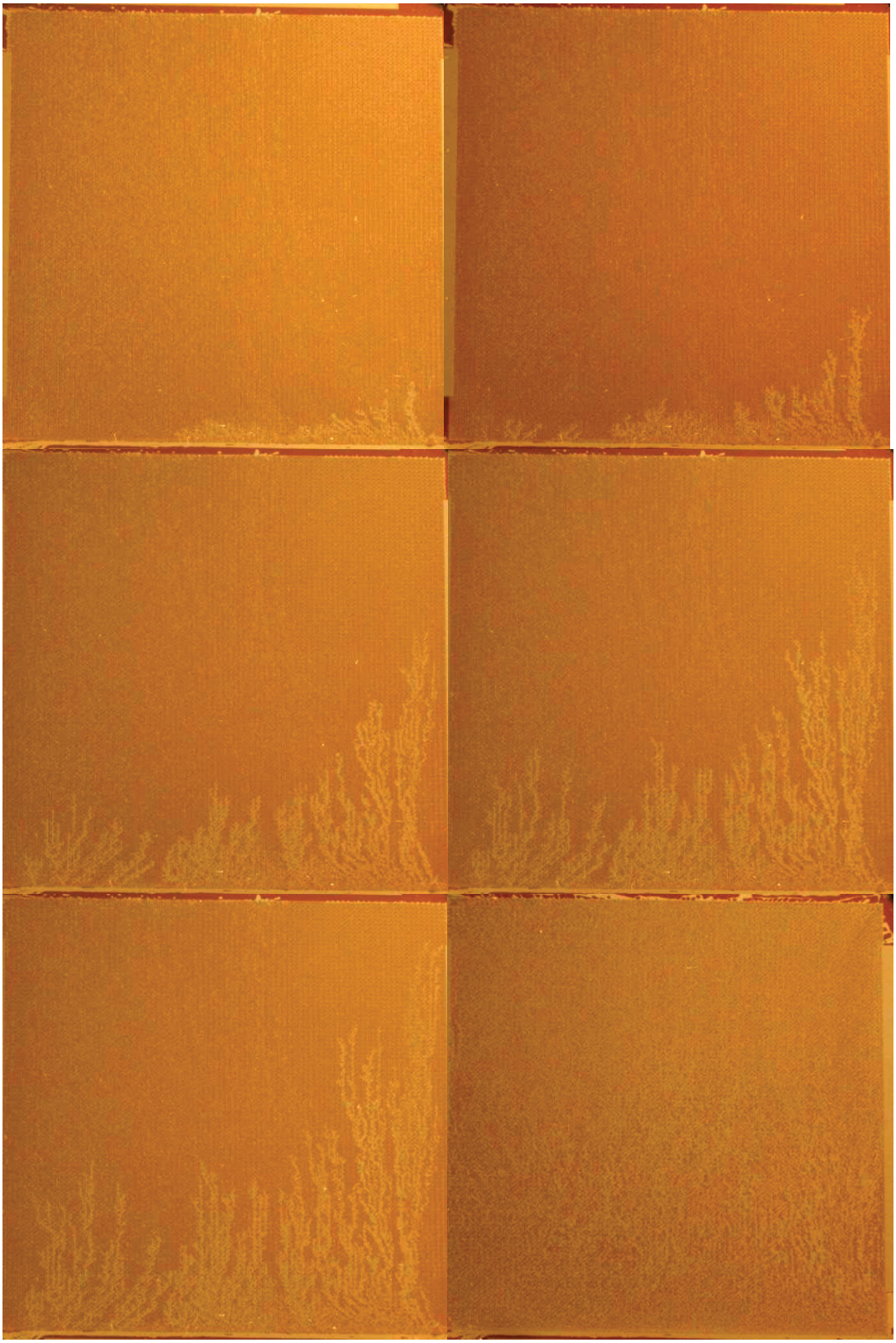

Figure 90: Conventional polymer flood FP3630, 500 ppm; BT-time: 25 min.

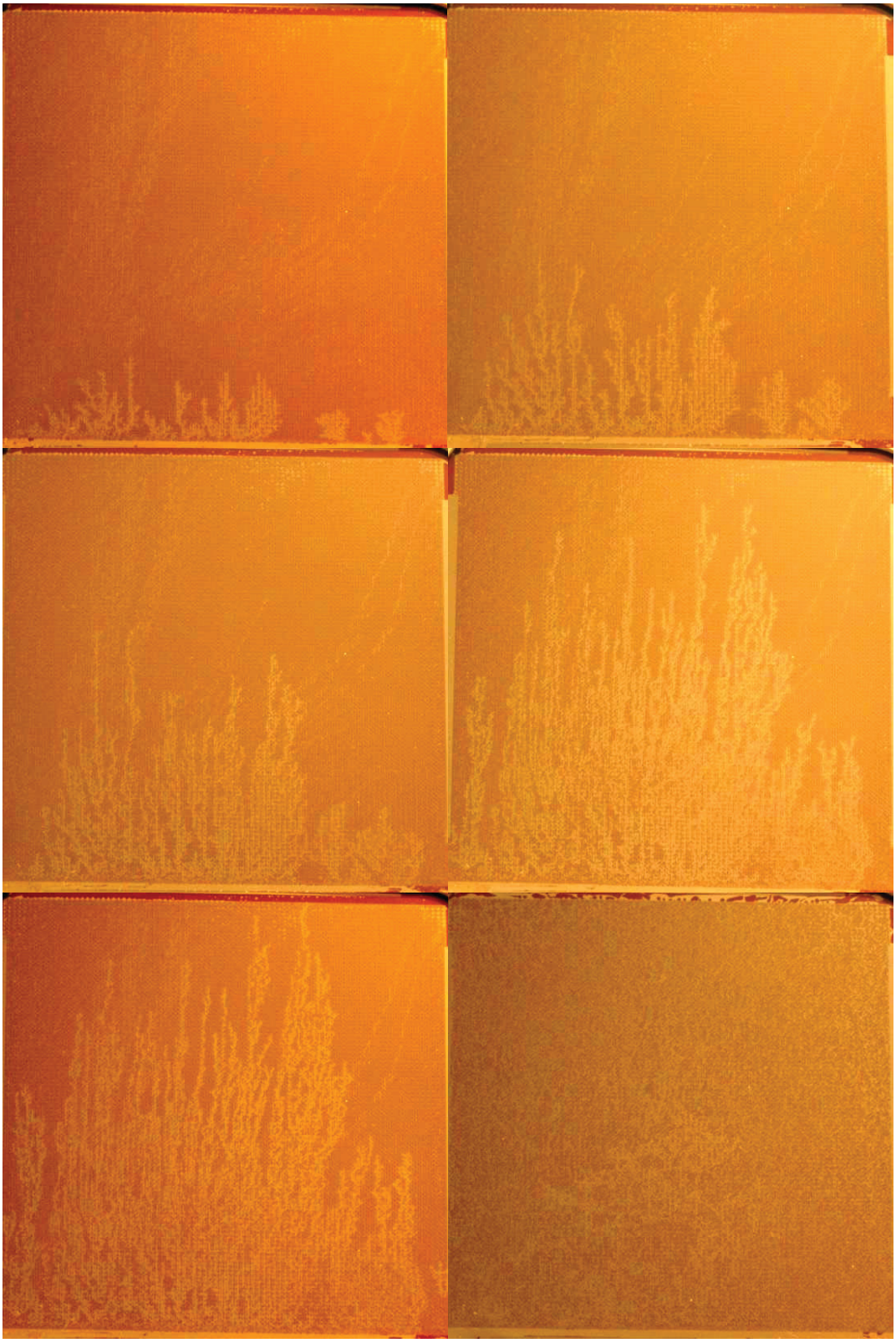

Figure 91: Conventional polymer flood FP3630, 750 ppm; BT-time: 81 min.

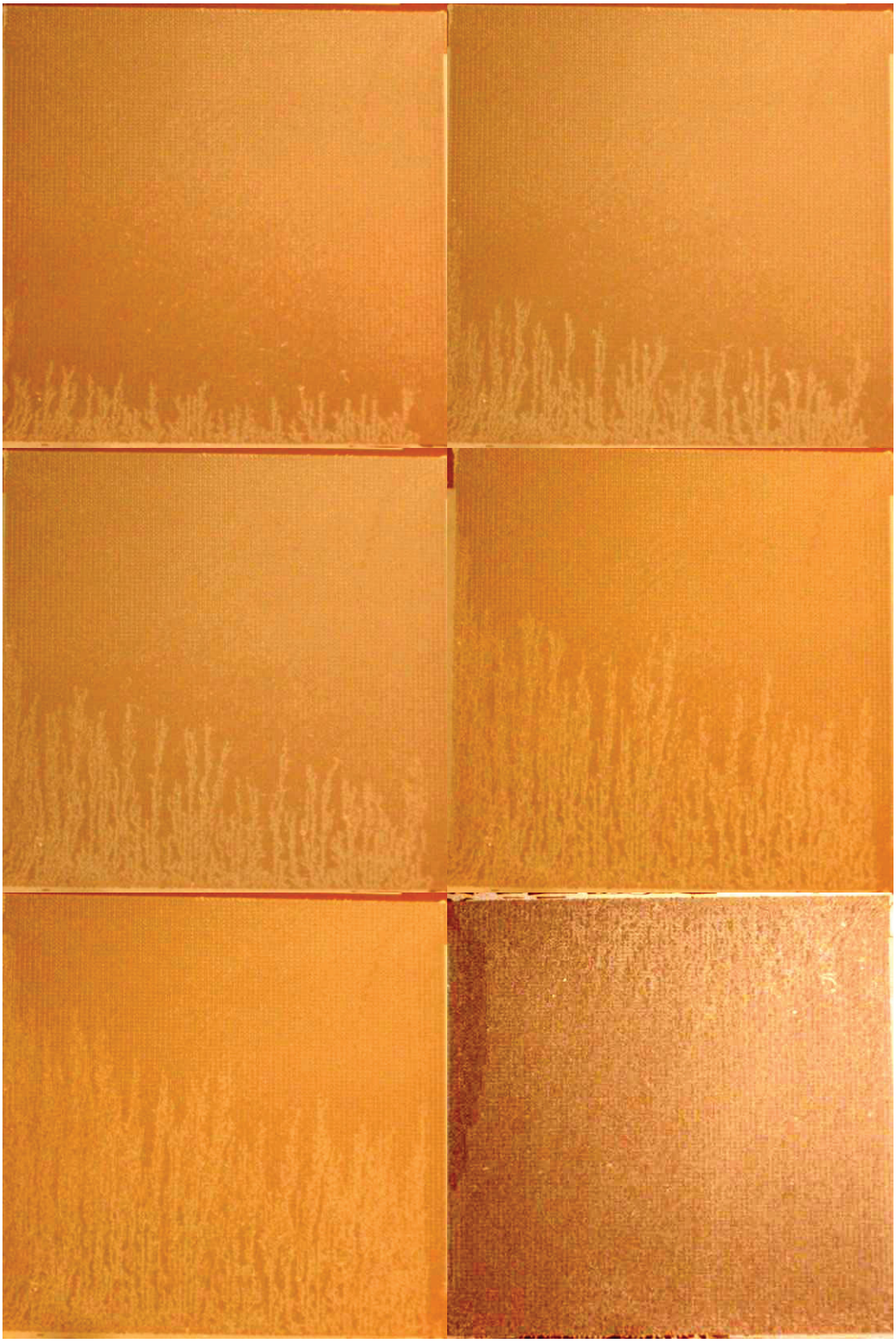

Figure 92:Conventional polymer flood FP3630, 1000 ppm; BT-time: 17 min.

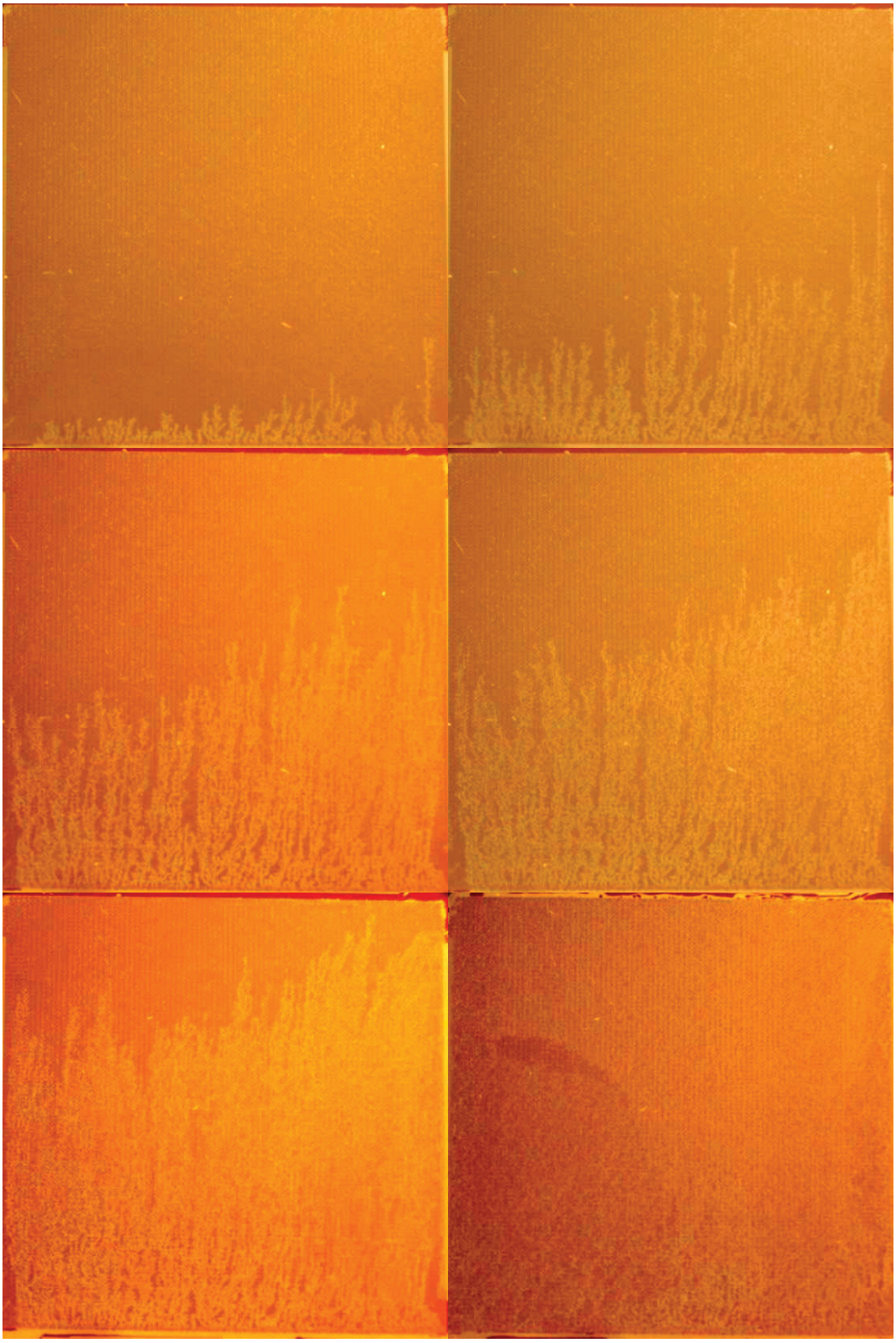

Figure 93: Conventional polymer flood FP3630, 1250 ppm; BT-time: 28 min.

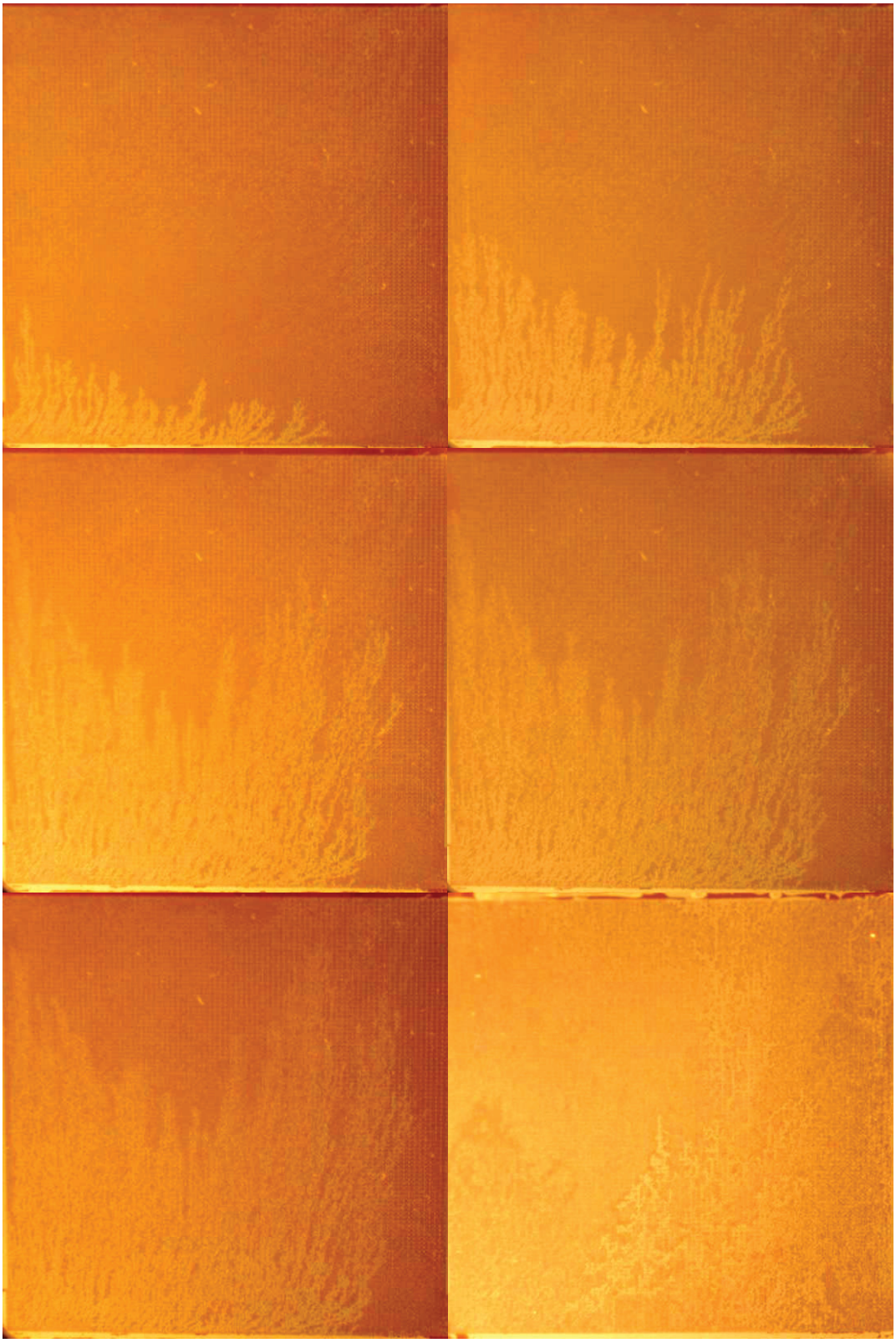

Figure 94: Conventional polymer flood FP3630, 1500 ppm; BT-time: 25 min.

	Brine	Associative Superpusher 255					
Concentration (ppm)		500	750	1000	1250	1500	2500
Permeability (md)	1311	905	1075	980	1160	1370	1422
BT-time (min)	71	51	50	91	107	64	213
Pore volume injected (ml)	0.54	0.39	0.38	0.69	0.81	0.48	1.61
BT-recovery (%)	17.6	16.9	21.4	27.9	38.8	30.4	9.43
22 hours recovery (%)	34.4	39.9	41.3	37.9	40.3	35.5	25.2

Table 16: Results for brine- and associative polymer flood experiments

	Brine	Conventional FP 3630				
Concentration (ppm)		500	750	1000	1250	1500
Permeability (md)	1311	1427	1151	1350	1200	1150
BT-time (min)	71	25	81	17	28	25
Pore volume injected (ml)	0.54	0.19	0.61	0.13	0.21	0.19
BT-recovery (%)	17.6	16.9	22.0	29.9	31.2	38.0
22 hours recovery (%)	34.4	37.4	34.5	31.5	33.8	36.5

Table 17: : Results for brine- and conventional polymer flood experiments

Finger Analysis and Sweep Efficiency

Finger analysis consists of the measurement of length and number of obvious fingers. The finger length was measured from the base line or from an average advancement of the front and was determined visually. Not every single finger is counted in this analysis. Only those which were easily detectable were taken into account.

An example of counted and measured fingers with a base line can be seen in Fig 94. This example below is from the breakthrough time of the 500 ppm conventional polymer solution. With increasing concentration, the number of fingers decreased as a consequence of the decreased mobility ratio. Finger length at a higher concentration which was caused by the edge fingers has to be taken with care when making further conclusions. But the general trend that the 1250 ppm and 1500 ppm polymer solution gave the best results with respect to the edge fingers can be seen in the following charts (Fig. 95 to Fig. 98) as well.

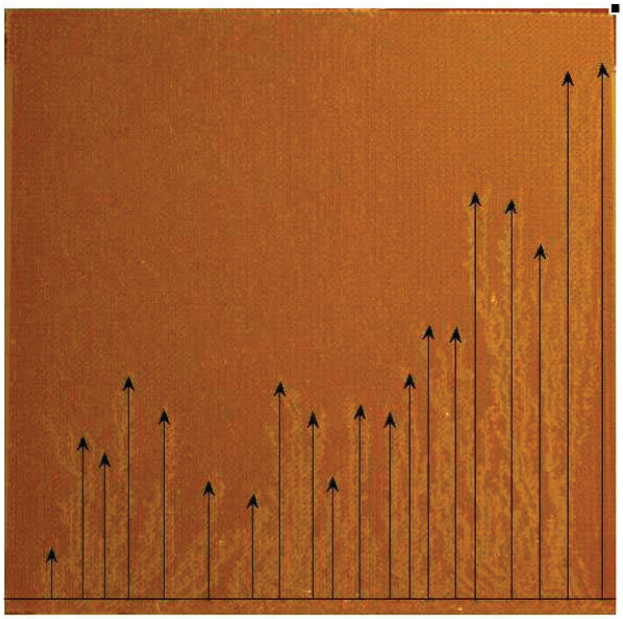

Figure 95: Meso scale photograph at breakthrough with finger base line and counted fingers

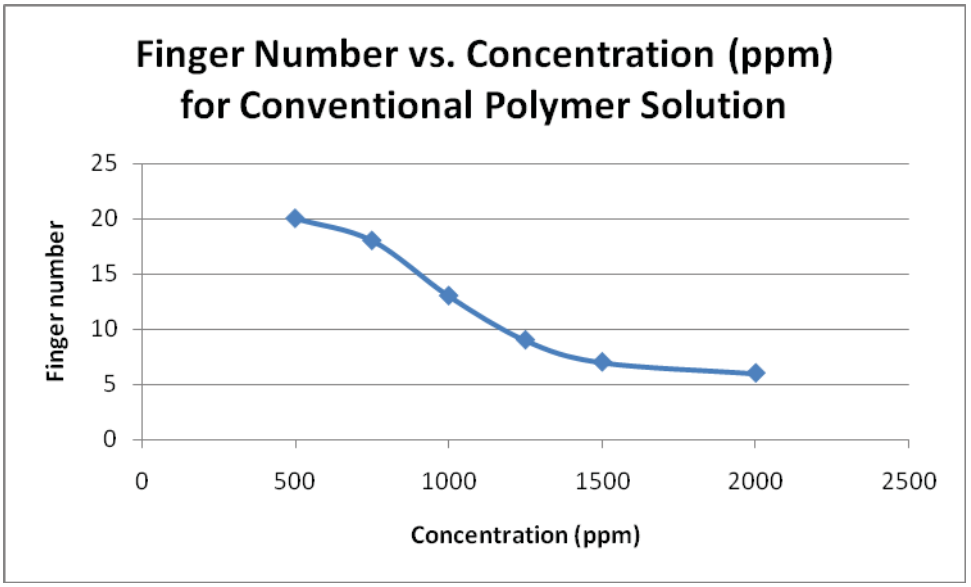

Figure 96: Effect of increasing concentration on finger number for conventional polymer

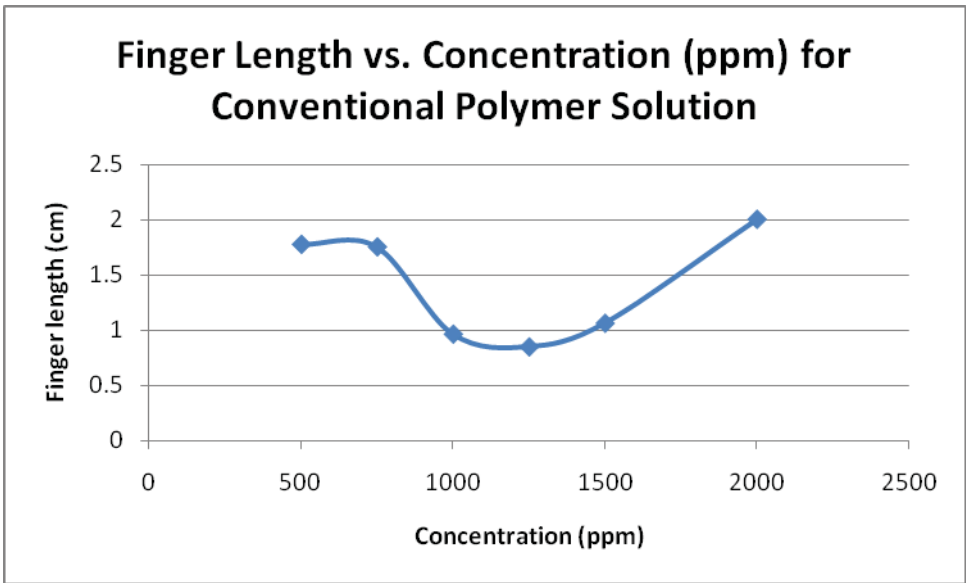

Figure 97: Dependency of finger length on polymer concentration for conventional polymer

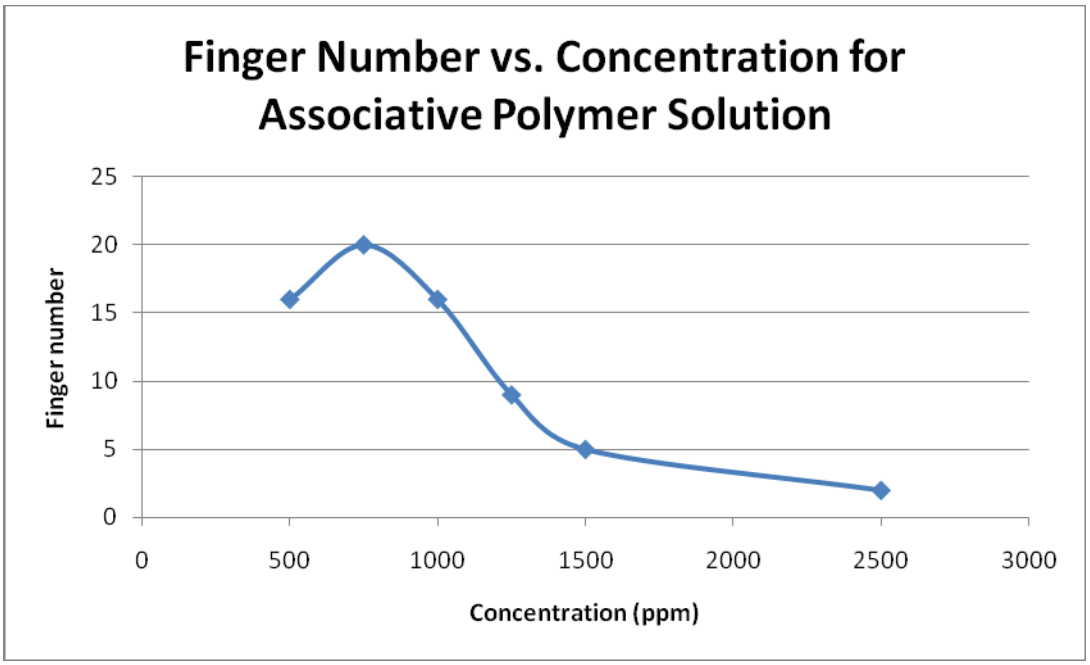

Figure 98: Effect of increasing concentration on finger number for associative polymer

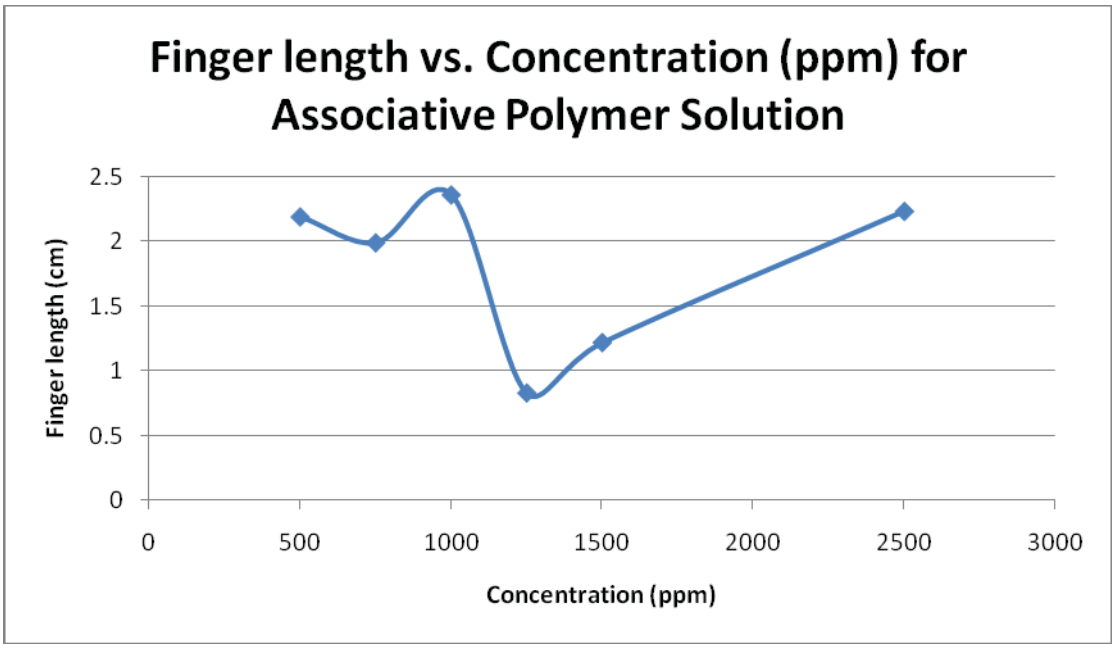

Figure 99: Dependency of finger length on polymer concentration for associative polymer

Swept Areas

Based on the meso scale photographs, the swept area at breakthrough time was determined. The similarity of swept and unswept areas made it impossible to process the picture with the computer. Hence, swept areas had to be marked manually ,because of the low colour contrast of the picture. Sweep efficiency was determined with G.I.M.P. image analyses procedure. Figure 99 to Fig. 101 below present the swept areas in black and the unswept in white after being processed from associative and conventional polymer solutions.

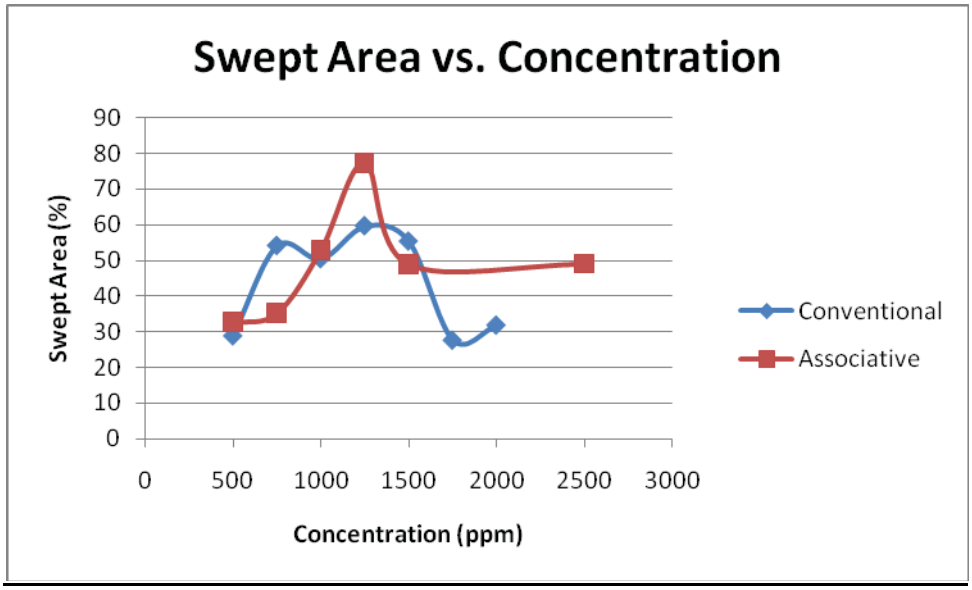

Figure 100: Swept areas for conventional and associative polymer solution

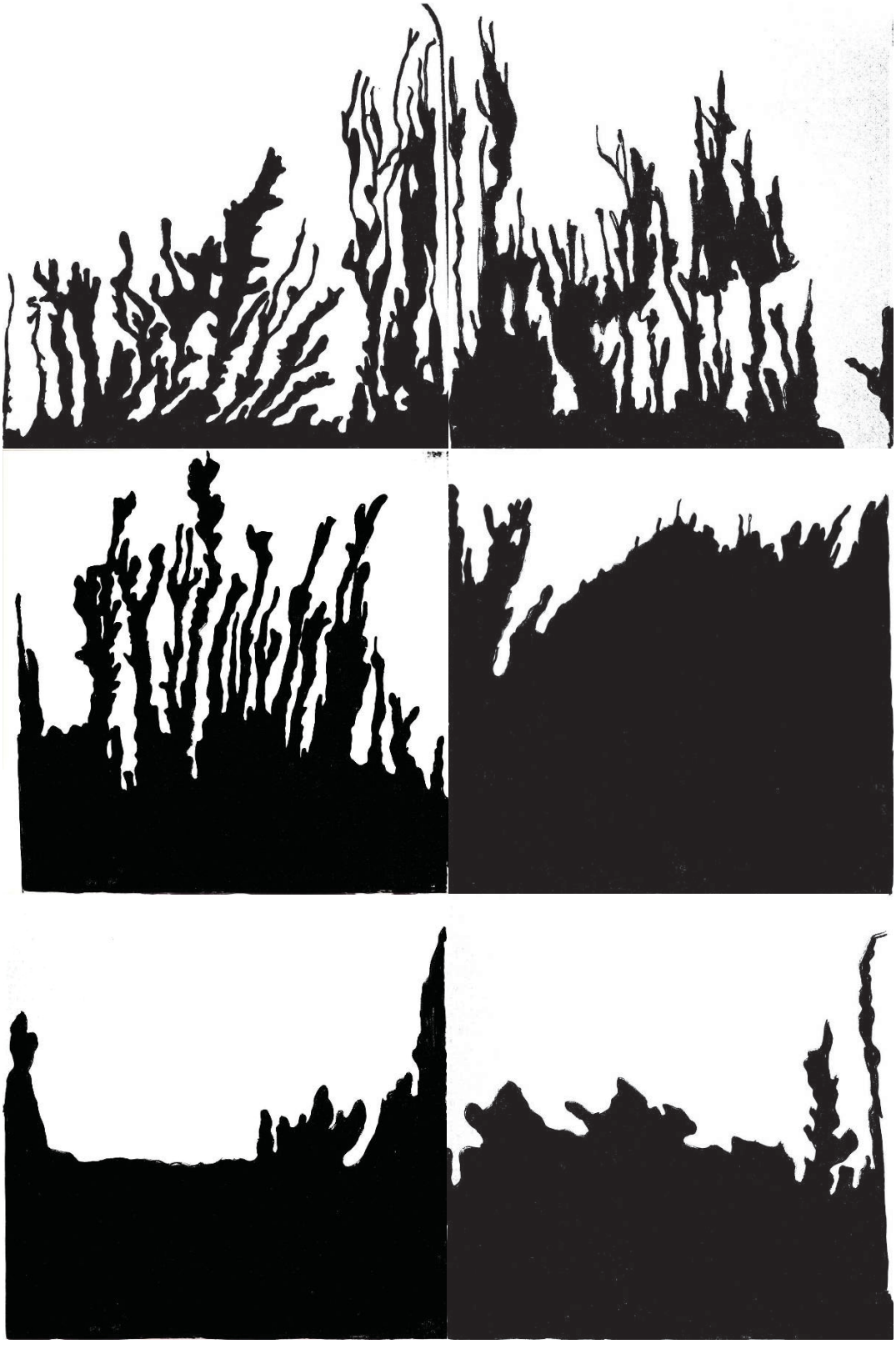

Figure 101: Processed binary images of associative polymer for swept area calculation. From top to bottom: 500 ppm, 750 ppm, 1000 ppm, 1250 ppm, 1500 ppm, 2500 ppm.

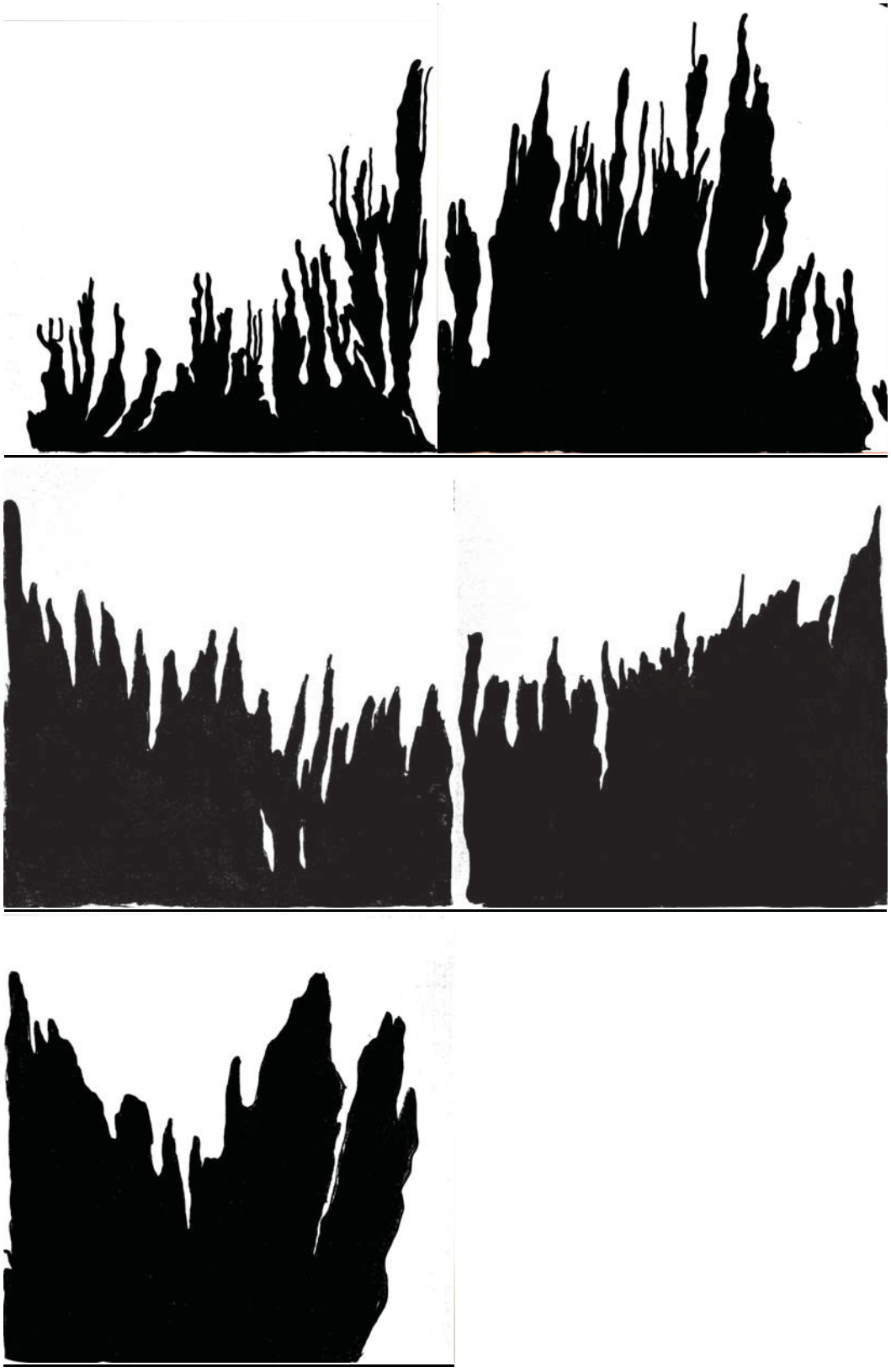

Figure 102: Processed binary images of conventional polymer for swept area calculation. From top to bottom: 500 ppm, 750 ppm, 1000 ppm, 1250 ppm, 1500 ppm

Combination Flood Experiment

The experiments mentioned above had the goal to find a polymer concentration which lead to a stable displacement. The cases in which a polymerflood is conducted in the secondary recovery stage are very rare. Normally polymer floods are started at tertiary recovery stage, when an intensive waterflood has already been done and water has already broken through. In this case a polymer solution is used to reduce the permeability of high velocity paths and contacts the bypassed oil. Consequently, the water production should be reduced and more oil produced.

In the micromodel it is not possible to wait for a waterflood breakthrough and then switch to the polymer solution to observe the above effect. Dimensions in the model are too small and it often takes less than 5-10 minutes, from breakthrough to a total swept area which is the time needed to switch from water to a polymer solution. First experiments were done in the way described above, but it was not observable if the fingers could be reduced after injecting the polymer solution.

So the further approach was to flood with water till half or a third of breakthrough and then switch to the polymer solution. The results showed a very positive effect of the associative polymers. The fingers developed initially had been smoothed by the polymer solution. Because of the very small contrast the changing front is marked with a black pen see Fig. 103. So, this result leads to the assumption that an initiation of a polymer flood after a water breakthrough can decrease the viscous fingering and therefore contact more areas in the reservoir which results in increased recovery.

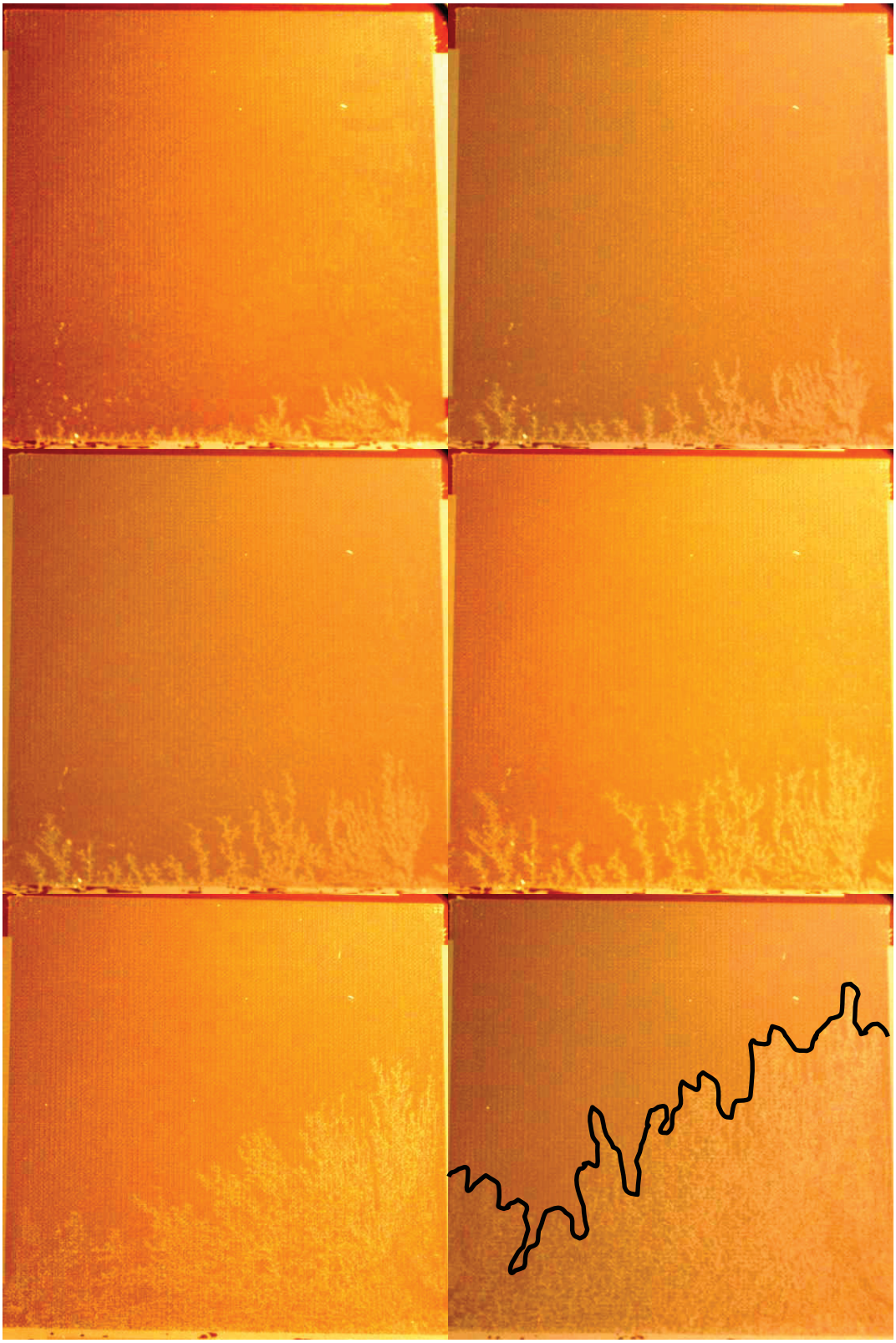

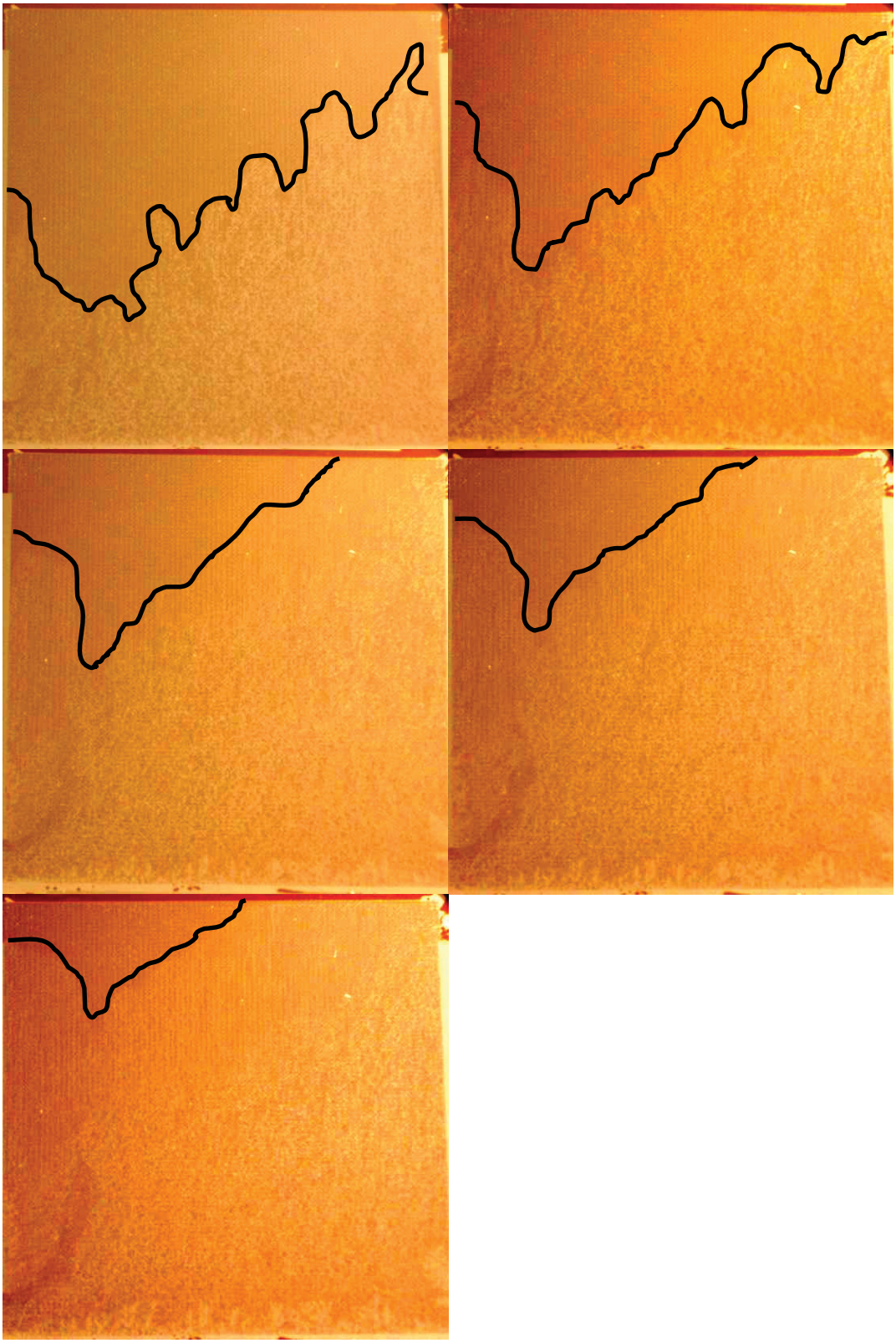

Figure 103: Combination flood. Switch from brine injection to polymer solution at picture 5 (third row second picture)

Residual Oil Recovery Experiment

This experiment was done with the purpose to investigate if the injection of a polymer solution can reduce the residual oil saturation. To observe this effect, the oil saturated micromodel was first flooded with water for 22 hours. After 22 hours no more oil production resulted from injecting more water.

At this time the brine vessel was disconnected, micro scale pictures were taken to determine the oil saturation and the polymer solution was injected into the micromodel. The flood was continued for a second 22 hour period. Finally pictures were taken and oil saturation was determined.

The comparison of the image analyses showed no additional oil production after the polymer injection.

Conclusions

The aim of this study was to observe the displacement process of polymer solutions. During the experiments, augmented associative and conventional polymers with different concentrations ranging from 500 ppm to 2500 ppm were used. Oil recoveries and sweep efficiencies were obtained by taking high resolution photographs at meso and macro scale and processing them further. Almost unchanged initial conditions and very careful experimental work led to reliable results. In addition to the conventional floods, combination floods had been conducted. The reason was to observe the effects of decreasing viscous fingers and the recovery of residual oil by polymer injection. This study reports experimental results showing that:

- Conventional brine flood with an unfavourable mobility ratio showed serious viscous fingers causing an early breakthrough and therefore poor sweep efficiency and recovery factor.

- By increasing the concentration stepwise the sweep efficiency at the breakthrough could be improved for associative and conventional polymer solutions. In some experiments an edge finger evolved, which probably caused an early breakthrough.

- Increased polymer concentration of associative and conventional polymers also led to a better recovery factor at breakthrough time.

- Sweep efficiency and recovery indicate that a polymer concentration of 1250 ppm (M=1.33) to 1500 ppm (M=0.97) led to the best results for the described conditions and fluids.

- The finger analysis also demonstrated a decreasing finger number and length with an increasing concentration.

- A stable displacement in the presence of only minor viscous fingers could only be observed for associative polymer solutions. A conventional polymer solution indicated viscous fingers for all used concentrations. Fingers of the

two polymer types differ in appearance and interval. Conventional polymer flood fingers seemed to be more tiny and closer together and merged towards the outlet fracture, whereas associative fingers tented to build thicker single fingers and to merge at a later stage of the flood.

- An associative polymer concentration of 2500 ppm led to a poor recovery and sweep efficiency. It was assumed that this concentration was too high and caused a very serious pore plugging by multi-layer polymer adsorption.

- No relation between ultimate recovery after flooding ten pore volumes and polymer concentration for both polymer types could be observed and measured.

- Already developed and advancing fingers could be thickened and even smoothed by the injection of an associative polymer solution.

- By the injection of an associative polymer solution after reaching the ultimate recovery with a water flood, no additional oil could be recovered, meaning that polymer flooding operations cannot recover any residual oil.

- Associative polymer solutions did not show any significant higher recoveries and swept areas at breakthrough than conventional polymers. However stable displacement was only obtained by an associative polymer solution.

- A residual resistance factor, R_{Rf} , of 1.5 was measured in an experiment. This value fits to other measured core experiments in literature.

Follow up

As a follow-up of this study, multiple repeated experiments should be conducted in order to determine to what degree standardization of initial conditions, and additionally to what degree varying the input parameters (i.e. viscosity and flow rate) can affect the anatomy of the displacement front. Further experiments with real cores investigating the polymer adsorption effect and polymer plugging would be of importance. Additionally computer tomography pictures analysing the saturations at different positions and times in the micromodel would enable the comparison to simulation programs.

Future experimets

References

1. R.Jennings et al. “Factors Influencing Mobility Control by Polymer Solutions”, SPE 2867, JPT Volume 23, (March1971)

2. Manning, R.K et al.:” Technical survey of polymer flooding projects”, Report DOE/ET/10327-19, (Sept.1983)

3. Forrest F. Craig Jr.: The reservoir engineering aspect of waterfloods, Monograph SPE

4. Van Meurs P. “The use of transparent Three-Dimensional Models for studying the mechanism of Flow processes in oil reservoirs”, SPE 000678, Trans., AIME 295-301, (1957)

5. BENHAM, A.L.” A model study of viscous fingers” SPE 513, (Juni 1963)

6. Saffman P.G. and Taylor G. I.,” The penetration of fluid into a porous medium or hele-shaw cell containing a more viscous liquid”, Proc. Royal society London Vol.213, 103-112, (1958)

7. Van Meurs P. and van der Poel C.” A theoretical description of water drive processes involving viscous fingers”, Trans, AIME, Vol. 213, Pages 103-112 SPE 000931, (1953)

8. W. Littmann, “Polymer flooding” ISBN 0-444-43001-6

9. Y. Du et al.: “Field-scale Polymer Flooding: Lessons Learned and Experiences Gained During Past 40 Years”, SPE 91787, (2004)

10. R.D. Kaminsky et al.:”Guidelines for polymerflooding Evaluation and Development” SPE 11200, (2007)

11. Jerry W. Lake, Enhanced Oil Recovery, ISBN 0-13-281601-6

12. Mojdeh Delshad et al.:" Mechanistic Interpretation and Utilization of Viscoelastic Behaviour of Polymer Solutions for Improved Polymer-Flood Efficiency", SPE/DOE 113620, (2008)

13. M, Pancharoen et al.:" Physical Properties of Associative Polymer Solutions ", SUPRI-A Stanford University Petroleum Research Institute Thirty-first Annual Report, (2008)

14. www.merriam-webster.com

15. www.brookfieldengineering.com/education/what-is-viscosity.asp

16. Sarah Inwood, "High Resolution, Microvisual Study of High Mobility Ratio, Immiscible Displacement", Stanford University, Master Thesis 2008,

17. Ashwini A. Upadhyaya," Visualization of Four-Phase Flowing Using Micromodels", Stanford University, Master Thesis 2001.

18. Mattax, C.C. and Kyte, J.R.: "Ever see a Water Flood", Oil and Gas Journal 115-128, (Oct. 1961)

19. Davis Jr., J.A. and Jones, S.C.: "Displacement Mechanisms of Micellar Solutions," JPT, SPE-1847, (Dec. 1968)

20. Owete, O.S. and Brigham, W.E.: "Flow Behaviours of Foam: A Porous Micromodel Study," SPERE 315-323, (Aug 1987)

21. Hornbrook, J.W., Castanier, L.M. and Petit, P.A.: "Observation of Foam/Oil Interactions in a New, High-Resolution Micromodel," SPE 22631,(Oct. 1991)

22. Keller, A.A., Blunt, M.J. and Roberts, P.V.: "Micromodel Observation of the Role of Oil Layers in Three-Phase Flow," Transport in Porous Media 26, 277-297, (1997)

23. Bruce T. Campbell. and Orr, F.M.: "Flow Visualization for CO2/Crude-Oil

Displacements," SPEJ 665-678, (Oct. 1985).

24. George, D.S.: "Visualization of Solution Gas Drive in Viscous Oil", Stanford University, Master Thesis 1999

25. Aktaz Filiz," The Reservoir Behaviour of Associative Polymers", Stanford University a. University Leoben, Master Thesis 2007

26. OMV, Alberta Research Council

27. SNF Floerger Technical Data Sheet

28. Mridul Kumar et al.:"High-Mobility-Ratio Waterflood Performance Prediction: Challenges and New Insights", SPERE 186-196, SPE 97671, (Feb. 2008)

29. D. Rousseau et. Al.:"Associative Polymers for EOR - Towards a Better Understanding and Control of Their Adsorption in Porous Media", EAGE, (June 2008)

30. http://snf.stanford.edu/Equipment/EquipByName.html

Nomenclature

ϕ	Porosity [%]
μ	Viscosity [cp]
λ_{1a}	Mobilty of brine after polymer flood [ ]
λ_1	Mobility of brine [ ]
λ_1'	Mobilty of single phase polymer [ ]
A	Area [cm²]
dl	Length [cm]
dp	Pressure [bar]
dx	Length [cm]
F	Force [N]
F´	Shear Rate [sec^{-1}]
f_o	Fractional Flow of oil [ ]
f_w	Fractional flow of water [ ]
k_{ro}	Relative permeability of oil [ ]
k_{ro}^*	Endpoint relative permeability of oil [ ]
k_{rw}	Relative permeability of water [ ]
k_{rw}^*	Endpoint relative permeability of water [ ]
M	Mobilty ratio [ ]
n_o	Oil exponent for saturation calculation [ ]
n_w	Water exponent for saturation calculation [ ]
N_p	Cumulative production [bbl/day]
n_{pl}	Fluid coefficient [ ]
q	Flow rate[m³/day]
R_{Rf}	Residual resistance factor [ ]
S	Shear stress [N]
S_{btp}	Saturation at polymer breakthrough [%]
S_{btw}	Saturation at water breakthrough [%]
S_{or}	Residual oil saturation [%]
S_{pf}	Saturation at the polymer front [%]
S_{wf}	Saturation at the water front [%]
S_{wi}	Initial water saturation [%]
S_{wor}	Water saturation at residual oil saturation [%]
S_{wr}	Connate water saturation [%]
u	Superficial velocity [cm/sec]
v	Velocity[cm/sec]
W_i	Injected pore volume [bbl/day]

Appendix

Appendix A

The Etching Process

The Etching process is done completely in the SNF and requires special training and equipment. Below all the equipment and machines which are used during this process are listed and introduced according to the production process from the beginning to the end[30].

Silicide Wet Bench

The Silicide Wet Bench is used for the cleaning of 3" or 4" silicon or SiGe wafers. Wafers containing Tungsten or Titanium silicides, but no other metals, may be processed here. This station contains sulfuric/peroxide hot pots, an HCl hot pot, and HF tanks in addition to dump rinse and spin-rinse-dry modules. The available chemical baths are:

- 90% Sulfuric Acid/Hydrogen Peroxide ("piranha") for resist strip
- 4:1 Sulfuric Acid:Hydrogen Peroxide for removal of trace organics
- 5:1:1 H2O:H2O2:HCl for removal of trace metal ions
- 50:1 HF, for oxide etching
- 6:1 BOE for oxide etching[30]

SVG Photoresist Spin Coater

The SVG (Silicon Valley Group) coater is an automated track system for dispensing photoresist on 4" silicon, glass, or quartz wafers. The system includes three stations: a prime oven which bakes the wafer and dispenses the adhesion promoter, HMDS; and a combination spinner, which dispenses photoresist, and a pre-bake oven which cures the resist. The uniformity of spun photoresists are typically +/- 100 Å[30].

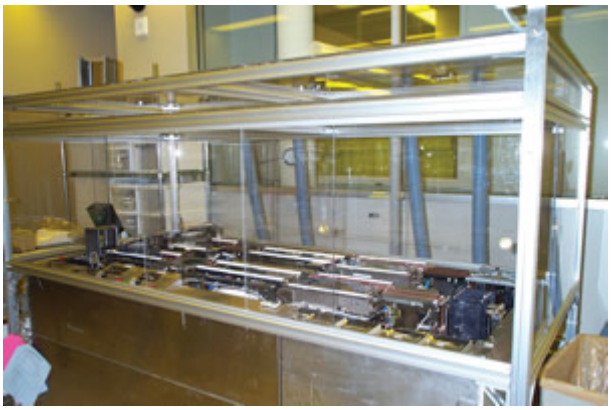

Figure 104: Photoresist Coater[30]

Karl Suss- Exposing

The Karl Suss MA-6 Contact Aligner system can perform precision mask-to-wafer front- or back-side alignment and near-UV photoresist exposure in any one of three modes (hard- and soft- contact, and high and low vacuum contact). The current configuration accomodates 3" and 4" wafers and pieces. SNF has two MA-6 aligners[30].

SVG Developer

The SVG (Silicon Valley Group) developer is an automated system with two independent tracks for developing and post-baking exposed photoresist-coated 4" wafers. Each track system includes two stations: a spin station which dispenses and rinses away developer; and an oven station for post-bake[30].

Figure 105: Developing machine-chemical Wash[30]

STS Deep RIE Etcher

The STS etcher is used to remove specific parts of the resist or wafer.CF_3^+ and F act as the etching gases. Oxide or photoresist may be used for mask.

Etches up to 6 µm/minute.

Metals may not be used as an etch mask, though they can be used as a mask stop Au, Cr, Ni, and magnetics are never allowed in the machine[30].

Figure 106: STS-Etching machine with control computer[30]

ZYGO White-Light 3D Surface Profiler

The Zygo White-Light 3D Surface Profiler provides fast, non-destructive, quantitative surface characterization of step heights, texture, roughness, and other surface topography parameters. The measurement technique is non-contact, three-dimensional, scanning white light and optical phase-shifting interferometry[30].

The Zygo is based on scanning white-light interferometry, a traditional technique in which a pattern of bright and dark lines (fringes) result from an optical path difference between a reference and a sample beam. Incoming light is split inside an interferometer, one beam going to an internal reference surface and the other to your sample. After reflection, the beams recombine inside the interferometer, undergoing constructive and destructive interference and producing the light and dark fringe pattern.

Available objectives are: 2.5X, 10X, 20X, and 50X with additional zoom from 0.5 to 2X

Field of view ranges from 0.14 x 0.11mm (50X) to 2.82 x 2.11mm (2.5X)

Vertical resolution is 0.1 nm

Minimum lateral resolution is 0.22 µm (50X objective, 2X zoom) [30]

Figure 107: Zygo-electron microscope[30]

Appendix B

MATHLAB Routine

```
function average=zoom(dirname)
black=0;
white=0;
schnittwhite=0;
schnittblack=0;
averagewhite=0;
averageblack=0;
summe=0;
cd(dirname)
names=dir('*.JPG');
nnames=length(names);
prozent=zeros(nnames,1);
oil=zeros(nnames,1);
for i=1:nnames
   fname=names(i).name
   X  =imread(fname);
   X=imcrop(X,[400 250 3200 2500]);
   A  =X;
   for m=1:2500
      for n=1:3200
            indi=0;
            black2=0;
            if ((X(m,n,1)>79) && (X(m,n,2)>108) && (X(m,n,3)>80))
               white=white+1;
               X(m,n,1)=250;
               X(m,n,2)=250;
               X(m,n,3)=250;
               indi=1;
            else
               black=black+1;
               X(m,n,1)=0;
               X(m,n,2)=0;
               X(m,n,3)=0;
```

```
            end
        end
      end
    datei=['blackwhite' fname ];
    imwrite(X,datei,'jpg');
    white=white/80000
    black=black/80000
    imshow(X);
    schnittblack=schnittblack+black;
    schnittwhite=schnittwhite+white;
    summe=0;
    oil(i)=black-26.00;
    black=0;
    white=0;
    pause
  end
  averagewhite =schnittwhite/nnames
  averageblack =schnittblack/nnames
  oil
```

Appendix C

Experimentnr.:13 **Date:** 12/03/2008 **MMnr.:** m9(01/03/2008)

# of experiments with same MM: 1

Description: Associative Polymerflood with S255 (500 ppm)

Oil(name/μ): OMV **Flooding fluid(name/ppm/μ):** S255; 500ppm
200 g brine
0.1 g S255

Flow test: const. pressure & const. flow rate

			INPUT					**OUTPUT**
P2 (psig)	P2 (atm)	P1 (atm)	Q (mL/min)	Q (mL/s)	Area (cm^2)	L (cm)	viscosity (cP)	k (darcy)
40	3.72	1.00	0.378	0.0063	0.0125	5	1.0	0.9261
30	3.04	1.00	0.277	0.0046	0.0125	5	1.0	0.9047
20	2.36	1.00	0.179	0.0029	0.0125	5	1.0	0.8771
10	1.68	1.00	0.088	0.0014	0.0125	5	1.0	0.8624
							average	0.89267

			INPUT					**OUTPUT**
P2 (psig)	P2 (atm)	P1 (atm) >	Q (mL/min)	Q (mL/s)	Area (cm^2)	L (cm)	viscosity (cP)	k(darcy)
37	3.2	1.0	0.35	0.0058	0.0125	5	1.0	0.92707
32	3.18	1.00	0.3	0.005	0.0125	5	1.0	0.91875
21	2.43	1.00	0.2	0.0033	0.0125	5	1.0	0.93333
11	1.75	1.00	0.1	0.0016	0.0125	5	1.0	0.89099
							average	0.91755

Calculated perm.: 905 md

Cleaning: CO2

Brine saturation:

Starttime: 10.55 **Startvol.:** 74.00 ml **Vol. inject.:** 14.00ml

Endtime: 11.55 **Endvol.:** 60.00 ml

Oil saturation:

Starttime: 12.00 **Startvol.:** 59.9 ml **Vol. inject.:** 0.5ml

Endtime: 20.20 **Endvol.:** 59.4 ml

Micro scale pictures were taken after every hour to investigate how the saturation changes after time

Image analysis results assuming 22.1 % porosity

	1 hour	2 hours	3 hours	4 hours	5 hours	8 hours
Black %	46.43	46.85	46.68	45.9	46.58	46.094
White %	53.57	53.15	53.32	54.1	53.42	53.905
Egde %	25.2	25.2	25.2	25.2	25.2	25.2
Oil sat. %	21.23	21.65	21.48	20.7	21.38	20.894

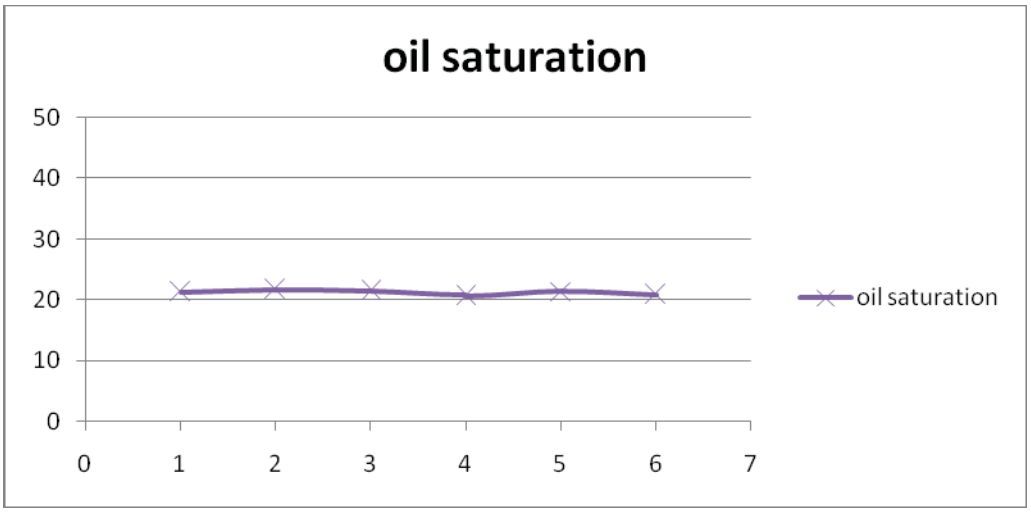

The uneven illumination of the pictures leads to some errors in the image analysis process!!!

Flooding:

Starttime: 20.45 **Startvol.: 55.16** **Vol. inject.: 0.132ml**

Endtime: 18.45 **Endvol.: 55.03**

Flowrate:0.0001 ml/min

The injected volume corresponds approximately to 10 pore volumes of the micromodel.

Pump recordings during flood

min.	6	**9**	**15**	**22**	**26**	**31**	**38**	**52**	**63**
psi	**6**	**5**	**5**	**5**	**5**	**5**	**6**	**6**	**6**

Breakthrough after 51 min.

After the breakthrough a front is developing very slowly from the inlet fracture towards the outlet fracture, which can be a polymer plugging front.